AN INVESTIGATION INTO THE FRAGMENTATION AND ISOMERIZATION PRODUCTS OF SMALL ALDEHYDES: AN ELECTRON BOMBARDMENT MATRIX ISOLATION STUDY

by

Matthew Robert White

A thesis submitted to the Department of Chemistry

In conformity with the requirements for

the degree of Master of Science

Queen's University

Kingston, Ontario, Canada

(June, 2009)

Abstract

The gas-phase chemistry of butanal, propanal, and acetaldehyde has been investigated using electron bombardment matrix isolation techniques. Each aldehyde was diluted in excess argon gas and subjected to electron bombardment with 300eV electrons. The products of subsequent reaction processes were matrix isolated and analyzed by FTIR absorption spectroscopy. Ionized butanal produced a variety of decomposition products including propane, propene, propyne, ethene, ethyne, CCCO, ketene, formaldehyde, CO, CH_2=$CHCH_2^{\bullet}$, $CH_2CHO^{\bullet}$, $HCO^{\bullet}$ and methane. Products resulting from ionized propanal included the ethyl radical, ethane, ethene, ethyne, CO, $CH_2CHO^{\bullet}$, $HCO^{\bullet}$ and methane. In both cases the products are believed to be formed from C—C cleavages of the parent ion followed by hydrogen atom scavenging and/or hydrogen atom abstraction from proximally located species. Dehydrogenation products of propane and ethane are proposed to result from product secondary ionization, a process dependent on high electron currents. Surprisingly, in the case of butanal, the McLafferty Rearrangement, a dominant process in electron ionization mass spectrometry, was not observed to occur.

Electron bombardment of acetaldehyde:Ar mixtures produced many decomposition products including methane, CO, $HCO^{\bullet}$, $CH_3CO^{\bullet}$, $CH_2CHO^{\bullet}$, $CH_3^{\bullet}$ and ketene. The isomerization product, vinyl alcohol, was also observed. As way of investigating the mechanisms of the above products, experiments were performed in which the acetaldehyde:Ar mole ratio was varied. Variations in the

acetaldehyde:Ar mole ratio produced dramatic variations in the products formed, demonstrating a transition from unimolecular chemistry at low acetaldehyde mole ratios, to processes consistent with bimolecular processes at intermediate mole ratios. Variations in the total flow rate of gas resulted in nonsystematic changes in product yields but provided further evidence for unimolecular methane formation via the elimination of neutral CO. Finally, an investigation into the mechanism of vinyl alcohol using the acetaldehyde isotopomer, CD_3CHO, in conjunction with computational methods provided further evidence that enol formation occurs as a result of a direct 1,3-H-transfer and not consecutive 1,2-H-transfers.

Acknowledgements

I must first thank all of the faculty and staff within both the Trent and Queen's chemistry departments for making this possible and for teaching me so much along the way. I have been lucky enough to have had many great professors who have influenced my education in profound ways.

One of those professors is my supervisor, Dr. J. Mark Parnis. He was always available to answer my questions, shed light on problems, and to listen to my concerns. I could not have asked for a better supervisor and mentor. I owe him a tremendous amount of gratitude for truly making this a worthwhile experience.

I also owe much thanks to all of the members of the Parnis lab. Both Dr. Matthew Thompson and Kaitlynn King provided much help and insight throughout my research. I would further like to thank my other fellow lab mates, Brandi West, Emily Clair and Laura Prest, for their friendship and support. Two final people from the Parnis lab that I would like to thank are Stephen Walker and Adam Malcolm. The good times I have shared (and will continue to share) with these two 'bros' are something I will cherish forever. They have both become two of my closest friends and without their support and distractions, obtaining this degree would have been a lot more difficult and a lot less fun.

I must also thank all of the people from the Trent University Varsity Swim Team for helping me to keep my life balanced. I could never have imagined how deciding to swim again could have so dramatically changed my life for the better.

I owe a giant thank you to Scott Farrow, my mentor, my swim coach, and one of my best friends.

I would like to give a special thank-you to my family. I am forever grateful for having two amazing parents. Thank you Mom and Dad for supporting me and for teaching me all of those little life lessons along the way. Similarly, I would like to thank my grandmother, Nanny, for always believing in me and for making me feel like I could succeed at anything I pursued. Finally, I am grateful to both my older sister Jen (and her family, my brother-in-law Ben, and my nephew Ethan) and my older brother Andy for teaching me so much, and for all of the good times we have shared.

To Mom, Dad and Nanny

Table of Contents

List of Figures and Schemes

List of Tables

Chapter 1
Introduction

1.0 General overview and scope of this work

The field of mass spectrometry has traditionally been used to study gas-phase chemistry. Ionization of a molecule typically imparts a certain amount of excess internal energy into the incipient cation which then becomes distributed throughout the vibrational modes of the molecule. This distribution of energy, coupled with the fact that one-electron oxidation can lead to structural changes in the molecule, can produce a diverse and interesting set of reactions with which the technique of mass spectrometry can analyze. Thus, upon ionization of the precursor, typical unimolecular fragmentation and/or bimolecular reactions occur whereby the subsequent products can be analyzed, most commonly by their differing mass-to-charge ratios (m/z). Mass spectrometry, along with photoionization spectroscopic techniques, has excelled at indirectly determining structures of molecular ions as well as gaining insight into energetics, reaction rates and mechanisms.[1] Despite this, there is much knowledge about the structure and energy levels of reaction products and intermediates, including neutral species that can be obtained from the use of infrared spectroscopy particularly when coupled to the technique of matrix isolation. Although matrix isolation has generally been used as a tool to characterize unstable or reactive molecules, this method has been found to provide a novel and complementary way of examining decomposition and isomerization chemistry as specifically

seen in our lab through studies concerning oxalyl chloride[2] and, more recently, acetone[3] and dimethyl ether.[4] An electron-bombardment source coupled to a matrix isolation spectroscopy set-up (EBMIS) based on the design of Szczepanski *et al.*[5] was used in those studies, as well as in the present work.

The success of the previous work has prompted further investigations into the chemistry of other small organic compounds. Thus, the present work focuses on three small aldehydes: acetaldehyde, propanal and butanal. Although each molecule has extensive literature concerning its gas-phase chemistry, there is still much to be gained through an EBMIS study of each. For example, isomers possessing the same m/z ratio are unable to be distinguished via mass spectrometric methods; however, isomers are easily distinguished through the use of infrared spectroscopy. Matrix isolation also enables the direct observation and characterization of reaction intermediates, which, in doing so, sheds mechanistic light onto previously gray areas of the gas-phase chemistry.[6] Finally, the use of the EBMIS apparatus provides a range of variables which can be carefully controlled such that their impact on the observed chemistry can be seen and subsequently interpreted.

In general, examining the chemistry of acetaldehyde, propanal and butanal through the EBMIS apparatus presents a new and valuable way of approaching gas-phase chemistry. This thesis is an attempt to gather new information on the gas-phase chemistry of those three aldehydes. In the end, it

is hoped that through the work herein, their various decomposition and isomerization pathways and mechanisms will be more fully understood.

1.1 Matrix Isolation

The term matrix isolation refers to the technique of trapping molecules or atoms in solidified inert gases. The technique was originally developed in the early 1930's where organics were frozen into clear glasses. The goal then was to find solvent mixtures which gave frozen glasses with good optical properties. For example, a mixture of ether, isopentane and ethanol, cooled to 77K, forms clear glasses that are completely transparent throughout the UV-visible region. However, the use of such glasses was clearly limited as they are not chemically inert and they give strong absorptions over wide regions of the infrared (IR) spectrum. Consequently, an important improvement on the technique was made upon the advent of noble gases as the matrix material. These closed-shell species are chemically inert and do not absorb in either the UV or infrared regions. The use of noble gases was first reported by George Pimentel in 1954 where his group reported the successful isolation of small organics (such us HN_3, NH_4 and NO_2) in xenon at 66K.[7] Although Pimentel is credited with the development of the modern matrix isolation technique, its practice was still limited by the relatively mild temperatures systems could reach. Even at 66K xenon formed matrices that were not very rigid resulting in diffusion and bimolecular interactions such as hydrogen bonding. Thus, the potential of matrix isolation was not fully actualized until lower temperatures could be obtained

which, in turn, resulted in the inclusion of other noble gases including argon. Once this happened matrix isolation began to have tremendous application and the technique continues to be a valuable tool in approaching a wide variety of chemical and physical problems.[8] This is apparent by the almost 18,000 research publications referencing matrix isolation as a technique. There have also been numerous monographs on the subject[6,9,10] and two bibliographical volumes for convenient reference of research articles concerning specific matrix isolation topics.[11,12]

Matrix isolation has been employed for a variety of uses; however, it is particularly well-suited for the study of transient species, which react rapidly or decompose under normal chemical conditions.[9] One of the first unstable molecules to be characterized and a landmark in the history of matrix isolation was the reporting of the infrared spectrum of cyclobutadiene.[13] In addition to studying unstable molecules, there have also been many studies of weakly bound complexes such as that found between acetone and water.[14] Efforts have even been made to use matrix isolation as a synthetic tool where novel reactions may proceed as different reaction pathways may be followed in low temperature conditions versus normal ambient conditions. An area of analysis that continues to be particularly fruitful is the mechanistic investigation of chemical reaction processes. For example, reactions in which intermediates are suspected but not directly observed are perfect candidates for a matrix isolation study as implicated short-lived intermediates can be successfully isolated and characterized. In this way, the physical underpinnings of otherwise inaccessible reactions can be

uncovered. Overall, the technique of matrix isolation can be exploited through the coupling of it with a variety of different techniques whether photolysis, microwave excitation, or as in the case of this work, electron bombardment.

A typical electron bombardment matrix isolation experiment consists of a gaseous sample containing the organic molecule (precursor) of interest entrained in an inert host gas (e.g. Ar, Kr, Xe, N_2) which can be directed at a controlled rate towards a cold surface kept at well below the freezing point of the host gas. While flowing, the gaseous mixture is subjected to collisions with an electron beam where ionization of the precursor occurs and typical gas-phase chemistry can ensue. As this occurs, a variety of products and intermediates, diluted in the host gas, co-condense onto the cold surface thereby isolating the various species from each other within the solidified host gas. The solidified host is referred to as the 'matrix' in which the various 'guest' molecules of interest are isolated. Figure 1 shows a cartoon representation of matrix isolated species. Once this condensation onto the cold surface occurs, spectroscopic investigation of products and any intermediates can be completed at leisure.

The stabilization of reactive or unstable species is thought to occur during the process of condensation onto the cold surface. As a result of the excess of inert gas this region can be characterized as having higher pressures than typical gas-phase environments. This relatively high pressure results in a significant reduction of the mean free path of any product or intermediate that was produced subsequent to ionization of the precursor. Consequently, repeated collisions

between the products/intermediates and the host gas occur which causes energy to transfer between them. In the case where the host is a rare-gas atom, energy leaves the excited species and is transferred to the rare-gas as additional translational energy. If inert molecules such as N_2 or CH_4 are used as the host they can provide increased energy transfer as they have additional degrees of freedom found in both vibrational and rotational modes. As energy is repeatedly transferred from any excited species to the host material in addition to the lower temperatures accessed as the various species start to condense, normally unstable or reactive species become quenched, below any energy barriers required for reaction thereby trapping them into their respective potential energy wells. This process of energetically quenching excited-state species is termed collisional deactivation. The combined result of the host gas and the cold surface is a matrix of isolated, stable, and rotationally rigid species. Consequently, once the matrix has been formed there is essentially a static system that can be probed with a variety of spectroscopic techniques. This fact leads to two of the main advantages of matrix isolation over other methods. First, the matrix can be collected over hours or even days such that the issue of sensitivity is mitigated and second, the system can be studied without time constraints.

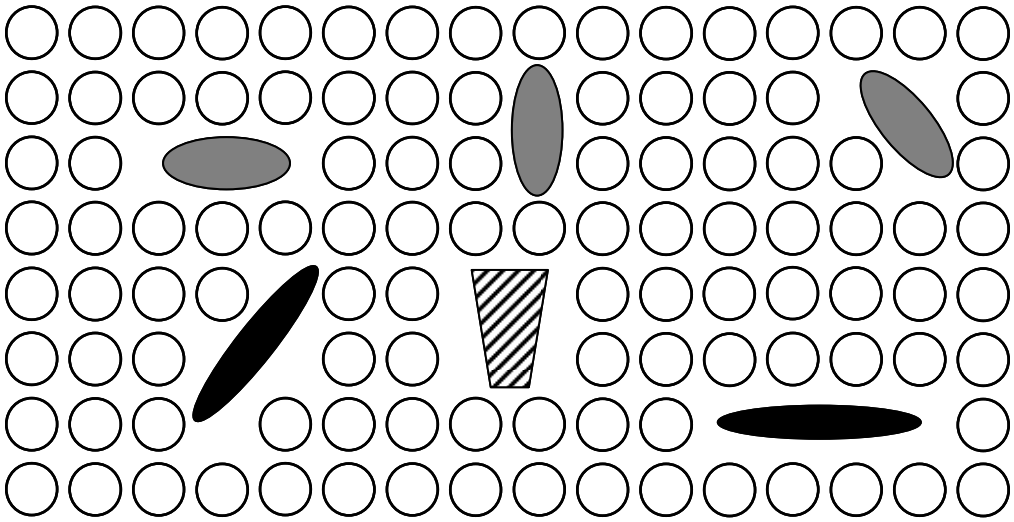

Figure 1: Representation of matrix isolated species in a host gas (clear circles). The rigid host isolates the various species from each other thereby preventing bimolecular interactions.

The isolation of species from one another is an important characteristic of the matrix which is ensured by choosing an appropriate concentration of the original gaseous mixture such that there is a great excess of host gas. Typically, the ratio of precursor (guest species) to host gas is kept no higher than 1:400. The rare-gases such as argon, krypton and xenon form face-centered cubic crystal structures. Except for very small species such as hydrogen that can occupy the tetrahedral and octahedral interstitial holes of the lattice, most molecules occupy substitutional sites.[10] As most molecules are much larger than single rare-gas atoms, matrix isolated species must occupy multiple substitutional sites, in which several adjacent matrix atoms are replaced. Consequently most molecules are surrounded by at least twenty argon atoms thereby effectively isolating key species from each other. Once the matrix has been formed diffusion of molecular species is prevented as long as low enough temperatures are maintained. A general rule is that a matrix may be taken as rigid as long as the temperature is 30% of its freezing point. For example, if argon were being used as the host gas the temperature would have to be kept below 25K (since the freezing point of argon is 83.9K and 0.3 x 83.9 = 25) in order to ensure the rigidity of the matrix. Thus, as long as a low enough temperature is reached to obtain a rigid matrix, bimolecular reactions are inhibited. Furthermore, because such low temperatures must be used, even modest reaction barriers prove to be substantially large as there is minimal thermal energy available to overcome them. As a result even very thermodynamically and kinetically favorable unimolecular dissociations become

unfeasible once the matrix has been formed. Sometimes the system is warmed to promote diffusion and to initiate further chemistry in a process called annealing.

One complicating factor is that although molecular diffusion is inhibited, free electrons are able to easily diffuse throughout the matrix. In the process of ionization a large number of lower energy secondary electrons are produced along with charged species. These secondary electrons are attracted to the positively charged molecules in the matrix. Normally in the gas-phase ion-electron recombination would impart enough energy into the incipient neutral to cause rapid decomposition. However, if neutralization occurs while the ion is embedded within the matrix, the matrix cage would effectively quench the energy of neutralization and therefore the neutral counterpart of the ion would remain.

$$A^{+\bullet} + e^- \rightarrow A \qquad (1)$$

$$A^{+} + e^- \rightarrow A^{\bullet} \qquad (2)$$

Evidence for the neutralization of charged species can be found in previous studies (see Parnis et al. for example) performed in our lab where there were disfavored neutral isomer species as well as low yields ion products.

Matrix isolation continues to be a valued technique for the investigation of gas-phase chemistry; however, there are many other methods that can be used as matrix isolation is not without some disadvantages. These include that matrix isolation experiments requires extensive equipment in order to reach appropriate temperatures and further that there can be some complications arising from

matrix interactions with the generated species. The particular advantage of matrix isolation in conjunction with infrared spectroscopy will be highlighted in the next section.

1.2 Fourier transformed infrared spectroscopy (FTIR) and matrix isolation

Many spectroscopic techniques have been employed for probing matrix-isolated species. The most common techniques include UV/visible and infrared (IR) absorption spectroscopy, and electron spin resonance spectroscopy (ESR).[15] The spectroscopic tool used in this research is IR spectroscopy for which it is pertinent to give an appropriate theoretical background particularly as it applies to matrix isolation.

A non-linear molecule composed of 'n' atoms possesses 3n degrees of freedom. Three of these refer to translational movement, and another three refer to rotational motion, both through Cartesian space. This leaves 3n-6 degrees of freedom for vibrational motion (3n-5 if linear, as only two degrees are present for rotational motion). Vibrational motion can be thought of as internal motion whereby the various atoms within a given molecule are constantly moving with respect to each other in a periodic fashion at a discrete energy. Typically the energy is reported as a wavenumber ($\bar{\nu}_k$) defined as the number of waves in one centimeter and where k corresponds to the k^{th} vibrational normal mode.

$$E = hc\bar{\nu} \qquad (3)$$

where h is Planck's constant (6.314 x 10^{-34} J/s), c is the speed of the light (2.998x10^{10} cm/s).

The energy of this periodic motion falls in the infrared region of the electromagnetic spectrum (4000-400 cm^{-1}). Infrared spectroscopy exploits this molecular vibration as, if a molecule is impacted with infrared light of a specific quantized energy that exactly matches the energy of a given vibration then the energy will be absorbed as excited molecular vibration. One caveat to this is that in order for a vibration to absorb the light, the vibrational mode must produce a change in the dipole moment of the molecule. A change in dipole moment results in a fluctuating electric field with which the oscillating electric field of the impinging infrared radiation can interact. An infrared absorption spectrum that reports these absorptions does not consist of discrete lines as vibrational excitation is accompanied by changes in rotational energy as well, and consequently vibrational spectra appear as bands that vary in their broadness.[16]

In general, vibrational modes are classified as either involving stretching or bending motion. Stretching motions can be predicted mathematically through the use of an approximate model. Even in polyatomic molecules, stretching modes can be simplified to involve the motion of only two atoms. Thus, the classic solution of the harmonic oscillator problem for a diatomic can be applied, with application of Hooke's law, in general to calculate the vibrational energy of a given stretch.[17]

$$\overline{\nu}_s = \frac{1}{2\pi c}\left(\frac{k}{\mu}\right)^{1/2} \qquad (4)$$

Where c is the speed of light (2.998 x 10^{10} cm/s), k is the force constant of the given stretching bond, and μ is the reduced mass ($\mu = m_a m_b / m_a + m_b$) for two nuclei, a and b, undergoing the stretching motion.

From this equation it is apparent that the vibrational wavenumber is proportional to the force constant of the bond, and therefore the stronger the bond the greater the energy of the vibration. Furthermore, in general the wavenumber is inversely related to the reduced mass; however, sometimes this is not clear. For example, comparing the C—H stretch with the F—H stretch on the basis of the reduced mass of the vibration would lead to the conclusion that the F—H bond should occur at a lower frequency than the C—H bond. However, while the reduced mass increases, there is a greater change in the force constant and therefore the F—H stretch absorbs at a higher frequency. In general, the distinct stretching motion of specific functional groups leads in large part to the usefulness infrared spectroscopy exhibits in characterizing different molecules. The functional group region is typically assigned to the 4000-1300 cm^{-1} region.[16] For example, the hydrogen-bonded O—H stretch occurs as a broad feature at about 3600 cm^{-1} whereas the C=O stretch of an aldehyde occurs as a large sharp feature at about 1700 cm^{-1}. Because functional groups display such varied absorption frequencies molecules containing different functional groups are easily distinguished from just minimal analysis of their respective infrared spectra.

In contrast to stretching motion, bending motion is more complicated in that it is difficult to reduce it in a way akin to that done for stretching motion. The energy of bending motion is lower than that of corresponding stretching modes, and the region of the IR spectrum in which bending modes are observed generally appears quite convoluted compared to the functional group region discussed above. This region, typically assigned to the 1300-900 cm^{-1} portion, is referred to as the fingerprint region. The fingerprint region is particularly useful for confirming specific structures over others, as although functional groups can absorb at almost identical frequencies when present on different molecules, they will still have unique fingerprint regions in which to distinguish them.

Infrared spectroscopy would be conveniently simple if each vibrational mode acted completely independently of the other, and if only one transition was observed for each mode; however, this is not the case and hence there are many complicating factors that make analysis of IR spectra more involved. By the Boltzmann distribution equation it can easily be shown that the vast majority of molecules, at ambient conditions, occupy the ground vibrational level.[17] As previously stated, when a molecule absorbs infrared radiation, the vibrational transition (Δn) is accompanied by a rotational transition (ΔJ), both of which, according to the harmonic-oscillator model, must obey particular selection rules which are $\Delta n=1$ and $\Delta J=\pm 1$ respectively. Thus, the most common absorption observed in the infrared spectrum is the $n_0 \rightarrow n_1$ transition; this is typically called the fundamental mode. Indeed, experimentally it is found that the vibrational spectrum of a diatomic molecule consists of a dominant line corresponding to

that transition, but there also exist weaker modes at approximately integral multiples of the fundamental. They are slightly less than integral multiples of the fundamental as the equal spacing of vibrational modes assumes that vibrations are harmonic whereas they are described more properly by an anharmonic potential where the spacing between vibrational modes decreases as further states are obtained (see figure 2). These weaker modes correspond to transitions other than the fundamental such as from $n_0 \rightarrow n_2$. When the anharmonicity of the potential is accounted for the selection rule, $\Delta n=1$, no longer applies, and Δn can theoretically have any integral value. Such absorptions, other than the fundamental, are called overtones. In addition to the presence of overtones, combination bands in which more than one normal mode is simultaneously excited can appear in the resulting infrared spectrum. Finally, a multitude of coupled interactions are possible. For example, the symmetric and antisymmetric stretching modes of carbon dioxide reflect mechanical coupling of individual CO stretches which results in the antisymmetric mode appearing at a wavenumber higher in frequency than observed for carbonyl groups in aldehydes and ketones.[16] Coupling of modes is contingent on certain factors, one being that vibrations must have the same symmetry. Furthermore, coupling can occur between the fundamental mode and overtones or combination bands. Such interactions are known as Fermi resonances. An example of Fermi resonance is the doublet that can appear for the C=O stretch of cyclopentanone where the fundamental mode of the C=O stretch couples with the overtone or combination band of an adjacent CH_2 group.

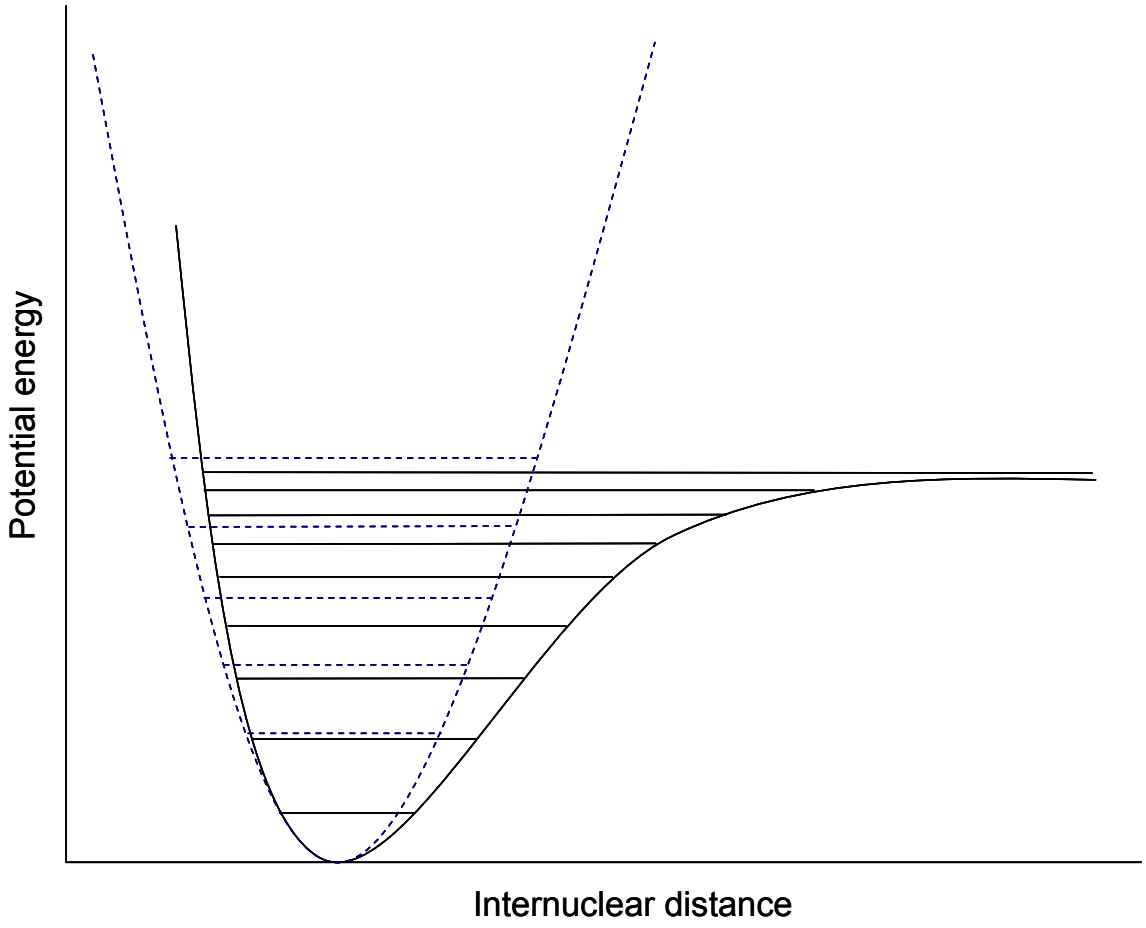

Figure 2: Harmonic (dashed-blue) and anharmonic potential energy curves for an arbitrary electronic state.

Although overtones, combination bands, and Fermi resonance can hinder spectral analysis, in most cases these features are present only as very weak modes and therefore traditionally do not drastically impact spectra interpretation.

If there is a degree of ambiguity surrounding the assignment of a vibrational mode to a specific molecule then often one way to confirm the assignment is the use of isotopic substitution. Isotopic substitution has been called the "gold standard" for molecule identification in both gas-phase and matrix isolation studies. In this work, where aldehydes are used and most vibrational modes involve hydrogen motion, it is most beneficial to use fully deuterated analogues to confirm the characterization of particular products. Remembering equation (3) it is known that the vibrational wavenumber is related to the force constant and the reduced mass. Since the force constant is roughly equivalent whether the atom is hydrogen or deuterium, the only change should stem from the different reduced masses.[18] A ratio of $\overline{\nu_H} / \overline{\nu_D}$ can be expressed as:

$$\frac{\overline{\nu_H}}{\overline{\nu_D}} = \frac{\frac{1}{2\pi c}\left(\frac{k}{\mu_H}\right)^{1/2}}{\frac{1}{2\pi c}\left(\frac{k}{\mu_D}\right)^{1/2}} \qquad (5)$$

This simplifies to give:

$$\frac{\overline{\nu_H}}{\overline{\nu_D}} = \left(\frac{\mu_D}{\mu_H}\right)^{1/2} = \sqrt{2} \qquad (6)$$

Thus, the ratio of a stretching vibration position involving hydrogen to the same vibrational wavenumber position involving deuterium is approximately 1.4 when the H/D experiments are compared. Bending vibrations have different ratios, however, but the difference is appreciable enough to be useful to confirm spectral assignments.

When infrared spectroscopy is used in conjunction with matrix isolation a host of other aspects must be considered. In the gas-phase, although molecules are found primarily in the ground vibrational state, at ambient conditions there is enough thermal energy which enables molecules to statistically populate a variety of different rotational levels. As a result, spectra of molecules in the gas-phase are often convoluted by rotational fine-structure. Figure 3 illustrates what such fine-structure appears as for carbon dioxide and water. As is apparent, such rotational complexity would make analysis much more demanding. A particular advantage of matrix isolation is that a molecule trapped in a host-gas cage at ~15K is held rigid and consequently rotational movement is inhibited. This translates into the disappearance of the rotational fine-structure leaving only clear, distinct vibrational modes. Thus, matrix isolation enables gas-phase chemistry to be probed easily with infrared spectroscopy.

Although molecules are isolated from each other in the matrix, they can still interact with the host-gas and even inert rare-gas atoms can impact, albeit in subtle ways, the resulting absorption spectra.

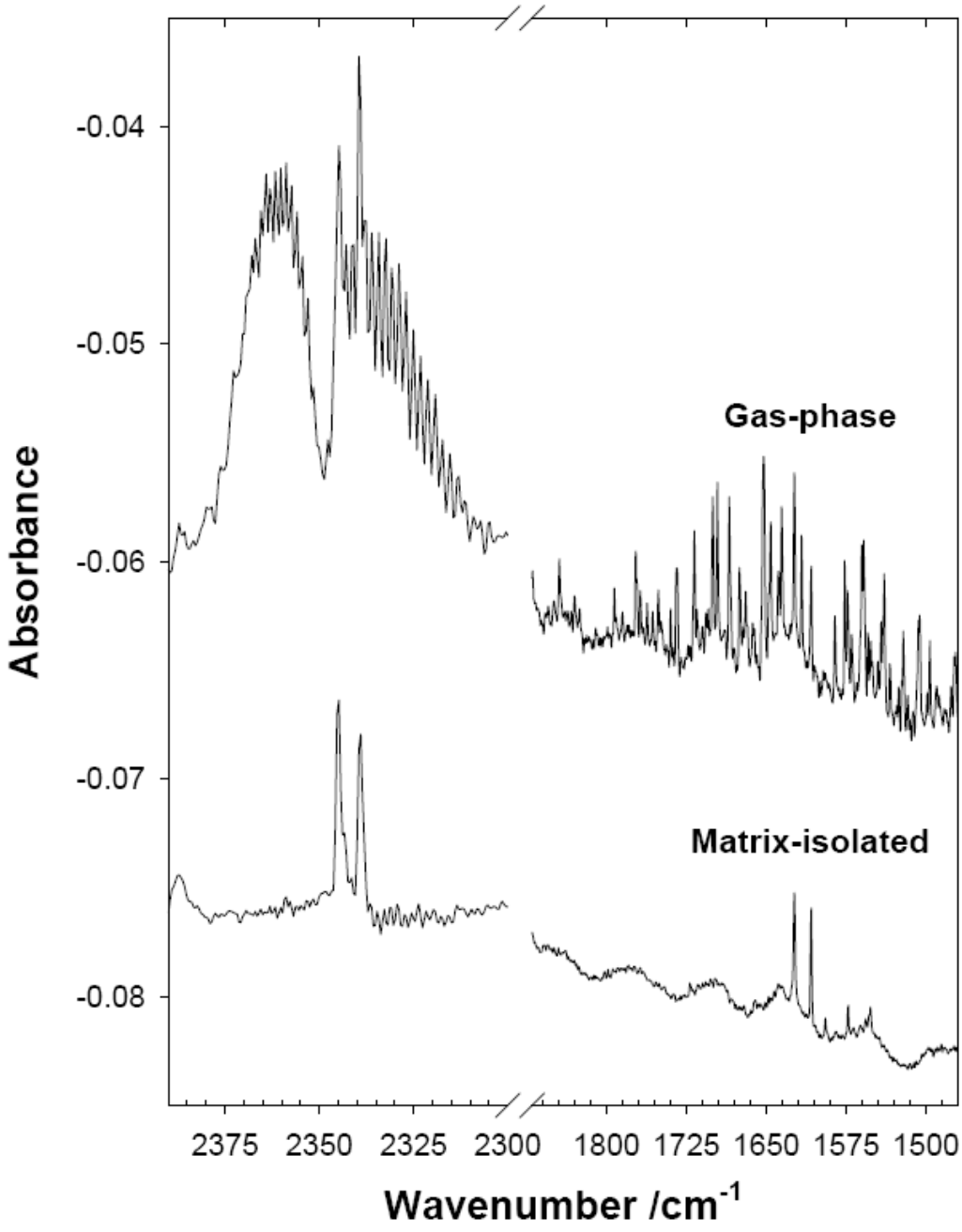

Figure 3: Comparison of the infrared absorptions of gas-phase CO_2 (left) and H_2O (right) versus matrix-isolated CO_2 and H_2O.

In the case of argon, vibrational shifts occur from non-specific matrix-guest interactions that can alter the electronic structure of the guest and subsequently the vibrational spectrum. In general this phenomenon is referred to as matrix-site effects. The vibrational wavenumber of modes of matrix-isolated species may differ from the value reported for the same mode in the gas-phase ($\Delta v = v_{gas} - v_{matrix}$). The larger Δv is, the greater the electronic interaction between a given molecule and the host-gas. The alteration of the vibrational absorption wavenumber is generally minor as the fundamental absorptions of most species isolated in an argon matrix lie within 1% of the gas-phase band centers, and very few deviate by more than 2%. For example, the gas-phase value for the deformation mode of methane is reported to be 1306 cm^{-1} but the same mode of methane, matrix-isolated in argon, absorbs at 1304 cm^{-1}; this is a very minor difference.

It is also important to note that the vibrational shift of modes can vary depending on how the molecule is oriented in the matrix. As previously discussed, there is more than one way of a molecule occupying a substitutional site within the matrix lattice, and thus, how the molecule is positioned within the cage of inert gas dictates how its electronic structure will be perturbed. Because a molecule can experience different matrix-guest interactions one vibrational mode may appear as two or more different peaks, each slightly shifted in wavenumber. For example in Figure 3 the antisymmetric stretch of CO_2 actually appears as a doublet resulting from the different positions of CO_2 within the matrix giving rise to two different matrix-site effects.

1.3 General concepts in gas-phase chemistry

Gas-phase chemistry is a well studied field both theoretically and experimentally. One-electron oxidation creates a localized area of charge resulting in structural changes within the molecule, including the weakening of bond strengths. Concordantly, working in the gas-phase allows access to what might normally be disfavored in solution. The rich and diverse chemistry that results makes this area of chemistry particularly interesting.

Although in this work the precursor of interest is not an isolated entity and many bimolecular processes are possible, a lot of the same theory and principles used for unimolecular decomposition of isolated ions in the gas-phase can be applied to elucidate the experimental findings of the EBMI apparatus. Thus, it is appropriate to consider some of the basic concepts entailed within gas-phase chemistry, and further to discuss some of the other prevalent methods for its study.

The currently accepted theoretical model for describing gas-phase chemistry is the Rice-Ramsperger-Marcus-Kassel (RRKM) theory. A complete description of this theory is beyond the scope of this work but can be found in the monograph by Robinson and Holbrook.[19] A simpler theory referred to as *quasi-equilibrium theory* (QET) also pertains to unimolecular decompositions, but instead assumes that energized molecules may only internally redistribute energy.[20] A simplified version of the QET with its basic assumptions is

presented by Gross[20], and a review of those assumptions is useful towards gaining at least a shallow understanding of the physical basis of decomposition.

First, ionization occurs vertically as opposed to adiabatically in that the molecular geometry of the incipient ion does not change and relax to a lower energy confirmation. According to the Born-Oppenheimer Approximation the nuclear motion involved in the vibrational modes of a molecule can be ignored in the context of the electronic motion which is assumed to be practically instantaneous. Thus, when ionization of a molecule takes place, the position of the various atoms within a molecule can be assumed to be held constant, as the molecule transfers to a cationic potential energy surface. Each vibrational level has associated with it an electronic wavefunction. The Franck-Condon principle states excitation occurs via vertical transitions, and the probability for an electronic transition is greatest where the wavefunctions of the both the ground state and the ionized state overlap the most significantly. Furthermore, the ion will have many low-lying excited electronic states which form a continuum and consequently energy transitions will occur between the excess electronic energy into vibrational energy. The low-lying excited electronic states will not be repulsive and therefore the molecule will remain intact long enough for the excess electronic energy to become randomly distributed as vibrational energy. The rates of dissociation of the ion are determined by the probabilities that randomly distributed energy becomes concentrated in specific regions leading to dissociations, or rearrangements.[20] Finally, if the initial ion has sufficient energy,

the fragment ion may also have enough energy to undergo further secondary decomposition.[20]

QET has particularly been applied when dealing with the rates of unimolecular reactions; however, within the context of this work it is important only to mention the difference in rates between simple cleavages and rearrangement reactions. A molecule undergoing fragmentation through a simple heterolytic bond cleavage possesses what is called a loose transition state in that the molecule does not have to be in any particular orientation in order for the decomposition to occur. All a cleavage reaction requires is sufficient energy to overcome the particular bond dissociation energy. However, some unimolecular fragmentations occur via rearrangement processes. In this case, the molecule must obtain a particular orientation in order for the reaction to proceed and thus the transition state for a reaction is labeled as a tight transition state. Although rearrangements can occur at lower energies than cleavages as a result of their thermodynamic stability, if an excess of energy is obtained for both reactions to occur then the cleavage reaction will dominate kinetically as a result of the loose transition state (Figure 4). As is particularly evident from Figure 4, the energy that an ionized molecule is imbued with has a direct impact on the subsequent chemistry that can occur. For example, an ion with low excess internal energy may show a drastically different product distribution than the same ion left with a large amount of excess energy. The amount of internal energy that a molecule is left with upon ionization is contingent on the process used to cause ionization.

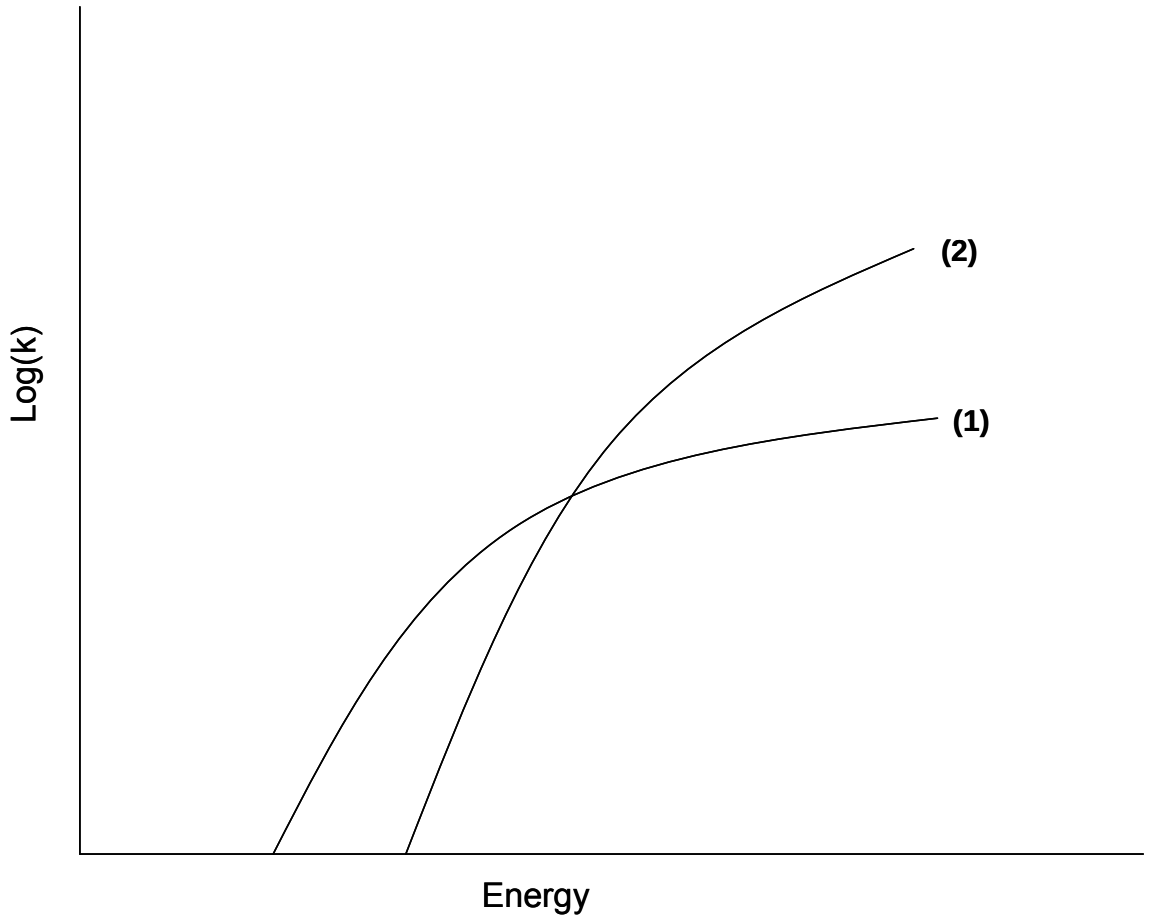

Figure 4: Comparison of how the logarithm of the rate constant, k, changes with energy for a reaction with a tight transition state (TS) (1) and a reaction with a loose TS (2). As higher energies are obtained the reaction with the loose TS out-competes the reaction with the tight TS.

Ionization processes are fundamental in any discussion of gas-phase ion chemistry. Evidence of this can be seen in the abundance of ionization techniques used in mass spectrometry. Generally speaking two broad classes of ionization methods are invoked depending on the degree of fragmentation desired upon ionization. Molecules and atoms are characterized by a certain ionization potential (IP), which is defined as the minimum amount of energy that has to be absorbed by an atom or molecule in its ground state to form an ion (also in its ground state) by the ejection of an electron. Often, the energy absorbed by a molecule during ionization exceeds its ionization potential and thus, ionization leaves the molecule with a large excess of internal energy to be dispersed throughout the vibrational modes of the molecule. Moreover, this dispersed vibrational energy often exceeds bond dissociation energies and hence extensive fragmentation occurs. Unimolecular fragmentation reactions can be characterized by their appearance energy, which is the minimum amount of energy needed to be transferred to the neutral precursor to lead to a specific fragmentation and therefore detection of a given product.

In the context of the apparatus used in this research three plausible ionization processes are possible: electron ionization, charge transfer ionization and Penning ionization. In electron ionization, energetic electrons interact with the molecule causing a transient electronic disturbance that may cause excitation, or if this disturbance is of energy in excess of the ionization potential of the molecule, ionization will occur by the ejection of an electron from the valence shell.

$$Ar + e^{-} \rightarrow Ar^{+\bullet} \qquad (7)$$

In charge transfer ionization a charged molecule interacts with a molecule of lesser electron affinity and subsequently pulls an electron from the neutral species thereby neutralizing itself and ionizing the other species. In this work where the precursor is diluted in excess argon, charge transfer ionization would most likely occur between argon (ionized through electron ionization as shown above) and the precursor, M as follows:

$$Ar^{+\bullet} + M \rightarrow M^{+\bullet} + Ar \qquad (8)$$

The thermodynamics of charge transfer ionization is dictated by both the ionization potential of the neutral and the electron affinity of the radical cation. The electron affinity (EA) of a radical cation is defined as the energy released when that species gains an electron. Some of this energy may be transferred as translational motion; however, most of the energy is carried away as excess internal energy by the incipient ion. The minimum amount of internal energy possessed by a molecule, M, upon charge transfer ionization, is given by:

$$E_{\text{internal}}(M^{+\bullet}) \geq EA(Ar^{+\bullet}) - IP(M) \qquad (9)$$

The ionization energy of argon is 15.8eV whereas that of a typical organic species such as an aldehyde is around 10eV. Consequently, by equation (9) this would leave the ionized species with up to 6eV of excess internal energy, or approximately 580kJ/mol. Typical C—C bond energies are well below this value, and therefore this is enough energy to cause extensive fragmentation of the

precursor molecule. An alternative to charge transfer ionization is Penning ionization (schemes (10) and (11)) where an internally excited argon atom (but not ionized) interacts with a precursor, transfers its energy and, in doing so, causes ionization of the precursor depending on the energy of the original excited state of the atom.

$$Ar + e^{-} \rightarrow Ar^{*} \qquad (10)$$

$$Ar^{*} + M \rightarrow M^{+\bullet} \qquad (11)$$

If the ionization energy of the precursor is lower than the energy of the metastable state of the excited argon atom then ionization will occur. These ionization schemes will be revisited in the next chapter in the context of previous studies performed with the EBMI apparatus.

1.4 References for Chapter 1:

[1] Jacox, M.E. *Int. J. Mass. Spectrom.* **2007**, 267, 268.

[2] Fridgen, T.D.; Parnis, J.M. *J. Phys. Chem. A.,* **1997**, 101, 5117.

[3] Parnis, J.M.; King, K.; Thompson, M.G.K. *J. of Mass. Spectrom.* **2009**, in press.

[4] Thompson, M.G.K.; Parnis, J.M. *J. Phys. Chem. A.* **2008**, 112, 12109.

[5] Szczepanski, J.; Roser, D.; Personette, W.; Eyring, M.; Pellow, R.; Vala, M. *J. Phys. Chem.*, **1992**, 96, 7876.

[6] Dunkin I.R. *Matrix Isolation Techniques: A practical approach.* Edited by Harwood L.M. and Moody C.J. Oxford University Press Inc., New York, USA, **1998**.

[7] Whittle, E.; Dows, D.A.; Pimentel, G.C. *J. Chem. Phys.*, **1954**, 22, 1943.

[8] Bondybey, V.E.; Smith, A.M.; Agreiter, J. *Chem. Rev.* **1996**, 96, 2113.

[9] Andrews L. *Chemistry and physics of matrix-isolated species.* Edited by Andrews L. and Moskovits M. Elsevier Science Publishers, New York. **1989**.

[10] Cradock, S.; Hinchcliff, A.J., *Matrix Isolation: A Technique for the Study of Reactive Inorganic Species,* 1st Ed., **1975**, Cambridge University Press, Cambridge.

[11] Ball, D.W.; Kafafi, Z.H.; Fredin, L.; Hauge, R.H.; Margrave, J.L., Eds., *A Bibliography of Matrix Isolation Spectroscopy 1954-1985*, **1988**, Rice University Press, Houston.

[12] Oshsner, D.W.; Ball, D.W.; Kafafi, Z.H., Eds. *Bibliography of Matrix Isolation Spectroscopy 1985-1997*, **1998**, National Technical Information Service, Washington.

[13] Lin, C.Y.; Krantz, A.J. *J. Chem. Soc., Chem. Commun.*, **1972**, 1316, 1111.

[14] Zhang, X.K.; Lewars, E.G.; March, R.E.; Parnis, J.M. *J. Phys. Chem.*, **1993**, 97, 4320.

[15] Fridgen, T.D. *Ph.D. Thesis*, Queen's University, Kingston, Ontario, Canada, **1999.**

[16] Silverstein, R.M.; Webster, F.X.; Kiemle, D.J. *Spectrometric Identification of Organic Compounds,* 7th Ed., Wiley, New York, **2005**.

[17] McQuarrie, D.A. *Quantum Chemistry*. University Science Books, Sausalito CA, USA, **1983**.

[18] Nakamoto, K.; *Infrared and Raman Spectra of Inorganic and Coordination Compounds, Part A, B.* 5th Ed., Wiley, New York, **1997**.

[19] Robinson, P.J.; Holbrook, K.A. *Unimolecular Reactions*, Wiley-Interscience, New York, **1972**.

[20] Gross, J. *Mass Spectrometry, a textbook.* Springer, New York, **2004**.

Chapter 2

Literature Review

2.0 Background of the EBMIS apparatus

The initial methods for generating molecular fragments and novel species to be studied using matrix isolation included reactive atomic sources, photolysis lamps, lasers, and radiolysis.[1] Relatively low energy electrons had been used heavily in gas-phase mass spectrometric studies, but such electron ionization methods were not initially applied to matrix isolation work.

The possible benefits of an electron bombardment matrix isolation technique were first partially realized through the early work of Milligan and Jacox[2] and Breeze *et al.*[3] The negative ion NO_2^- was generated through the electron bombardment of NO_2:Ar mixtures and was subsequently characterized using infrared spectroscopy.[2] In the latter study the ions $Ni(CO)_3^-$, $Cr(CO)_5^-$ and $Fe(CO)_4^-$ were isolated in inert gas matrices through the electron bombardment of their neutral precursors.[3] The generation of positive ions was accomplished through the work of Knight and co-workers in 1983.[4] In this work a new experimental method was presented utilizing electron bombardment for the generation and trapping of cation and neutral radicals in neon matrices at 4 K for electron spin resonance (ESR) studies.[4] The electron bombardment technique was noted for its efficiency and flexibility over other methods, such as photoionization, as the electron flux and energy could easily be varied over a

wide range.[4] Thus, using that technique, ESR spectra of $^{13}CO^+$, H_2O^+, and N_2^+ were obtained.[5] Among these early studies coupling electron bombardment and matrix isolation for the production and spectroscopic characterization of novel species was research performed by Suzer and Andrews.[6,7] Using a thermionic tungsten filament low energy electrons (30-200eV) were produced that continuously bombarded water-argon mixtures during condensation onto the deposition window. This resulted in the production and subsequent IR characterization, for the first time, of the OH^- ion as well as OH radicals, both of which were confirmed via appropriate isotopic substitution experiments.[6] Subsequent to that paper, was a similar study where NH_3/Ar mixtures were electron bombarded which produced matrix isolated NH_2^- and NH_2 as confirmed by IR spectroscopy.[7]

A modification by Szczepanski *et al*.[8] of the EBMIS apparatus performed in the experiments described above ensured that the ionization of the gaseous mixtures was occurring in the gas-phase, prior to condensation onto the deposition window, by directing the electron beam to an anode adjacent to the growing matrix. In this way the electron beam intersected the gas mixture just in front of the matrix deposition window, prior to the event of condensation. The apparatus used in this work is based on this original design and therefore it is worth taking a more detailed review of the early work to originate from that apparatus, in which many important facets of the EBMIS apparatus were first explored. Using that apparatus, studies concerning the generation and characterization of relatively large molecular ions that do not undergo extensive

decomposition were undertaken. In particular, mixtures of carbon tetrachloride, argon, and naphthalene were electron bombarded which produced fragments associated with carbon tetrachloride (CCl_3•Cl, $CCl_3^{+\bullet}$, CCl_3, and Cl^-), as well as the naphthalene radical cation ($N^{+\bullet}$). The characterization of the naphthalene radical cation was important as its spectrum correlated to modes from unidentified infrared emission features observed in interstellar space. The addition of carbon tetrachloride (CCl_4) was used as an ionization enhancer and as a matrix charge stabilizer. It was thought that ionization of naphthalene (N) occurred via either charge transfer ionization with $CCl_3^{+\bullet}$ or through Penning ionization with argon (as argon was the most abundant gas) since the energy of the excited metastable state of argon is higher than the ionization potential of naphthalene.

$$CCl_3^{+\bullet} + N \rightarrow CCl_3 + N^{+\bullet} \qquad (12)$$

$$Ar + e^- \rightarrow Ar^* + e^- \qquad (13)$$

$$Ar^* + N \rightarrow N^{+\bullet} + Ar \qquad (14)$$

Furthermore, the addition of CCl_4 was imperative as it resulted in the formation of Cl^- counterions. Electron impact of argon atoms produces low energy electrons which can be captured by the neutral Cl atoms (due to its large electron affinity) formed from fragmentation of CCl_4 to produce Cl anions. These anions balance the excess charge created by the naphthalene radical cations. In order to successfully produce and characterize ions, corresponding counterions must also be present to balance the charge. Szczepanski *et al.*[8] point out that the potential

1 cm in front of the matrix window containing only positive ions and the rare gas is approximately one megavolt. Such an enormous potential is unfeasible and therefore charged species require the formation of counterions. In the earlier studies, where anions were produced, the counterion was the proton-bound argon dimer, Ar_2H^+.

2.1 Background of the EBMIS work in the Parnis Lab

As mentioned above the EBMIS apparatus in the Parnis lab originated from the design by Szczepanski *et al.*[8] and has been in operation for over 10 years. The understanding of the apparatus has evolved over those years as continued research revealed further aspects that were previously not considered. It is thus pertinent to review the chemistry that has stemmed from the apparatus used in this work so as to describe the knowledge that has been continually developed over the years and which has subsequently guided this current research.

2.1.1 Ionization mechanism of electron bombardment of dilute precursor:Ar mixtures

As first discussed in chapter 1 there are three ionization mechanisms that could account for the ionization of the precursor in the gas-phase: (1) direct electron ionization (2) charge-transfer ionization with the inert host gas and (3) Penning ionization with the inert host gas. There have been several excellent studies from the Parnis lab that have explored the issue of which mechanism the precursor is being ionized under. The results from three separate studies by

Fridgen and Parnis[9], Fridgen *et al.*[10], and Thompson and Parnis[11] all independently confirm that ionization of the precursor is occurring via a charge-transfer process.

Among the early EBMIS studies in the Parnis Lab was a study of the gas-phase ion chemistry of oxalyl chloride ($C_2Cl_2O_2$) by Fridgen and Parnis.[9] Electron bombardment of mixtures of oxalyl chloride (OxCl) in either argon or krypton produced a variety of decomposition products that were successfully trapped and characterized upon condensation into the matrix. The products Cl_2CO, $ClCO^{\bullet}$, CO, and CCl were all successfully characterized using IR spectroscopy. The radical, $ClCO^{\bullet}$ (16), was thought to form as a secondary product from further fragmentation of the initially formed $Cl_2CO^{+\bullet}$ (15) ion.

$$OxCl^{+\bullet *} \rightarrow CO + Cl_2CO^{+\bullet *} \quad (15)$$

$$Cl_2CO^{+\bullet *} \rightarrow Cl^{\bullet} + ClCO^{+} \quad (16)$$

Sometimes primary fragmentation products are formed with enough excess energy that they can then undergo further decomposition chemistry. In this case secondary product formation was suspected as when samples were spiked with nitrogen it was found that increasing the amount of nitrogen decreased the formation of $ClCO^{\bullet}$ and instead greater amounts of the initial product Cl_2CO were observed. Nitrogen was thought to have acted as an energy sink where the excess energy of the primary product, $Cl_2CO^{+\bullet}$, was sufficiently quenched by the triple bond of the inert nitrogen gas thereby preventing further secondary fragmentation from occurring. From the work of Szczepanski *et al.*[8] it

was believed that the ionization of the precursor was most likely due to Penning ionization with the argon host gas; however, Fridgen and Parnis[9] initiated the hypothesis that, based on the product distribution of oxalyl chloride, ionization of the precursor was actually occurring via charge transfer with the host gas. The thermodynamics of Penning ionization with argon could not explain the products that were observed in the resulting spectra. The excited metastable states of argon are 11.5, 11.6, 11.7, and 11.8 eV above the ground state.[12] Additionally, any higher energy states are known to rapidly relax radiatively to these lower energy states and therefore would not be able to contribute to Penning ionization.[12] These energies are below the threshold for the observed C—C cleavage of oxalyl chloride (resulting in the Cl_2CO and $ClCO^{\bullet}$ products) and therefore the appearance of these products could not be understood under a Penning ionization scheme.[9] In contrast, the ionization energy of argon is 15.8 eV[13] and therefore charge transfer ionization would leave the incipient ion with a greater amount of internal energy which exceeds the necessary energy to cause C—C cleavage. The absence of the product ethylenedione (OCCO) was also explained by attributing ionization to a charge transfer process, as its appearance energy from ionized oxalyl chloride is 15.7 ± 0.1 eV[14], which is just below the ionization potential of argon. Consequently, there would be insufficient energy to promote this decomposition pathway to a significant extent, which explains its absence from the product spectra. Penning ionization could also explain this experimental finding however. Although not entirely conclusive, the results of

Fridgen and Parnis[9] provided strong evidence that ionization of the precursor was occurring from charge transfer ionization with the host gas.

A later EBMIS study concerning the fragmentation and isomerization products of dihalomethanes further added to the growing body of evidence in support of the charge transfer mechanism of precursor ionization. When CH_2Cl_2/Ar mixtures were subjected to electron bombardment followed by matrix isolation a variety of decomposition products were observed which included: $CCl_2^{+\bullet}$, $ClHCl^-$, $CHCl_2^\bullet$, $CHCl_2^+$, $CCl^\bullet$, $HCCl^{+\bullet}$, and HCCl. In addition to the many fragmentation products, the isomer, isodichloromethane (CH_2Cl-Cl) was also observed. The study by Fridgen *et al.* highlights the utility of the EBMIS apparatus as both products that were expected from previous mass spectrometric studies (such as $CCl_2^{+\bullet}$ and $CHCl_2^+$) as well as neutral species whose presence was previously only inferred, were both directly characterized using infrared spectroscopy. Similar to the earlier work with oxalyl chloride, the ionization mechanism was investigated through comparing the product distribution of EBMI experiments performed on mixtures of CH_2Cl_2 in argon, krypton or xenon respectively. In this case CH_2Cl_2 was a particularly useful molecule to examine as its ionization energy and the appearance energies of subsequent decomposition pathways appeared throughout the energy range accessible through the use of argon, krypton and xenon. The ionization potential of dichloromethane is 11.3eV which lies between the first excitation energies of neutral argon (11.6 and 11.7eV) and those of neutral krypton (10.6 and 9.9eV). The first two excited metastable states of xenon lie even lower in energy at 9.5

and 8.3eV respectively. Thus, if ionization were occurring in the EBMIS system as a result of Penning ionization only collisions with argon would result in the ionization of the precursor, dichloromethane. Subsequently, only experiments where argon was the host gas would produce observable ion fragmentation chemistry. However, it was observed that similar chemistry occurs regardless of the choice of host gas. Mixtures of CH_2Cl_2/Ar, CH_2Cl_2/Kr, and CH_2Cl_2/Xe all produced ion decomposition fragments upon electron bombardment. This indicated that ionization was occurring in all cases and therefore must have been occurring via charge transfer as the ionization potential of argon, krypton and xenon (15.8, 14.0 and 12.1eV)[13] all lay above the 11.3eV ionization potential of dichloromethane. Furthermore, because krypton and xenon both have lower ionization potentials compared to argon it was suggested that the range of decomposition pathways should be reduced progressively as the host gas was changed to these other inert gases. For example, the appearance energy for reaction (17) is 12.7eV.

$$CH_2Cl_2^{+\bullet} \rightarrow H_2 + CCl_2^{+\bullet} \qquad AE=12.7eV \qquad (17)$$

This appearance energy lies below the ionization potential of argon and krypton but above the ionization potential of xenon. Therefore, the $CCl_2^{+\bullet}$ product should be observed when argon or krypton matrices are used but not when xenon is chosen as the host gas. This was observed experimentally which suggests that the energetics of decomposition correlates with the charge transfer mechanism. Despite this success there were still some lingering inconsistencies such as why

the product $CCl^{\bullet}$ was observed when xenon was used when the appearance energy of this process lies above the ionization potential of xenon. To explain this Fridgen *et al.* suggested that some of the $CH_2Cl_2^{+\bullet}$ ions may have been formed through direct electron ionization with the 300eV electron beam where the $CCl^{\bullet}$ would then be expected to be formed.

The energetics of ionization was recently reinvestigated by Thompson and Parnis. Dilute mixtures of dimethyl ether (another simple organic molecule) subjected to electron bombardment followed by matrix isolation produced several decomposition products as shown below.

$$CH_3OCH_3^{+\bullet}/Ar \rightarrow CH_4 + H_2CO + HCO^{\bullet} + CO + Ar_2H^{+} \qquad (19)$$

Although evidence supporting the charge transfer mechanism was substantial at this point, it was still not clear exactly how much energy the incipient ion was receiving from the process. The maximum internal energy of an incipient ion possesses post ionization from $Ar^{+\bullet}$ is given by IP(Ar) – IP(Precursor) (see chapter 1). In that work, the maximum excess energy a newly formed dimethyl ether radical cation would posses is IP(Ar)-IP(CH_3OCH_3) which is 15.8eV-10.0eV equaling 5.0eV. Although this gives an upward boundary, some of this energy may be given off as enhanced translational energy of the argon atom, and thus the exact amount of internal energy possessed by the incipient ion was still in question. Through a comparison of the observed products of dimethyl ether within the EBMIS system to the known energetically mapped pathways from threshold photoelectron-photoion studies (TPEPICO) it was put forth that the

energy of the dimethyl ether cation is formed in the 15-15.8eV appearance energy range. A previous TPEPICO study by Butler *et al.*[15] concerning dimethyl ether reported the relative ion yields in the form of a breakdown curve over a photoionization range of 10-18eV. The yields reported for various ions at an energy range around 15eV were found to correlate well the observed products resulting from decomposition of dimethyl ether within the EBMIS system. By that argument it was believed that the dimethyl ether cation was formed in the 15-15.8eV energy range. There were, however, some ostensible inconsistencies between the results of Thompson and Parnis and the TPEPICO results of Butler et al. For example, an expected product based on the TPEPICO results is the methyl radical, $CH_3^{\bullet}$, but this was not observed. Furthermore, the unexpected product CO was observed. These products were believed to be a result of re-encounter chemistry where, as a result of the higher pressures of the EBMIS system, newly created products are capable of re-encountering each other which possibly leads to further chemistry and different products. The unexpected formation of CO was explained in this way, where a methyl radical would re-encounter HCO and through hydrogen abstraction ultimately form the products CO and CH_4 (this also explains, partially, the absence of CH_3 in the product spectrum).

Despite the overall consistency displayed between the results of the EBMIS system and other gas-phase methods such as TPEPICO, there are differences that can emerge from the altered conditions of the EBMIS system versus the traditional low pressure gas phase environment. Nevertheless, the

mechanism and energetics of charge transfer ionization within the EBMIS system used in this work is now well understood as a result of the aforementioned studies. Other work stemming from the EBMIS apparatus in the Parnis lab has focused on other areas such as isomerization chemistry and in further probing the differences between the EBMIS environment versus traditional low pressure systems. The work investigating the diverse chemistry of acetone is particularly relevant as it prompted the further investigation of the chemistry acetaldehyde which is the focus of this thesis.

2.1.2 EBMIS investigations of acetone chemistry/keto-enol tautomerization

As with the other EBMIS investigations of small organic molecules, electron bombardment of acetone/argon gas mixtures above a cryogenic matrix isolation deposition window led to the direct observation of several neutral fragmentation products which included the acetyl and methyl radicals ($CH_3CO^{\bullet}$, and $CH_3^{\bullet}$), carbon monoxide (CO), ketene (CH_2CO) and methane (CH_4).[16] Zhang *et al.*[16] also reported the formation of the enol isomer of acetone, 1-propen-2-ol, which was thereby characterized for the first time by infrared spectroscopy. This result was specifically important as keto-enol tautomerization has been the subject of much research with numerous experimental and theoretical papers exploring the thermodynamics and kinetics of such isomerization. It is therefore prudent to spend some time reviewing the general background of keto-enol tautomerization.

Neutral enol isomers are inherently difficult to characterize as, in aqueous solution, neutral enol isomers are thermodynamically less stable than their keto counterparts and consequently the equilibrium established between the two tautomers is completely dominated by the keto form. Acetone, for example, in aqueous solution, exists as an equilibrium mixture of more than 99.9% keto tautomer and less than 0.1% enol tautomer.[17] Consequently, ascertaining spectroscopic information on enol tautomers has not been straightforward to achieve. Zhang *et al.*, however, recognized that acetone was a perfect candidate to examine as it is one of the simplest members of a group of carbonyl compounds of the [CH_3COR] type (R=H, CH_3 etc…). In this group the relative thermodynamic stability of the enol to the keto tautomer of a given ion is reversed with respect to that of the corresponding neutral forms. An extensive study by Holmes and Lossing[18] compared the gas-phase heats of formation of 13 enol positive ions of aliphatic aldehydes, ketones, acids, and esters with those measured for the corresponding keto forms and in all cases found the enolic ions are much more stable thermodynamically by amounts ranging from 14 to 31 $kcalmol^{-1}$. For example, the acetone radical cation lies 14 $kcalmol^{-1}$ above its enol isomer, 1-propen-2-ol.[18] Despite this favorable thermodynamic stability of the enol tautomer, gas-phase formation of the acetone radical cation by electron ionization under typical mass spectrometric conditions is known to follow decomposition routes rather than the isomerization pathway leading to the cationic enol isomer. This is a result of the large energy barrier (37 $kcalmol^{-1}$) between the two isomers which makes tautomerization unfavorable under

traditional mass spectrometric conditions.[19] Thus, instead of undergoing isomerization, the acetone radical cation undergoes α-cleavage to form the methyl radical and the acetyl cation (see Figure 5). As a result of the large activation energy of the isomerization pathway for the process to occur it must be facilitated through a catalytic ion-molecule interaction with an appropriate base that can act as a proton shuttle. The base would abstract the proton from one available site and transfer it to the oxygen to form the enol isomer. Benzonitrile[20], methanol[21], and isobutylnitrile[22] have all been employed as base catalysts that promote proton-transfer and cause the tautomerization of the acetone radical cation to its enolic form. Furthermore, it was shown by Trikoupis *et al.* that this proton-transfer mechanism can occur through self-catalysis where a neutral acetone itself acts as the catalytic base. A more detailed description of the proton-transfer catalysis can be found later in the section reviewing the tautomerization mechanisms of the acetaldehyde radical cation.

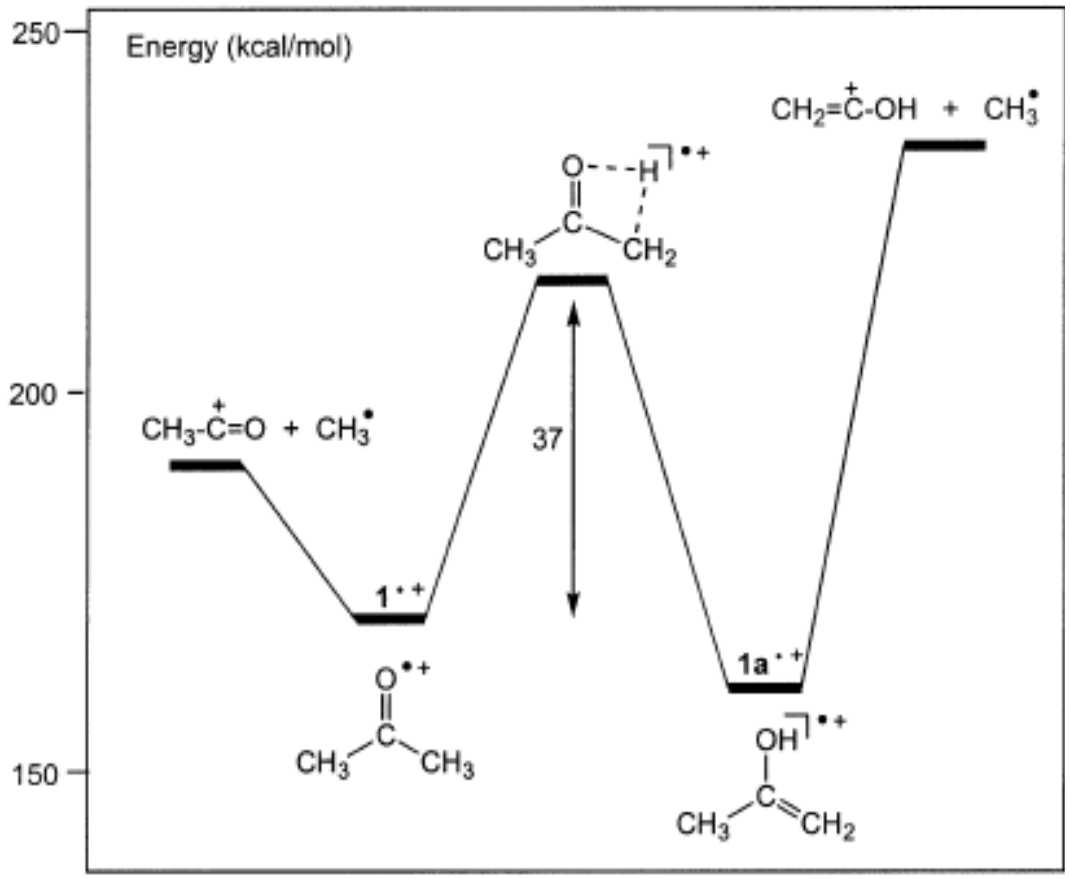

Figure 5: From Trikoupis *et al.* [23] Energy level diagram of the isomerization and decomposition pathways of the acetone and enol radical cations.

At the time when Zhang *et al.*[16] first characterized the enol isomer it was believed that the isomerization to the enol radical cation was a result of a gas-phase unimolecular ion process involving an excited electronic state of the acetone radical cation. It was known that acetone radical cations formed in their ground electronic *X* state, decompose on the picosecond timescale and therefore it would be unlikely that acetone ions in their *X* state would lead to the enol isomer. Thus, it was proposed instead, that the acetone radical cation was being formed in the excited electronic *A* state, for which lifetimes are relatively long. The formation of the neutral 1-propen-2-ol was then achieved through neutralization by secondary electrons followed by immediate stabilization by the surrounding matrix. Overall then the mechanism of enol formation was believed to follow a process involving acetone ionization, isomerization, neutralization and stabilization.

Recently the chemistry of acetone, including the mechanism of tautomerization, was revisited in hopes of better understanding the process in light of the self-catalysis studies by Trikoupis *et al.*, and in addition to the observation that there are differences in product formation in the EBMIS system versus traditional low-pressure mass spectrometric sources. It was concluded by Parnis *et al.*[24] that the isomerization of acetone, within the EBMIS system, occurs via an ion-molecule self-catalysis between ionic acetone and neutral acetone in a similar way to that originally reported by Trikoupis *et al.*[23] Beyond confirming the purported mechanism of acetone tautomerization, the work by Parnis *et al.* also helped understand how specific controllable variables of the EBMIS system can

Scheme 1: Net reaction processes showing the formation of ethane, ethene, ethyne, CCCO and CO.

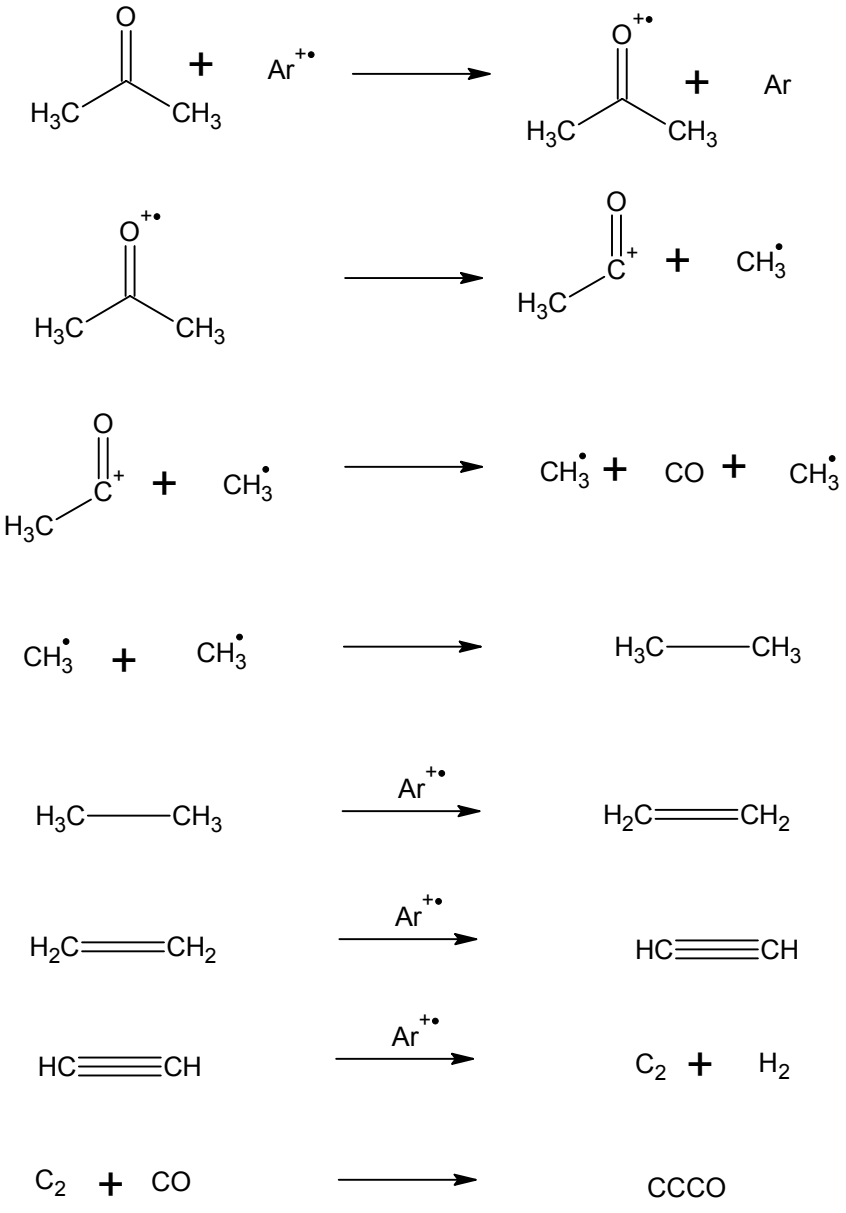

be altered to as to affect the resultant chemistry. In contrast to the earlier work by Zhang *et al.* the acetyl and methyl radicals were not observed in appreciable yields but rather the dehydrogenation products ethene, ethyne and CCCO were observed in addition to CO, methane, ketene and ethane. It was purported that the formation of the dehydrogenation products ethene, ethyne, and CCCO is due to the secondary ionization of ethane produced from methyl radical recombination (Scheme 1). This was based on the observation that increasing the measured current of the electron beam, which the gaseous mixture was subjected to, caused a dramatic increase in dehydrogenation products while concurrently producing a noticeable decrease in the ethane yield. A series of experiments were also performed where the influence of acetone partial pressure was examined. Experiments were performed where the ratio of acetone to argon was varied from 1:100 and diluted progressively to 1:10,000. It was believed that higher partial pressures of acetone promote ion-molecule chemistry and at lower partial pressures the observed chemistry transitions into more traditional unimolecular decomposition chemistry. A plot of normalized product yield versus the partial pressure of acetone found that products purported to result from bimolecular processes maximize at intermediate concentrations of acetone. Thus, products such as ketene, ethane and 1-propen-2-ol all showed similar behavior as the acetone partial pressure is varied. Overall, it was realized that variables such as electron current and the partial pressure of the precursor can cause dramatic changes in the observed chemistry, and by noticing how the

product yields are altered upon changing these variables valuable mechanistic information can be discovered.

The interesting chemistry of the studies reviewed throughout section 2.2 all show that the EBMIS apparatus provides a novel and complementary method of exploring gas-phase chemistry as opposed to methods that are more usually employed. The small organic species that were the focus of these earlier studies has prompted the investigation of the isomerization and decomposition chemistry of other simple functional groups. Thus, three small aldehyde species have been examined in this thesis: acetaldehyde, propanal, and butanal. It is thus necessary to review the current knowledge of their respective gas-phase chemistry.

2.2 Gas-phase chemistry of butanal

The 70eV electron ionization mass spectrum of butanal (C_4H_8O) shows various fragment ions stemming from simple bond cleavages such as $CH_2CH_2CHO^+$ (m/z 57), CH_2CHO^+ (m/z 43), CHO^+ (m/z 29) and CH_2CH^+ (m/z 27). A photoionization mass spectrometric study by Traeger and McAdoo[25] of a variety of $C_4H_8O^{+\bullet}$ isomers measured the appearance energies of CH_2CHO^+ along with $CH_2CH_2CHO^+$. In the case of butanal those two products correspond to decomposition products resulting from β and γ C—C bond cleavages of the parent ion. Thus, for butanal, the measured appearance energies corresponding to β and γ cleavage respectively were found to be 10.19 and 10.18eV.

$$CH_3CH_2CH_2CHO^{+\bullet} \rightarrow CH_2CHO + CH_3CH_2^{\bullet} \qquad AE=10.19eV \qquad (20)$$

$$CH_3CH_2CH_2CHO^{+\bullet} \rightarrow CH_2CH_2CHO^{+} + CH_3^{\bullet} \qquad AE=10.18eV \qquad (21)$$

As butanal is a relatively large aldehyde to work with, the energetics of the various possible decomposition routes are not as well characterized as other smaller molecules which have been favored for their simplicity. However, in addition to the products above that result from simple bond cleavages, the EI mass spectrum of butanal also shows peaks corresponding to vinyl alcohol and ethene. These products have been shown to be a result of a γ-H shift with β-cleavage—a famous reaction known as the McLafferty Rearrangement (McLR). Threshold photoionization studies by Traeger and Djordjevic[26] have found the appearance of this process to be 10.46eV.

$$CH_3CH_2CH_2CHO^{+\bullet} \rightarrow CH_2CHOH^{+\bullet} + CH_2{=}CH_2 \qquad AE=10.46 \qquad (22)$$

The McLR has become the most studied of all gas-phase rearrangements, which stems from the continuing debate over the mechanism of the reaction.[27] The McLR can, in principle, occur either as a concerted process with the γ-H-shift occurring simultaneously with the β-cleavage, or it can occur as a stepwise process with the γ-shift occurring first creating a distonic (radical and ionic character in different locations on the molecule) intermediate that then fragments through β-cleavage (Figure 6). Thus, despite the scarcity of literature concerning the energetics of simple decomposition routes, butanal has been a fundamental focus of studies investigating the McLR. The initial goal of this thesis was to ascertain spectroscopic evidence of the putative distonic intermediate and therefore confirm that the McLR occurs via stepwise process and therefore it is

important to give the background surrounding the research into the mechanism.

2.2.1 Mechanistic studies of the McLafferty Rearrangement

Since the discovery of the McLR over fifty years ago the mechanism has been probed using a variety of techniques. As early as 1974, in a review of the reaction, claims on the nature of the McLR have been made (in that review it was that the McLR is stepwise in nature).[28] A perusing of the literature shows that although many studies convincingly conclude that the McLR must occur via a stepwise route, there are also many valid studies, in contrast, that conclude that the McLR is a concerted process. This continued controversy over the mechanism has resulted in a multitude of studies concerning the McLR.

A comprehensive 1992 study by Stringer *et al.* [27] using kinetic isotope effects found the reaction to proceed as a stepwise process. In that study, ^{13}C and ^{2}H isotope effects were measured for the McLR of the known precursors 2-ethyl-1-phenylbutan-1-one, 3-ethylpentan-2-one and heptan-4-one. The various isotope effects measured were, in all cases, consistent with a stepwise mechanism with two rate-determining steps. However, an earlier study by Stone *et al.*[29] on the isotope effects on the McLR of the benzyl ethyl ether radical cation concluded that the mechanism was concerted. Another experimental study using infrared multiple photon dissociation (IRMPD) of the butyrphenone cation again supported the stepwise mechanism.[30] IRMPD uses a laser of a specific wavelength to couple to a vibrational mode(s) of the molecule and induce bond dissociation. By studying the product yield in relation to the length of the laser

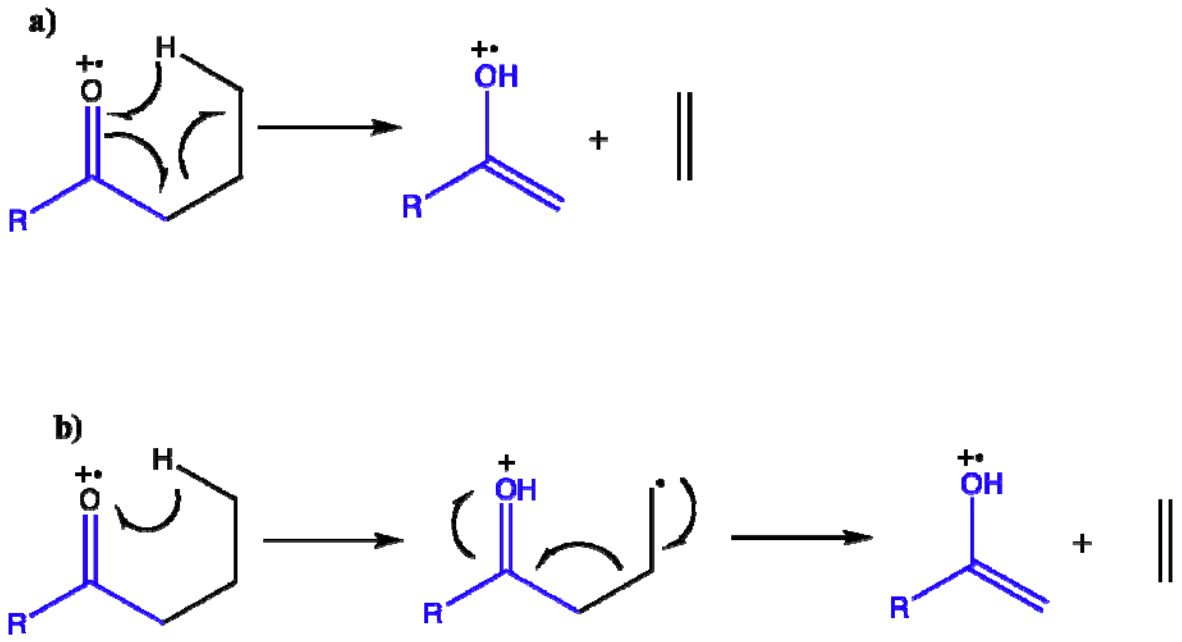

Figure 6: a) the concerted mechanism of the McLR and b) stepwise mechanism of the McLR.

pulse, it was found that the results were inconsistent with a concerted interpretation of the mechanism, but consistent with the stepwise process.

In addition to the experimental studies above, the development of the serious application of computational chemistry to chemical problems created another tool with which to probe the McLR and consequently there are many computational studies exploring the mechanism of the reaction. Conveniently, the butanal radical cation is the simplest compound for modeling the McLR and it is used almost exclusively in the computational studies.

An early study by Ha *et al.*[31] found the mechanism of the McLR to be concerted. Based on calculated reaction barriers it was found that the rate-determining step is the β-cleavage and that the transition state for that process in the concerted mechanism is lower than in the stepwise process.[31] It was therefore concluded that the McLR of the butanal radical cation should be concerted in nature. However, later Liu and Pulay[32] published results refuting the study put forth by Ha *et al.* on the basis of incorrect transition state structures in their calculations. It was found that the transition states used by Ha *et al*. were actually higher order saddle points containing two negative vibrational modes. Thus, using the appropriate transition state structures Liu and Pulay[32] completed optimizations and single-point energy calculations. Using those calculation methods a transition state structure for the concerted process could not be found (a proper transition state consisting of one negative vibrational mode) and thus it was concluded that the reaction actually occurs as a stepwise process.

Another computational study was performed on the butanal radical cation by Trigueros *et al.*[33] using the semi-empirical methods: MNDO (Modified Neglect of Differential Overlap) and AM1 (Austin-Model 1). It was found that the concerted mechanism possesses 14.9 kcalmol^{-1} lower activation energy than the stepwise mechanism. In all cases, frequency calculations were performed to ensure proper minima, as well as to ensure the appearance of one negative vibrational mode in their transition state structures.

The emergence of more powerful computers and better computational methods made an updated computational study of the McLR overdue. This occurred in 2007 by Norberg and Salhi-Benachenhou.[34] Optimization of the various minima and transition states (again using the butanal radical cation as the precursor) were performed using density functional theory (DFT) with the B3LYP and BHandHLYP functionals as well as with MP2 theory. In all cases the triple-ξ valence basis set 6-311+G(d,p) was used. Single-point energy calculations were performed on the MP2 optimized structures at higher levels including the CCSD(T) level. In these calculations it was found that the concerted γ-H-shift barrier was 37.7kcal/mol while for the stepwise pathway it was only 2.2kcal/mol. In the same paper, it also purports that the semi-empirical study by Trigueros *et al*. was flawed in that their concerted transition state structure had an incorrect structure where the O—H bond length was actually that of protonated formaldehyde and thus is not associated with the concerted McLR.

2.3 Gas-phase chemistry of propanal

The gas-phase chemistry of propanal has been investigated extensively. $C_3H_6O^{+\bullet}$ isomers are particularly suitable for study as their size is large enough that a variety of different decomposition processes are possible but small enough to ensure simplicity as well as to facilitate appropriate high-level computational calculations.[35] The electron ionization mass spectrum of propanal shows peaks associated with the molecular ions: $C_3H_5O^+$ (m/z 57), $C_2H_6^+$ (m/z 30), CHO^+ (m/z 29), $C_2H_4^+$ (m/z 28), $C_2H_3^+$ (m/z 27) and $C_2H_2^+$ (m/z 26). The energetics and mechanisms of the many decomposition routes associated with propanal have been explored both experimentally[35,36,37,38,39] and theoretically[40,41,42].

Of particular note is the threshold photoelectron-photoion coincidence (TPEPICO) study of Dannacher and Stadelmann.[35] There the calculated appearance energies for the major decomposition pathways are presented as shown below.

$CH_3CH_2CHO^{+\bullet} \rightarrow CH_3CH_2CO^+ + H^\bullet$ AE=10.31eV (23)

$CH_3CH_2CHO^{+\bullet} \rightarrow C_2H_5^+ + CO + H^\bullet$ AE=12.30eV (24)

$CH_3CH_2CHO^{+\bullet} \rightarrow C_2H_6^{+\bullet} + CO$ AE=11.40eV (25)

$CH_3CH_2CHO^{+\bullet} \rightarrow CH_2O^{+\bullet} + C_2H_4$ AE=12.18eV (26)

$CH_3CH_2CHO^{+\bullet} \rightarrow C_2H_4^{+\bullet} + CO + H_2$ AE=11.74eV (27)

$CH_3CH_2CHO^{+\bullet} \rightarrow C_2H_5^+ + HCO^\bullet$ AE=11.69eV (28)

$CH_3CH_2CHO^{+\bullet} \rightarrow C_2H_3^{+\bullet} + CO + H_2$ AE=13.56eV (29)

$CH_3CH_2CHO^{+\bullet} \rightarrow HCO^+ + C_2H_5^\bullet$ AE=11.67eV (30)

$CH_3CH_2CHO^{+\bullet} \rightarrow C_2H_4^{+\bullet} + CH_2O$ AE=11.83eV (31)

$CH_3CH_2CHO^{+\bullet} \rightarrow CO^{+\bullet} + C_2H_6$ AE=13.89eV (32)

$CH_3CH_2CHO^{+\bullet} \rightarrow C_2H_3^+ + H^\bullet + CO + H_2$ AE=14.18eV (33)

From this it is apparent that the formation of the dehydrogenated products such as $C_2H_3^+$ and $C_2H_4^{+\bullet}$ result from secondary metastable dissociation through loss of H_2 from the original products $C_2H_5^+$ and $C_2H_6^{+\bullet}$ respectively. Dehydrogenation in this manner was also proposed by Liu *et al.* based on multiphoton ionization studies of propanal.

An interesting aspect surrounding the fragmentation of propanal upon ionization surrounds the formation of $CH_3CH_3^{+\bullet}$ via the elimination of neutral CO. The fragmentation of several $C_3H_6O^{+\bullet}$ isomers to $CH_3CH_3^{+\bullet}$ represent the majority of the dissociations known to produce alkane cations in the gas-phase, as more often alkanes are eliminated as neutral radical species. This process is known to be competitive with the α-cleavage and subsequent $H^\bullet$ loss from the parent ion. The fact that $CH_3CH_3^{+\bullet}$ formation competes with the $H^\bullet$ loss from $C_3H_6O^{+\bullet}$ isomers (with the CCCO framework) has been an issue of contention as the first reaction has a substantially higher threshold energy (11.40eV versus 10.31eV, see above) and a tighter transition state.[42] The tighter transition state regarding the formation of $CH_3CH_3^{+\bullet}$ and CO stems from the implicated ion-neutral complex required for this dissociation as shown below.

$$CH_3CH_2CHO^{+\bullet} \rightarrow [CH_3CH_2....H.....CO]^{+\bullet} \rightarrow CH_3CH_3^{+\bullet} + CO \qquad (34)$$

It is been observed however, that at intermediate energies beginning at the threshold energy of 11.40eV until approximately 12.0eV, that CO elimination outcompetes $H^{\bullet}$ loss. A theoretical study by Hudson *et al.*[42] investigated the factors behind this result and it is suggested that the dependence on energy of a rate of a simple unimolecular fragmentation is usually directly related to the number of rotational degrees of freedom in the products. Because an atom does not posses rotational states there are correspondingly fewer low frequency (as rotations are low frequency motions) modes in transition states for losses of atoms versus those for losses of polyatomic fragments and thus the latter transition states are more readily obtained. Hudson *et al.*[42] suggest that this is a newly recognized factor in determining the dependence of dissociation reaction rates on internal energy. Thus, because $H^{\bullet}$ is an atom and thereby has fewer rotational degrees of freedom than a molecule, the formation of $CH_3CH_3^{+\bullet}$ is able to outcompete the other reaction at the aforementioned energies. The reason $CH_3CH_3^{+\bullet}$ formation diminishes at even higher energies (>12.0eV) is attributed to the very rapid dissociation to $CH_3CH_2^{\bullet} + CHO^{+}$ (AE=11.67eV) and/or $CH_3CH_2^{+} + CHO^{\bullet}$ (AE=11.69eV) at these high energies, thus preventing the required intermediate ion-neutral complex from existing long enough for H-transfer to occur. An extensive paper by Griffin et al.[43] investigates other examples of where alkyl loss surprisingly is able to dominate over $H^{\bullet}$ loss,

2.4 Gas-phase chemistry of acetaldehyde

Acetaldehyde (C_2H_4O) has been extensively studied and there are many studies exploring both the mechanism and energetics of the acetone isomerization and decomposition pathways upon ionization. The EI mass spectrum of acetaldehyde is dominated by four major peaks which represent the fragmentation products: CH_3CO^+ (m/z 43), CH_2CO^+ (m/z 42), HCO^+ (m/z 29) and CH_3^+ (m/z 15).

Two independent threshold photoelectron-photoion (TPEPICO) studies have been conducted measuring the appearance energies of the decomposition pathways of acetaldehyde.[44,45] The appearance energy concerning the formation of the formyl cation (HCO^+) has also been measured separately using photoionization mass spectrometry.[46] The appearance energies for all observed ions from electron impact of acetaldehyde have further been measured.[47] Below are the appearance energies for the major decomposition pathways as summarized by Głuch *et al.*

$$CH_3CHO^{+\bullet} \rightarrow CH_3CO^+ + H^\bullet \qquad AE=11.00 \pm 0.1 \qquad (35)$$

$$CH_3CHO^{+\bullet} \rightarrow CH_2CO + H_2 \qquad AE=12.70 \pm 0.1 \qquad (36)$$

$$CH_3CHO^{+\bullet} \rightarrow HCO+ + CH_3 \qquad AE=12.20 \pm 0.1 \qquad (37)$$

$$CH_3CHO^{+\bullet} \rightarrow CO+ + CH_4 \qquad AE=11.90 \pm 0.15 \qquad (38)$$

$$CH_3CHO^{+\bullet} \rightarrow CH_4^{+\bullet} + CO \qquad AE=12.80 \pm 0.1 \qquad (39)$$

$$CH_3CHO^{+\bullet} \rightarrow CH_3+ + HCO^\bullet \qquad AE=13.30 \pm 0.1 \qquad (40)$$

In addition to the extensive studies concerning the decomposition pathways of acetaldehyde, much work has also been devoted to both the energetics and mechanism of the isomerization reaction to vinyl alcohol. Vinyl alcohol was first characterized by matrix isolation work performed by Hawkins and Andrews.[48] The chemistry of tautomerization was introduced earlier when reviewing the previous work concerning acetone. Like acetone, the enol isomer (vinyl alcohol) of cationic acetaldehyde is thermodynamically more stable than the corresponding keto form. A theoretical study by Bertrand and Bouchoux[49] found that cationic vinyl alcohol is 55kJ/mol more stable than cationic acetaldehyde. Another theoretical study by Hudson and McAdoo[50] further examined the tautomerization of cationic acetaldehyde and enol isomers from the perspective of possible orbital symmetry constraints involved in the purported 1,3-H shift that occurs during tautomerization.

As previously discussed there is a substantial energetic barrier preventing direct isomerization between the two isomers and consequently the reaction must be initiated by the use of an appropriate catalyst. Two studies have explored the mechanism in which a catalyst promotes the enolization of the acetaldehyde radical cation. Using Fourier transform ion cyclyotron resonance (FTICR) experiments, van der Rest *et al.*[51] were able to show that a variety of molecules catalyze the hydrogen transfer which converts ionized acetaldehyde to its vinyl alcohol counterpart. In particular methanol was used as a catalyst in an attempt to elucidate the specific reaction pathway and determine if the reaction

occurs either by a direct 1,3-H transfer (41) or by two consecutive 1,2-H transfers (42).

$$CH_2\mathbf{H}CHO^{+\bullet} \rightarrow CH_2{=}CHO\mathbf{H}^{+\bullet} \qquad (41)$$

$$CH_3C\mathbf{H}O^{+\bullet} \rightarrow CH_2\mathbf{H}CO\mathbf{H}^{+\bullet} \rightarrow CH_2{=}C\mathbf{H}O\mathbf{H}^{+\bullet} \qquad (42)$$

As isolated ions the barrier between the two isomers is greater than 38 kcalmol^{-1}; however when solvated by the use of a methanol catalyst the barrier was found to be 12.3 kcalmol^{-1} thus demonstrating the catalytic effect.[51] It was concluded by van der Rest *et al.*[51] that although the isomerization can theoretically occur by either a 1,3-H transfer or by a double 1,2-H-transfer, when methanol is used the former mechanism is favored. A comprehensive investigation by Haranczyk *et al.*[52] investigated computationally the various possible catalysis models for enolization of the acetaldehyde radical cation. Two relevant mechanisms that were considered were: (1) Proton-transport catalysis (43) and (2) Quid pro Quo (QpQ) (44).

$$HAB^{+\bullet} + M \rightarrow AB^{\bullet} \text{ - - - } HM^{+} \rightarrow ABH^{+\bullet} + M \qquad (43)$$

$$HAB^{+\bullet} + \mathbf{H}R \rightarrow HAB\mathbf{H}^{+} \text{ - - - } R^{\bullet} \rightarrow AB\mathbf{H}^{+\bullet} + HR \qquad (44)$$

Importantly, the catalyst used must have an appropriate proton affinity as originally suggested through investigations into the catalyst induced 1,2-H shift of methanol to its distonic isomer $CH_2OH_2^{+\bullet}$ by Gauld and Radom.[53] The proton affinity (PA) of the catalyst should be greater than the PA of the original site of

abstraction, but less than the PA of the incipient radical. In terms of (43) this would mean that the following would be true:

$$PA\ (AB^{\bullet}\ \text{on A}) < PA(M) < PA\ (AB^{\bullet}\ \text{on B}) \qquad (45)$$

The necessity of having a catalyst of appropriate PA has been termed Radom's criterion. The self-catalysis of acetaldehyde was also considered at it was found that the PA of neutral acetaldehyde is in accordance with Radom's criterion.[52] It was concluded that the most facile way for the acetaldehyde ion to rearrange to its enol form from self-catalysis is via the QpQ mechanism (44). Finally, in the EBMIS apparatus of the Parnis lab, Robinson[54] serendipitously characterized vinyl alcohol while studying the reactivity of acetaldehyde with O^- upon electron bombardment of acetaldehyde/N_2O/Ar mixtures. Robinson further investigated the mechanism of isomerization through a combination of deuteration experiments and computational calculations. It was tentatively concluded the enolization was occurring through a self-catalyzed 1,3-H transfer.

2.5 References for Chapter 2

[1] Suzer, S.; Andrews, L. *J. Chem. Phys.*, **1987**, 88, 916.

[2] Milligan, D.E.; Jacox, M.E. *J. Chem. Phys.* **1970**, 52, 3864.

[3] Breeze, P.A.; Burdett, J.K.; Turner, J.J. *Inorg. Chem.* **1981**, 20, 3369.

[4] Knight, L.B.; Bostick, J.M.; Woodward, R.W.; Steadman, J. *J. Chem. Phys.*, **1983**, 78, 6415.

[5] Knight, L.B. *Acc. Chem. Res.* **1986**, 19, 313.

[6] Suzer, S.; Andrews, L. *J. Chem. Phys.*, **1988**, 88, 916.

[7] Suzer, S.; Andrews, L. *J. Chem. Phys.*, **1988**, 89, 5347.

[8] Szczepanski J.; Roser D.; Personette W.; Eyring M.; Pellow R.; Vala M. *J. Phys. Chem.* **1992**, *96*, 7876.

[9] Fridgen, T.D.; Parnis, J.M. *J. Phys. Chem. A.* **1997**, 101, 5117.

[10] Fridgen, T.D.; Zhang, X.K.; Parnis, J.M.; March, R.E., *J. Phys. Chem. A.,* **2000**, 104, 3487.

[11] Thompson, M.G.K.; Parnis, J.M. *J. Phys. Chem. A.* **2008**, 112, 12109.

[12] Jacox, M.E. *Rev. Chem. Intermed*. **1978**, 2, 1.

[13] Gross, J. *Mass Spectrometry, a textbook.* Springer, New York, **2004**.

[14] Chen, H.; Holmes, J.L. *Int. J. Mass Spectrom. Ion Processes.* **1994**, 133, 111

[15] Butler, J.; Holland, D.M.P.; Parr, A.C.; Stockbauer, R., *Int. J. Mass. Spec. Ion Phys.*, **1984**, 58, 1.

[16] Zhang, X.K.; Parnis, J.M.; Lewars, E.G.; March, R.E. *Can. J. Chem.*, **1997**, 75, 276.

[17] Bruice, P.Y. *Organic Chemistry 4th Ed.* **2004**, Pearson: New Jersey.

[18] Holmes, J.L.; Lossing, F.P. *J. Am. Chem. Soc.*, **1980**, 102, 1591.

[19] Burgers, P.C.; Holmes, J.L. *Org. Mass. Spectrom.* **1982**, 104, 2648.

[20] Trikoupis, M.A.; Burgers, P.C.; Terlouw, J.K. *J. Am. Chem. Soc.* **1998**, 120, 12131

[21] Wang, X.; Holmes, J.L. *Can. J. Chem.* **2005**, 83, 1903

[22] Mourgues, P.; Chamot-Rooke, J.; van der Rest, G.; Nedev, H.; Audier, H.E.; McMahon, T.B. *Int. J. Mass Spectrom.* **2001**, 210, 429.

[23] Trikoupis, M.A.; Burgers, P.C.; Ruttink, P.J.A.; Terlouw, J.K. *Int. J. Mass. Spectrom.* **2002**, 217, 97.

[24] Parnis, J.M.; Thompson, M.G.K.; King, K. *J. Mass. Spectrom.* **2009**, in press.

[25] Traeger, J.C.; McAdoo, D.J. *Int. J. Mass Spectrom. Ion Processes*. **1986**, 68, 35.

[26] Traeger, J.C.; Djordjevic, M. *Eur. Mass Spectrom.* **1999**, 5, 319.

[27] Stringer, M.B., Underwood, D.J., Bowie, J.H., Allision, C.E. Donchi, K.F. and Derrick, P.J. *Org. Mass Spectrom.* **1992**, 27, 270.

[28] Kingston, D.G., Bursey, J.T. and Bursey, M.M. *Chemical Reviews,* **1974**, 74, 215.

[29] Stone, D.J.M., Bowie, J.H. and Underwood, D.J. *J. Am. Chem. Soc.* **1983**, 105, 1688.

[30] Osterheld, T.H. and Braumann, J.I. *J. Am. Chem. Soc.* **1990**, 112, 2014.

[31] Ha, T.K., Radloff, C. and Nguyen, M.T. *J. Phys. Chem.* **1986**, 90, 2991.

[32] Liu, R. and Pulay, P. *J. Comput. Chem.* **1992**, 13, 183.

[33] Trigueros, P.P., Casanovas, J., Aleman, C. and Vega, M.C. *J. Molec. Struct. (Theochem)*. **1992**, 277, 117.

[34] Norberg, D. and Salhi-Benachenhou, N. *J. Comput. Chem.* **2007**, 29, 392.

[35] Dannacher, J.; Stadelmann, J.P. *Int. J. Mass Spectrom.* **2001**, 208, 147.

[36] Harvey, Z.A.; Traeger, J.C. *J. Mass Spectrom.* **2004**, 39, 802.

[37] Polce, M.J.; Wesdemiotis, C. *J. Am. Soc. Mass Spectrom.* **1996**, 7, 573.

[38] Liu, H.X.; Li, Z.L; Qian, Y.L.; Wang, Y.; Wu, C.K. *Chemical Physics*. **1989**, 129, 495.

[39] Traeger, J.C. *Org. Mass Spectrom.* **1985**, 20, 223

[40] Bouchoux, G.; Luna, A.; Tortajada, J. *Int. J. Mass Spectrom. Ion Processes.* **1997**, 167, 353.

[41] Hudson, C.E.; McAdoo, D.J.; Traeger, J.C. *J. Am. Soc. Mass Spectrom.* **2002**, 13, 1235.

[42] Hudson, C.E.; McAdoo, D.J.; Griffin, L.L.; Traeger, J.C. *J. Am. Soc. Mass Spectrom.* **2003**, 14, 136.

[43] Griffin, L.L.; Traeger, J.C.; Hudson, C.E.; McAdoo, D.J. *Int. J. Mass Spectrom.* **2002**, 217, 23.

[44] Bombach, R.; Stadelmann, J.P.; Vogt, J. *Chemical Physics*. **1981**, 60, 293.

[45] Johnson, K.; Powis, I.; Danby, C.J. *Chemical Physics*. **1982**, 70, 329.

[46] Traeger, J.C. *Int. J. Mass Spectrom. Ion Processes*. **1985**, 66, 271.

[47] Gluch, K.; Cytawa, J.; Michalak, L. *Int. J. Mass Spectrom.* **2008**, 273, 20.

[48] Hawkins, M.; Andrews, L. *J. Am. Chem. Soc.* **1983**, 106, 2523.

[49] Bertrand, W.; Bouchoux, G. *Rapid Commun. Mass Spectrom.* **1998**, 12, 1697.

[50] Hudson, C.E.; McAdoo, D.J. *Int. J. Mass Spectrom.* **2002**, 219, 295.

[51] van der Rest, G.; Nedev, H.; Chamot-Rooke, J.; Mourgues, P.; McMahon, T.B.; Audier, H.E. *Int. J. Mass Spectrom.* **2000**, 202, 161.

[52] Haranczyk, M.; Burgers, P.C.; Ruttink, P.J.A. *Int. J. Mass Spectrom.* **2002**, 220, 53.

[53] Gauld, J.; Radom, L. *J. Am. Chem Soc.* **1997**, 119, 9831.

[54] Robinson, Mark. MSc. Thesis, Queen's University, Kingston, Ontario, Canada, **2005**.

Chapter 3
Experimental methods

3.0 Overview

The equipment used in order to perform typical experiments in this research includes a specially constructed gas-handling line in which samples were prepared and the electron bombardment matrix isolation infrared spectroscopy (EBMIS) apparatus itself. This section describes the technical details of such equipment, as well as the general experimental protocols employed for this work. Additionally, the details and theory concerning the theoretical methods used in this work are discussed.

3.1 Pumping systems

In both the gas-handling line and the EBMIS apparatus the maintenance of high vacuum conditions is imperative to ensure the purity of the sample prepared and subsequently to limit the contamination from atmospheric gas while performing the EBMIS experiment. High-vacuum conditions are also necessary in the EBMIS apparatus in order to facilitate the attainment of the cryogenic temperatures required for matrix isolation. In order to obtain high vacuum conditions a two-stage pumping system is employed. This pumping system is equivalent for both the gas-handling line, and the EBMIS apparatus. The first stage uses a mechanical rotary pump (model Edwards E2M2) to evacuate the system to a pressure on the order of 10^{-2} or 10^{-3} Torr. These pressures are measured using a Pirani gauge, the location of which can be seen by examining

Figure 7 for the gas-handling line and Figure 8 for the EBMIS apparatus. Although pressures around 10^{-3} Torr are low enough to provide an effective vacuum, contamination from ambient gas is still significant and thus attaining lower pressures is still necessary.[1] A second pumping system is activated to bring the system down to high vacuum pressures around 10^{-7}-10^{-8} Torr. These lower pressures are monitored using a cold cathode ion gauge (Figure 7 and Figure 8) which is activated only after the system has been partially evacuated through first using the rotary pump. The lower pressures can then be obtained using a silicon-based oil diffusion pump (model Edwards 63). A gate valve connecting the main mechanical pump and the diffusion pump can be used to isolate the diffusion pump when initially evacuating from high pressures. In a diffusion pump, oil is boiled under reduced pressure, and the resulting vapor passes at high velocity through one or more downward-pointing jets where the rapidly moving oil molecules collide with gas molecules and sweep them downwards where they are removed from the diffusion pump by the previously described rotary pump.

Through the use of two-stage pumping system just described pressures around 10^{-7} Torr can be reached in a matter of minutes. An alternative to the use of a diffusion pump is the use of a turbo pump; however, although turbo pumps are very effective they are both more expensive and require more maintenance. Diffusion pumps are reasonably cheap and they possess no moving parts and therefore require little maintenance. Whole pumping systems, comprising of a diffusion pump, mechanical pump, as well as corresponding connectors and

gauges can be bought as a single unit from several manufacturers. One problem with diffusion pumps is that the silicon oil is reactive with typical atmosphere gases. When the oil is significantly exposed to oxygen it is quickly oxidized to silicon dioxide based products (sand) thus rendering the pump defective. This is another reason why the diffusion pump is only activated, through opening the gate valve, once a pressure of $< 5 \times 10^{-2}$ Torr has been reached through the use of mechanical pump.

3.2 Preparative gas-handling line

All of the gas-mixture samples were prepared using a standard, stainless steel, high vacuum line (Figure 7), which was constructed within a fume hood and is separate from the EBMIS apparatus. The pressure of this line was kept under high-vacuum via the pumping system described above. At every connection within the line control valves are placed which allows for the manipulation of gas flow. A digital MKS Baratron pressure sensor was used to measure the pressures of the various reagents to an accuracy of 10^{-1} Torr. The argon gas cylinder as well as other replaceable gas and liquid reagents were fixed to the gas-handling line using airtight compression fittings. Liquid reagents, in which their vapor pressure must have exceeded 20 Torr, were contained in small long-necked glass flasks. All of the samples were prepared in 1-2 liter glass bulbs.

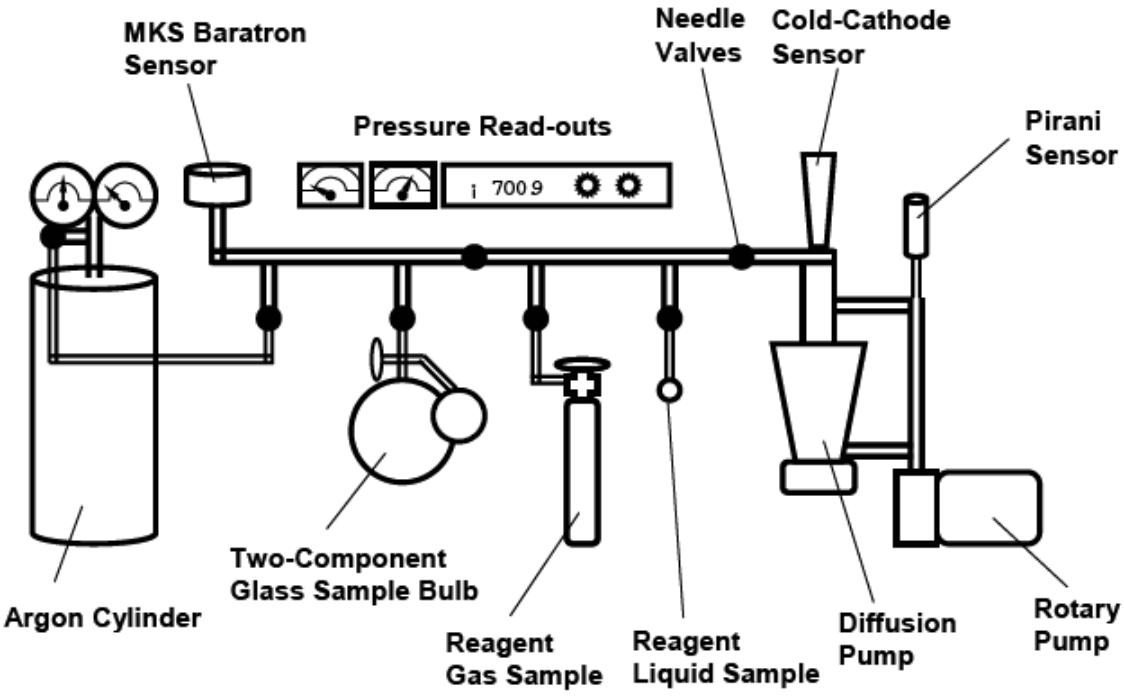

Figure 7: Schematic diagram of the gas-handling line used in sample preparation.

3.3 Experimental protocols for sample preparation

Prior to preparing a sample, a 1-2L glass bulb was first cleaned by placing it on the gas-handling line in order to be fully evacuated to high vacuum through the use of the pumping system. Typically, a bulb was placed on the line to be evacuated overnight.

In this research the liquids acetaldehyde (as well as its isotopomers), propanal, and butanal were used along with the inert rare host gas (typically argon) (Table 1). As a consequence of those reagents being in the liquid phase under ambient conditions, a specialized procedure was used in order to purify them to suitable levels to be used in matrix isolation experiments. To a given flask, 2-3mL of the species was added, and this flask was then connected to the line using the aforementioned compression fittings. The liquid reagent was then subjected to series of freeze-pump-thaw cycles in order to purify the liquid sample by removing dissolved atmospheric impurities. The liquid was first exposed to liquid nitrogen which freezes the liquid along with the dissolved impurities; however, the vapor gas occupying the head space of the flask remains unfrozen. Opening the frozen system to the vacuum line evacuates this vapor gas along with any impurities it contains. Once this initial pumping has occurred the flask was sealed off from the line and allowed to thaw thus completing the initial cycle. As thawing occurs dissolved impurities become vaporized so as to restore equilibrium between the liquid and vapor phases, and thus further impurities occupy the headspace of the flask which can again be

evacuated after freezing the liquid with liquid nitrogen. The freeze-pump-thaw cycle was performed three times to ensure the reagent was of sufficient purity.

Once a glass bulb had been evacuated, and the given liquid reagent had been purified, everything was then ready such that the gaseous sample could be prepared. Samples of specific reagent to rare-gas ratios were prepared by treating the reagents as ideal substances and introducing reagents on the basis of their pressures according to Dalton's law of partial pressures. For example, to prepare a sample in which the ratio of acetaldehyde to rare-gas was 1:400 required the introduction of 2.0 Torr of acetaldehyde, and 800.0 Torr of argon such that the total pressure inside the bulb would equal 802.0 Torr. Because the volume (V) and temperature (T) of the system is the same for each gas the relative mole ratio ($n_{CH_3CHO} \big/ n_{Ar}$) of each species can be given by the ideal gas law:

$$\frac{n_{CH_3CHO}}{n_{Ar}} = \frac{P_{CH_3CHO}V \big/ T}{P_{Ar}V \big/ T} = \frac{P_{CH_3CHO}}{P_{Ar}} = \frac{2.0Torr}{800.0Torr} = \frac{1}{400} \qquad (46)$$

In order to prepare such a sample, the gas-handling line was first isolated from the pumping system. The control valve connecting the port at which the flask containing the liquid was then slowly opened so as to draw off the desired vapor pressure into the system. The value of the pressure was measured using a digital MKS Baratron pressure gauge which had been zeroed. Once the desired amount of gas had been added to the system, the valve connecting the

flask to the line was sealed as well as the valve connecting the glass bulb to the line. The system was then evacuated until high vacuum conditions were re-achieved. At this point the line was again isolated from the pumping system, and argon gas was allowed to flow into the system by opening the valve connecting the line to an argon cylinder. Argon was flowed into the system until a pressure of approximately 200 Torr was reached, at which point the valve connecting to the glass bulb was opened whereby argon was further introduced into the system until the final desired pressure was achieved. This was done to ensure a pressure gradient was first established such that the initially introduced reagent would not escape from the bulb. Once the argon had been added the glass vessel was then sealed from the line, removed from the gas-handling line and was allowed to equilibrate overnight in order to achieve a homogeneous gas sample. The following table provides information on all of the reagents used in this research.

Table 1: Table of reagents used in this work, including purity and supplier information.

Reagents	Formula $_{(phase)}$	Purity	Supplier
Argon	$Ar_{(g)}$	99.995%	Matheson
Krypton	$Kr_{(g)}$	99.995%	Matheson
Acetaldehyde	$CH_3CHO_{(l)}$	99.5+%	Sigma-Aldrich
2,2,2-d_3-acetaldehyde	$CD_3CHO_{(l)}$	98 atom % D	Sigma-Aldrich
d_4-acetaldehyde	$CD_3CDO_{(l)}$	98 atom % D	Sigma-Aldrich
Propionaldehyde	$CH_3CH_2CHO_{(l)}$	99.7%	Sigma-Aldrich
Butanal	$CH_3CH_2CH_2CHO_{(l)}$	99%	Sigma-Aldrich
Deuterated water	$D_2O_{(l)}$	99% atom D	Sigma-Aldrich

3.4 EBMIS Apparatus

A schematic of the EBMI apparatus is shown in Figure 9 and is based on the original design of Szczepanski *et al*.[2] The apparatus consists of three important aspects: (1) gas sample flow into the reaction zone, (2) the cooling of the cold deposition window and (3) the electron source.

The glass bulb in which the sample was held was connected to the apparatus using an air tight compression fitting. The system was kept at high vacuum using the pumping system described above. The pressure of the system was monitored using both a Pirani gauge and a cold-cathode sensor (Figure 8). Control valves placed throughout the all-metal line were used to control gas flow. Once the valve sealing the glass bulb from the system was opened, the amount of sample gas could be measured using a reverse helicoid pressure gauge located immediately above where the bulb was fitted to the apparatus. The flow of matrix gas-sample into the reaction zone, towards the cold matrix window, was controlled using a MKS 1100 series mass-flow controller. This electronic valve can be set to a desire flow-rate and will flow gas at this fixed rate when activated. The pressure in the gas-sample bulb must be above 200 Torr in order for the mass-flow controller to function properly. Flow rates could be adjusted from 0.1cm^3/min to 5.0cm^3/min. A Teflon spout in the reaction chamber directs the gas towards the cold deposition window (Figure 9).

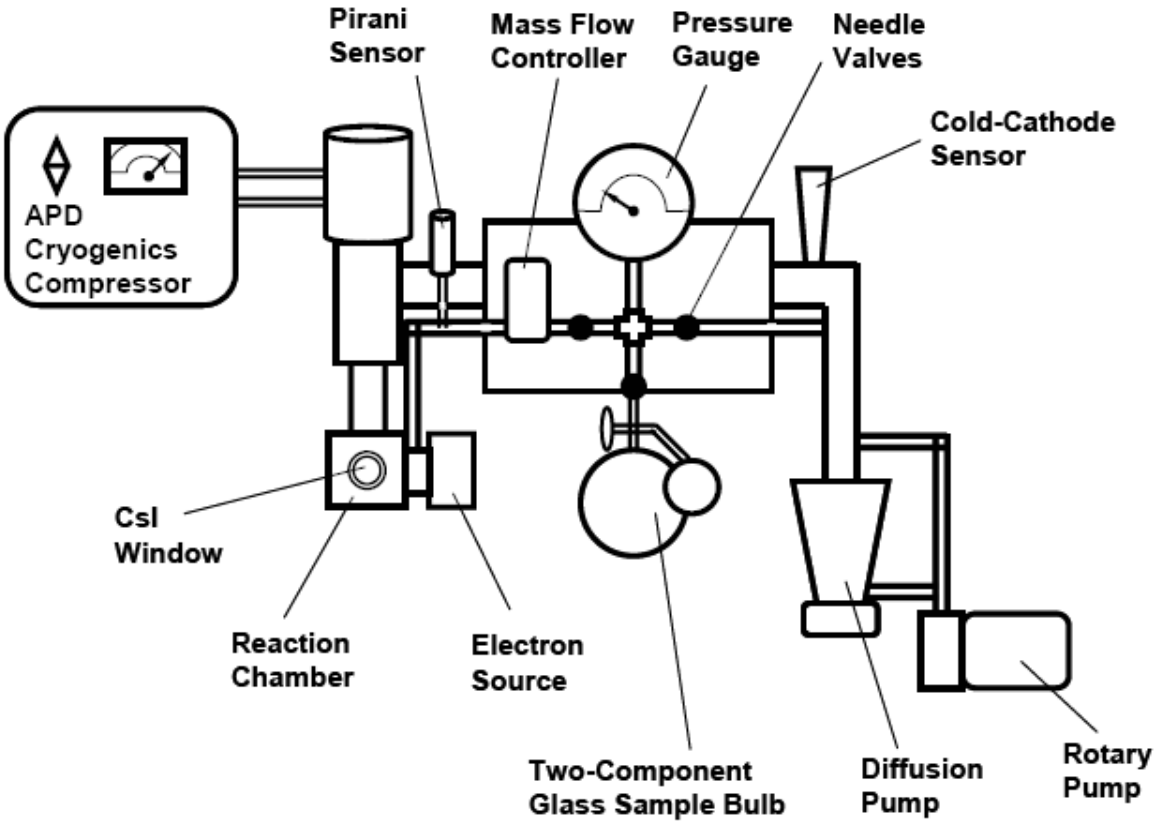

Figure 8: Schematic of the electron-bombardment matrix isolation (EBMI) apparatus.

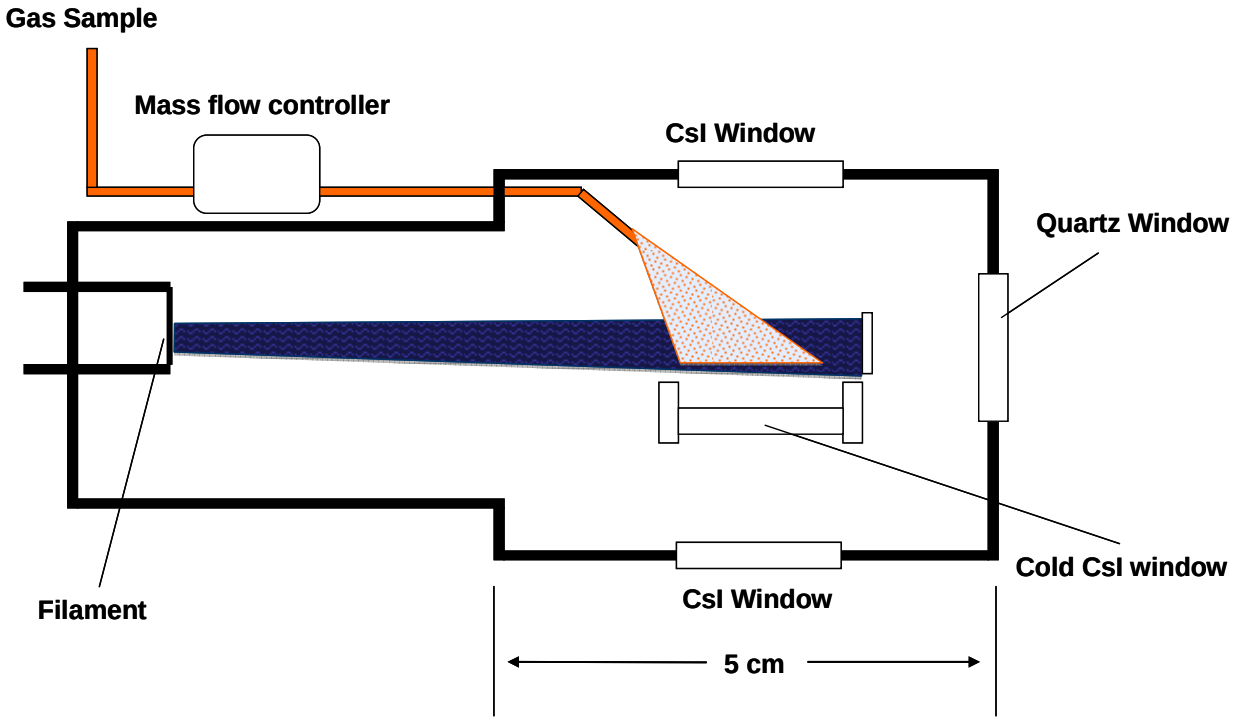

Figure 9: Top-view of the matrix isolation reaction chamber illustrating the thermionically generated electron beam as well as the flow of the gaseous mixture.

The deposition surface consisted of a CsI window held in a copper frame at the tip of an APD Cyrogenetics Displex closed-cycle helium refrigeration system which was comprised of a compact expander head connected to a helium compressor unit through a high pressure feed cable and low pressure return cable. Operating the helium compressor forces high pressure helium into the expander head system through the feed line. Once the helium reaches the expander head, it is allowed to expand through two stages controlled by a rotating valve. This is described in detail in the monograph by Dunkin.[1] The continuous cycle of helium gas from the compressor unit through to its expansion in the expander head causes the rapid cooling of the matrix tip, as a result of the Joule-Thompson effect. From the point the compressor unit is initially engaged it usually takes approximately one hour for the system to cool completely so as to attain a temperature of about 15K. This temperature can then be maintained for as long as the unit is turned on.

Finally, the electron beam is generated through the application of current to a thorium-coated tungsten filament, which simultaneously acts as the cathode. The anode (Faraday plate) and cathode were biased to ~-220V and +80V respectively which created a large potential difference of 300V. This large potential difference was necessary to create a large enough potential so as to drive the electrons over the relatively large distance separating the filament from the anode. A current of approximately 5.0 A was applied to the filament in order to cause the rapid ejection of electrons from the filament. The kinetic energy of the electrons can be described by:

$$E_k = qV \qquad (47)$$

Where, E is the kinetic energy, q is the charge, and V is the potential difference.

If the charge is the charge of an electron, e (1.6021 x 10^{-19} Coulombs), the potential difference is in volts, the energy is described in units of electron volts (eV) which is defined as the kinetic energy given to an electron when it is accelerates through a potential difference of 1V. Given that the potential difference is 300V (as explained above) the kinetic energy of the impinging electrons would be 300eV as shown below:

$$E_k = eV = e \bullet 300V = 300eV \qquad (48)$$

The electron current reaching the anode was measured using a picoampmeter capable of reading 10^{-1}nA to 2mA. The electron current could be controlled by altering the current applied to the filament. In this research the current was varied from 10microamps in some experiments to as high as 200microamp in others.

3.5 Experimental protocol for the EBMIS apparatus

The glass bulb was connected to the apparatus and the entire system was pumped to high vacuum overnight. The CsI deposition window was first cooled to approximately 15K using the compressor unit. At this point a reference deposit was first performed in which the gas was flowed towards the cold window without electron bombardment for a desired amount of time. Unless otherwise

indicated the flow rates were held at 1.0 cm^3/min and the total flow time was kept at 2 hrs. At the end of deposition a spectrum of the matrix was taken using a Bomem Michelson** 100 Fourier Transform Infrared Spectrometer. Spectra were collected for 100 scans at a resolution of 1cm^{-1}. Prior to deposition a background spectrum was taken as well. The reference spectrum was obtained in order to serve as a comparison to the eventual spectrum collected after electron bombardment. Subsequent to the recording the spectrum of the reference deposit, the compressor unit was shut off and the system warmed to over 200 K at which point the system was evacuated again to high vacuum conditions. Upon attaining vacuum conditions the system was re-cooled to approximately 15 K. The anode and cathode were then biased to create a potential difference of 300V and a current of 5.0A was applied to the filament. The sample was then deposited at the same rate for the same time as earlier except this time it was subjected to electron bombardment from the electrons ejected from the filament. In most experiments the current was kept at about 40microamps. Once the deposit time had elapsed the flow was ceased and a new spectrum was recorded.

3.6 Special procedure for deuterium labeled experiments

Deuterated acetaldehyde contains an acidic deuterium atom on the α-carbon which can easily undergo exchange with hydrogen atoms that coat the inside surfaces of both the gas-handling line and the EBMIS apparatus.

Consequently, special procedures were used to minimize the extent of this exchange.

When preparing a deuterated sample on the gas-handling line, the system was first exposed to deuterium oxide (D_2O) vapor. A small flask containing D_2O was connected to the gas-handling line and the vapor from the flask was used to expose the system to D_2O. After approximately 10 minutes of exposure the flask was sealed and the system was evacuated. This was repeated three times in order to ensure that the system was now replete with deuterium atoms, instead of hydrogen atoms.

For the EBMIS apparatus a glass bulb containing D_2O was connected to the apparatus, and the same procedure as described above was performed in which the system was repeatedly exposed to D_2O. With these extra steps performed the systems were now primed to be used with deuterated samples.

3.7 Theoretical Methods

In general computational chemistry has become a major tool to investigate a variety of chemical problems such as molecular geometry, reactivity, infrared spectra, and the physical properties of molecules.[3] In this work the use of computational chemistry was relegated to cases where previously uncharacterized molecules were among the predicted products where the vibrational modes of those molecules could be calculated and used as a guide in the analysis of the spectra. In this work Gaussian 03[4] was used for all calculations. Additionally GaussView[5] was used both to create input structures

and to visualize the optimized structures and their various vibrational modes. In all cases density functional theory was used with the restricted B3LYP functional and a 6-311G(d,p) basis set.

The B3LYP functional is based on the exchange-energy functional developed by Axel Becke in 1993, which was then modified by the introduction of the Lee, Yang, Parr (LYP) 1988 correlation-energy functional.[3] The B3LYP functional falls into the category of hybrid exchange-correlation functionals. These functionals use the exchange energy given by Hartree-Fock theory to substitute into the exchange-correlation functional developed by LYP, which is empirical in basis. The functional is shown below.

$$E_{xc}^{B3LYP} = (1-a_0-a_x)E_x^{LSDA} + a_0E_x^{HF} + a_xE_x^{B85} + (1-a_c)E_c^{VWN} + a_cE_c^{LYP} \qquad (49)$$

The E_x^{LSDA} term is the simplest exchange-correlation functional based on the local spin density approximation. The E_x^{HF} term is the Hartree-Fock exchange energy functional alluded to above, however it is still based on the Kohn-Sham orbitals of DFT. The E_x^{B85} term is the exchange functional developed by Becke. The E_c^{VWN} term is the Vosko, Wilk, Nusair function (VWN) and finally the E_c^{LYP} term is the LYP correlation functional. The parameters (a_0, a_x, a_c) were chosen based on how good the calculated values were using the functional, and in is way the functional is not as rigorous (from first principles) as other methods. Although, strictly not as rigorous as some other methods, as a result of the use of empirical parameters, the B3LYP is the best of the current functionals available and is widely used for both optimization and frequency calculations.

The 6-311G(d,p) basis set is a split valence set method. The core electrons are represented by a single contracted Gaussian consisting of six primitive Gaussian functions. The '6-311' designation indicates that this is a triple-ζ basis set in that the valence orbitals are split into three shells where the contracted Gaussians are represented by three, one and one primitive Gaussians respectively. Finally, the '(d,p)' designation indicates the addition of polarization functions which supplement the basis set with 6 d-type basis functions (represented by one primitive Gaussian each) on the heavy atoms and the 3 p-type basis functions on hydrogen (or helium if present).

Optimization calculations were performed at the B3LYP/6-311G(d,p) level of theory. Subsequent to the optimization calculations, frequency calculations were performed in order to calculate the vibrational modes of the desired molecule. This also served to ensure that the output structures of the optimization calculations were actually minima. Structures that are minima on the potential energy curve posses no negative frequencies whereas transition states (and higher order saddle points) are characterized by the presence of at least one negative frequency. Ensuring the output structures had only positive frequencies confirmed that that the structures were minima.

3.8 References for Chapter 3

[1] Dunkin I.R. *Matrix Isolation Techniques: A practical approach.* Edited by Harwood L.M. and Moody C.J. Oxford University Press Inc., New York, USA, **1998**.

[2] Szczepanski, J., Roser, D., Pesonette, W., Eyring, M., Pellow, R. and Vala, M. *J. of Phys. Chem.*, 96, **1992**, 7876.

[3] Lewars, E. *Computational Chemistry: Introduction to the theory and applications of molecular and quantum mechanics*. Kluwer Academic Publishers, **2003**.

[4] Gaussian 03, Revision C.01 Frisch, M. J.; Trucks, G. W.; Schlegel, H. B.; Scuseria, G. E.; Robb, M. A.; Cheeseman, J. R.; Montgomery, Jr., J. A.; Vreven, T.; Kudin, K. N.; Burant, J. C.; Millam, J. M.; Iyengar, S. S.; Tomasi, J.; Barone, V.; Mennucci, B.; Cossi, M.; Scalmani, G.; Rega, N.; Petersson, G. A.; Nakatsuji, H.; Hada, M.; Ehara, M.; Toyota, K.; Fukuda, R.; Hasegawa, J.; Ishida, M.; Nakajima, T.; Honda, Y.; Kitao, O.; Nakai, H.; Klene, M.; Li, X.; Knox, J. E.; Hratchian, H. P.; Cross, J. B.; Bakken, V.; Adamo, C.; Jaramillo, J.; Gomperts, R.; Stratmann, R. E.; Yazyev, O.; Austin, A. J.; Cammi, R.; Pomelli, C.; Ochterski, J. W.; Ayala, P. Y.; Morokuma, K.; Voth, G. A.; Salvador, P.; Dannenberg, J. J.; Zakrzewski, V. G.; Dapprich, S.; Daniels, A. D.; Strain, M. C.; Farkas, O.; Malick, D. K.; Rabuck, A. D.; Raghavachari, K.; Foresman, J. B.; Ortiz, J. V.; Cui, Q.; Baboul, A. G.; Clifford, S.; Cioslowski, J.; Stefanov, B. B.; Liu, G.; Liashenko, A.; Piskorz, P.; Komaromi, I.; Martin, R. L.; Fox, D. J.; Keith, T.; Al-Laham, M. A.; Peng, C. Y.; Nanayakkara, A.; Challacombe, M.; Gill, P. M. W.; Johnson, B.; Chen, W.; Wong, M. W.; Gonzalez, C.; and Pople, J. A.; Gaussian, Inc., Wallingford CT, 2004.

[5] GaussView, Version 3.09, Dennington II, Roy; Keith, Todd; Millam, John; Eppinnett, Ken; Hovell, W. Lee; and Gilliland, Ray; Semichem, Inc., Shawnee Mission, KS, 2003.

Chapter 4

An investigation into the fragmentation and isomerization reactions of small aldehydes: an electron bombardment matrix isolation study

4.0 Overview of chapter 4

This section presents the results in chronological order in which they were obtained. The original goal of this research was to gather spectroscopic evidence of the putative McLafferty Rearrangement (McLR) intermediate of cationic butanal. Upon failing to observe McLR products in appreciable yields the focus of this research was altered and it was decided that other aldehydes should be examined which led to research into propanal. Although the propanal radical cation experiences extensive fragmentation no isomerization was observed. Consequently, acetaldehyde which was known to isomerize to vinyl alcohol within the electron bombardment matrix isolation apparatus (EBMIS)[1] was used to investigate the interplay between isomerization and decomposition chemistry. Thus, the majority of research was focused around acetaldehyde, upon which the bulk of this thesis is centered.

4.1 EBMIS investigation into the gas-phase chemistry of butanal

A gaseous mixture comprising of a 1:800 mixture of butanal and argon was subjected to electron bombardment during a 2 hr deposit, at a gas flow rate of 1.0 cm^3/min onto a cold 15K CsI window. A current of 70μA from the electron beam was maintained throughout the deposition. The infrared spectrum that was subsequently obtained was compared to a reference spectrum where the same gaseous mixture was deposited under the same conditions except without electron bombardment. When no electron current is applied, all of the features in the spectrum correspond to absorptions of butanal monomers isolated in Ar or to small amounts of common matrix impurities such as H_2O, CO or CO_2. Comparison of the two spectra revealed that significant amounts of the original butanal had been destroyed judged by the drastic decreased in the size of peaks associated with butanal in the electron bombardment spectrum as well as by the emergence of a variety of new spectral features suggesting that many new products had been formed. A portion of the infrared spectrum of these matrices formed from butanal/Ar mixtures with and without electron bombardment are given in Figure 10, which serves as a general illustration of how the precursor is destroyed in typical EBMIS experiments. Unless otherwise indicated the reference spectrum will always be presented in black, and the electron bombardment spectrum will be in red. Figures 11 and 12 show portions of a 1:800 butanal/Ar spectrum shown as a difference spectrum where the reference spectrum has been subtracted from the spectrum obtained post electron bombardment. Thus, positive modes correspond to products and negative peaks represent the original butanal precursor.

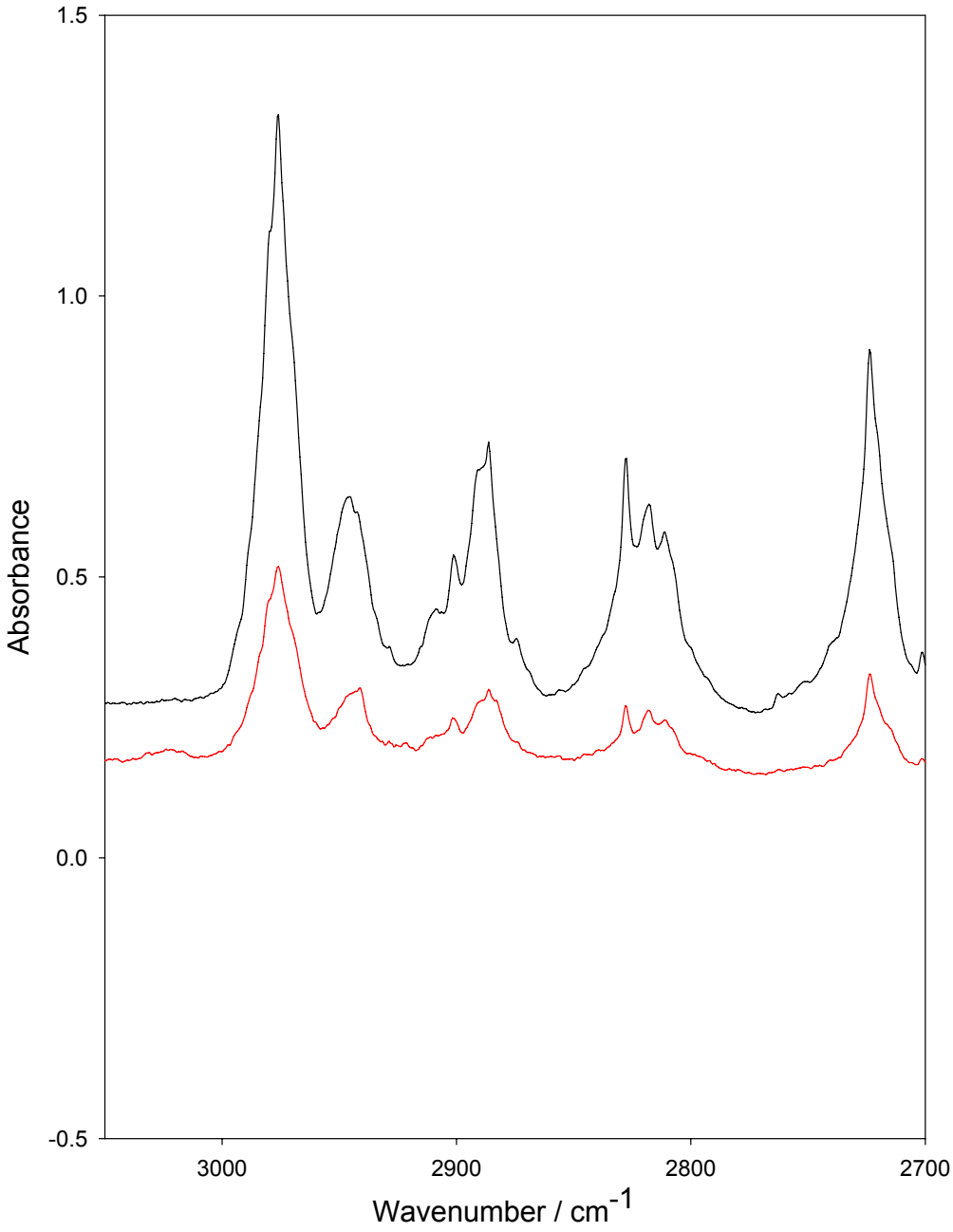

Figure 10: Portions of the FTIR spectrum of non-electron bombarded butanal/Ar matrices (black) as well as the spectrum of electron bombarded butanal/Ar (red). Illustrated is the pronounced destruction of CH stretching modes of butanal in the electron bombarded spectrum.

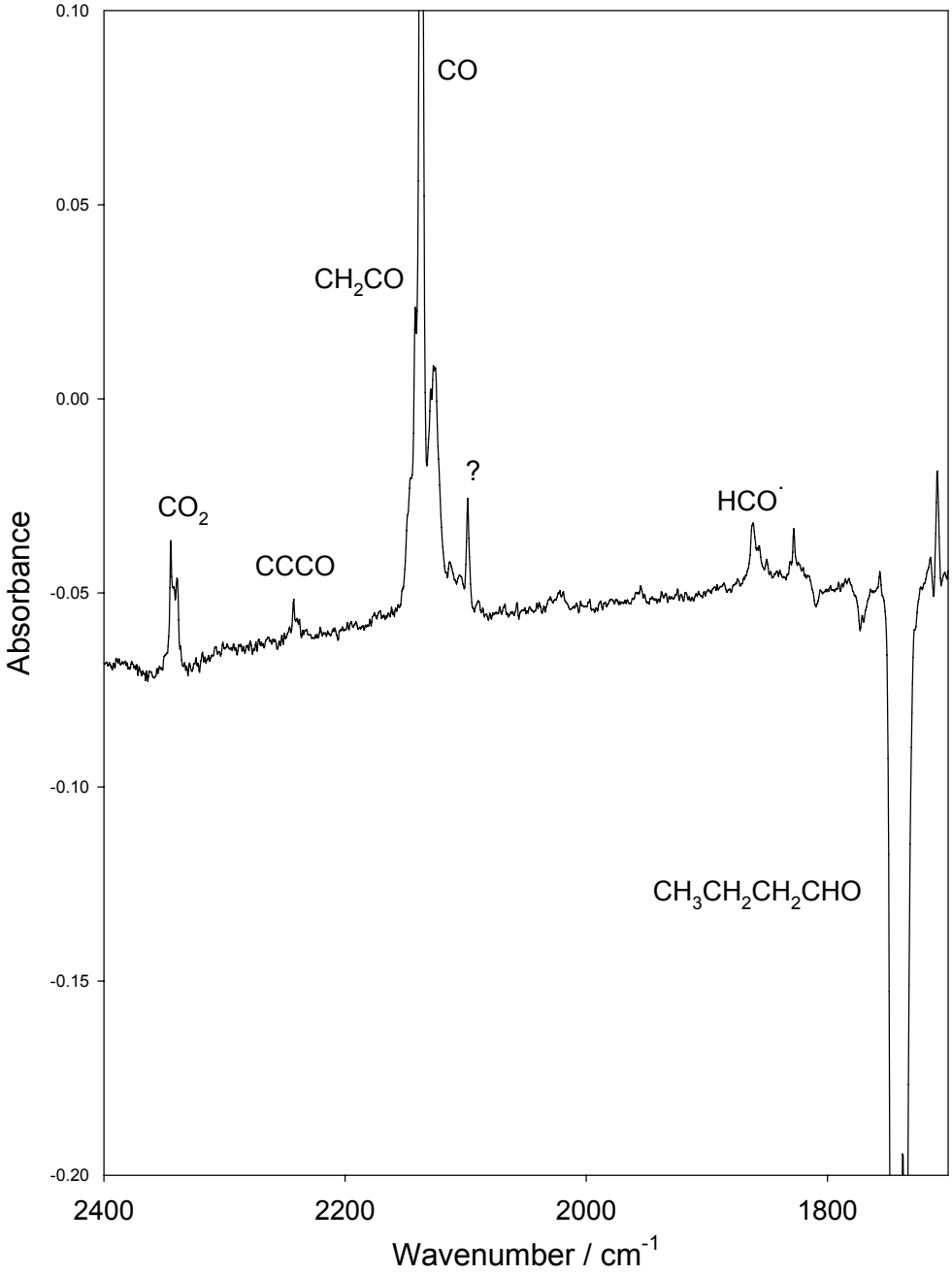

Figure 11: Portion of the infrared spectrum of a 1:800 butanal:Ar sample. Shown is a difference spectrum for the matrix formed under electron bombardment conditions from which the spectrum of a reference spectrum with no electron bombardment is subtracted.

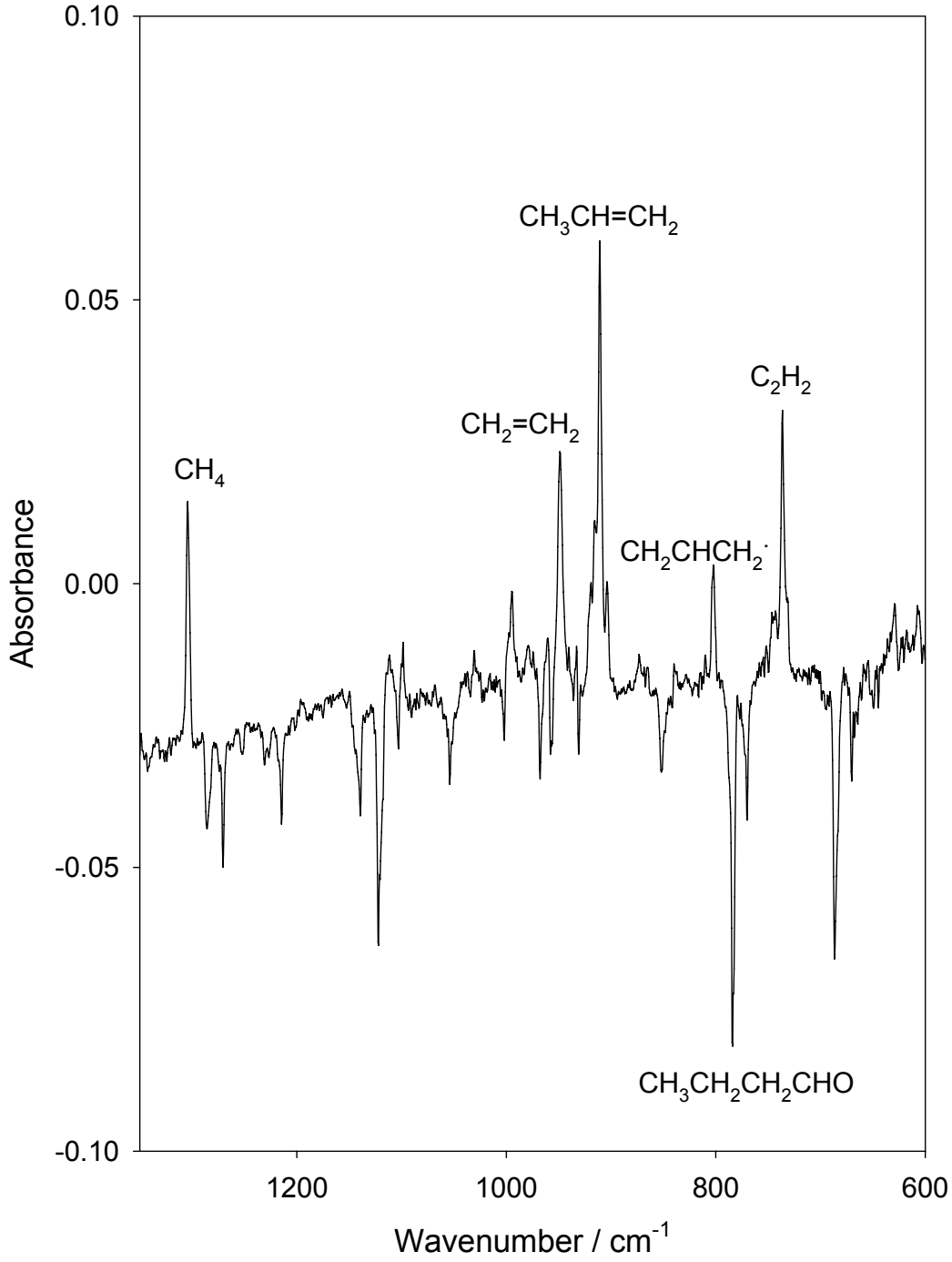

Figure 12: Portion of the infrared spectrum of a 1:800 butanal:Ar sample. Shown is a difference spectrum for the matrix formed under electron bombardment conditions from which the spectrum of a reference spectrum with no electron bombardment is subtracted.

A complete list of all assigned products and their corresponding products, as well as the remaining unidentified features can be found below in Table 2. As can be observed from the above spectra, electron bombardment of 1:800 butanal/Ar mixtures produces a variety of decomposition products. The alkanes methane ($1304cm^{-1}$)[2] and propane (2960, 2943, 1481 and $916cm^{-1}$) were both observed, the latter only in small yields. In addition to these hydrogenated species, many dehydrogenation products were also observed, including ethene (1439 and $949cm^{-1}$), ethyne ($736cm^{-1}$), propene (2922 and $911cm^{-1}$) and propyne ($2941cm^{-1}$). Radical species observed included $CH_2CHO^{\bullet}$ (1541 and $1373cm^{-1}$),[3] the allyl radical, $^{\bullet}CH_2CH=CH_2$ (803cm-1)[4] and the formyl radical, $HCO^{\bullet}$[5]. The remaining characterized features corresponded to ketene ($2142cm^{-1}$)[6], carbon monoxide ($2137cm^{-1}$)[7], formaldehyde (2798, $1498cm^{-1}$)[8], CCCO (2243, $579cm^{-1}$)[9,10] and finally the proton-bound argon dimer, Ar_2H^+ ($904cm^{-1}$)[11]. Unfortunately, there still remain a few unidentified features as found in table 2.

It was suspected that some of the above products were forming as a result of secondary fragmentation of primary products as a consequence of the rather large electron current (70μA) that was being applied throughout the deposit. Since it was known that by minimizing the electron current the formation of secondary products could be inhibited,[12] experiments were performed where the current was reduced to below 15μA for the entirety of the deposit. Reducing the current also drastically limits the amount of butanal precursor that is destroyed. For example, the percent destruction of a 1:800 butanal/Ar mixture when a 70μA current is applied was calculated to be 53%.

Table 2: Infrared absorption positions of products formed via electron bombardment of a 1:800 mixture of butanal/Ar. Shown also are the unidentified features many of which disappear when only a lower current is used14

$CH_3CH_2CH_2CHO$ in Ar with EB		$CH_3CH_2CH_2CHO$ in Ar with EB	
Product	**Wavenumber / cm^{-1} (relative intensity)**	**Product**	**Wavenumber /cm^{-1} (relative intensity)**
$CH_3CH_2CH_3$ (propane)	2960 (m)	Unassigned	3094 (m)
	2943 (m)		2098 (s)
	1481 (w)		2090 (m)
	916 (m)		1828 (m)
$CH_2CH_2CH_3$ (propene)	2922 (w)		1756 (m)
	911 (vs)		1709 (s)
$CHCCH_3$ (propyne)	2941 (s)		1696 (m)
H_2CCO (ketene)	2142 (s)		1679 (m)
CO	2137 (vs)		1637 (m)
	2125 (vs)		1456 (m)
CH_2CH_2 (ethene)	1439 (s)		1349 (m)
	949 (s)		1069 (m)
CHCH (ethyne)	736 (s)		1043 (m)
CCCO	2243 (m)		1031 (m)
	579 (m)		998 (m)
CH_4 (methane)	1304 (s)		974 (m)
H_2CO (formaldehyde)	2798 (w)		933 (m)
	1498 (m)		873 (m)
$CH_2CHCH_2^{\bullet}$ (allyl radical)	803 (s)		840 (m)
$CH_2CHO^{\bullet}$	1541 (w)		810 (m)
	1373 (m)		789 (m)
$HCO^{\bullet}$ (formyl radical)	1862 (m)		752 (m)
Ar_2H^+	904 (s)		746 (m)

peak area a large butanal feature at 2976cm^{-1} for the spectrum post electron bombardment and dividing it by the peak area of the same butanal feature but for the reference spectrum. In contrast, the percent destruction when a 15μA current was applied was found to be 29%. Unfortunately for butanal this line of analysis proves to be difficult as most of the products characterized correspond to dehydrogenated species. However, from a comparison of the spectrum generated from applying a 70μA current versus the spectrum generated from applying a 15μA current, it is noticed that the more fully dehydrogenated products, such as ethyne, decrease in size more drastically than the partially dehydrogenated products, such as propene and the allyl radical. Figure 13 below illustrates these differences. Propene, for example, appears as an appreciable peak in both spectra; however, ethyne appears as a substantial product in the 70μA spectrum but is a nonexistent feature in the 15μA spectrum.

Based on the electron impact mass spectrum of butanal where vinyl alcohol (m/z 44) is the base peak it was initially thought that butanal would undergo the McLafferty Rearrangement (McLR) and that the products vinyl alcohol and ethene would be observed. Indeed ethene was observed when a 70μA current was applied, however, surprisingly vinyl alcohol was not observed. It is therefore thought that ethene is formed through other decomposition pathways. It also thought the partial pressure of butanal in argon could be altered so as to promote the McLR to occur and thus a series of experiments were performed in order to examine the influence of butanal partial pressure in an attempt to maximize the formation of vinyl alcohol.

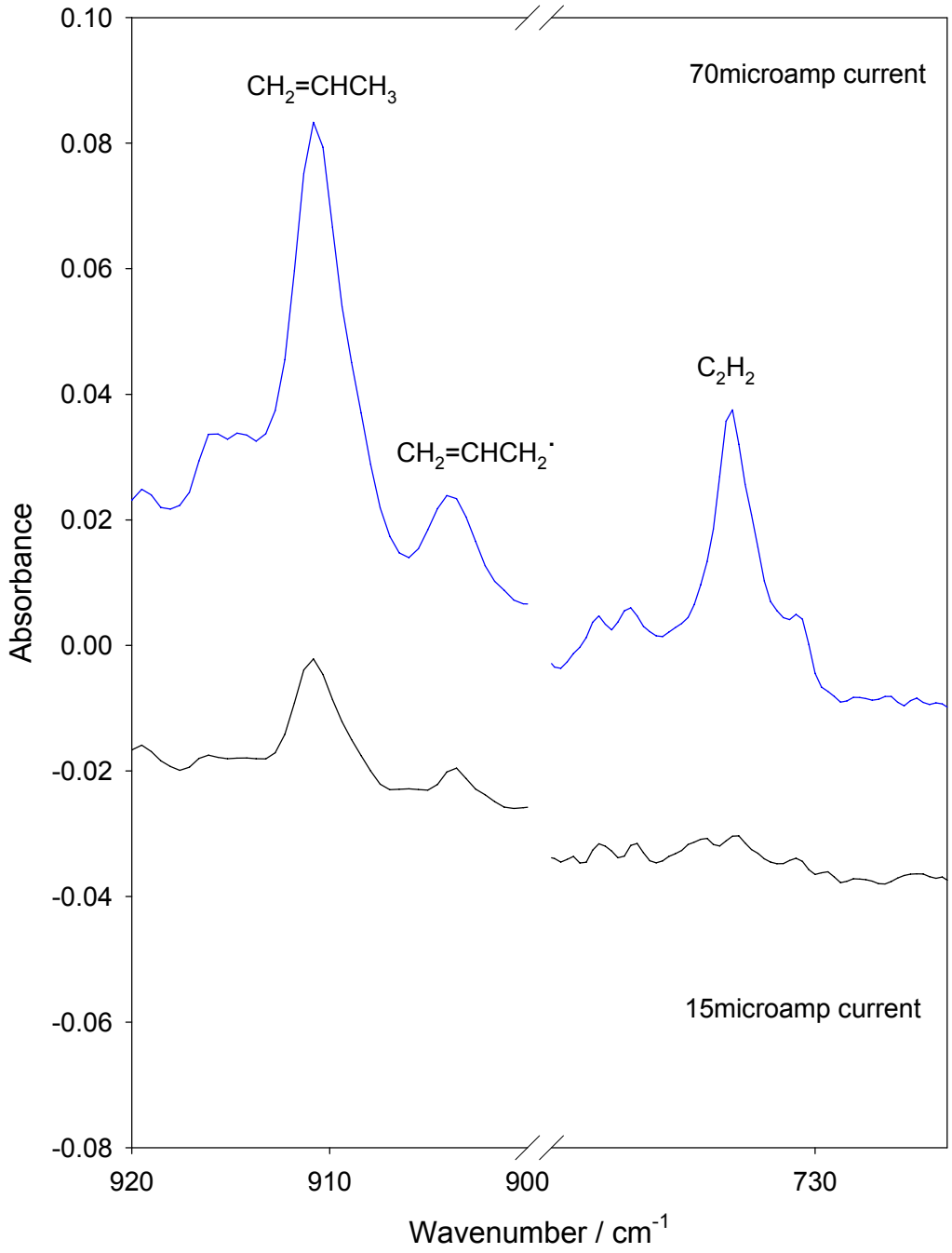

Figure 13: Comparison of the product yield for propene, the allyl radical, and ethyne between spectra obtained when either a 70μA current or 15μA current is applied.

As the original intent was to gather spectroscopic evidence of the putative McLR intermediate it was believed that to accomplish this, the McLR products must be obtained in high yields to indicate that the process was occurring to a significant extent. Experiments consisted of butanal/Ar mixtures of the following ratios: 1:400, 1:800, 1:1600, 1:3200 and 1:6400. In all cases the flow rate was kept constant at 1.0 cm^3/min as well as the flow time was kept at 2hrs and finally the electron current was held at approximately 50μA. In order to ensure consistency, an original glass bulb was prepared (see section 3.1) where the concentration of butanal was 1:400 and this bulb was progressively diluted to the lower concentrations. Figure 14 below shows the matrix isolated C—O stretching mode (1079 cm^{-1}) of vinyl alcohol at the top of the figure (black) as generated from an electron bombarded mixture of 1:400 acetaldehyde/Ar in addition to the same region shown for various mixtures of butanal/Ar where the butanal partial pressure was varied as shown. As can be observed from Figure 14 neither at high nor low partial pressures of butanal was vinyl alcohol generated as in all cases no mode at 1079 cm^{-1} is present. Thus, after some time was spent trying to optimize the conditions to maximize the efficiency of the McLR it was found that under all conditions within the EBMIS apparatus other fragmentation pathways were being favored. Consequently a decision was made to alter the focus of this research into understanding, more generally, the diverse chemistry that was occurring as evidenced by the various decomposition products observed as described above.

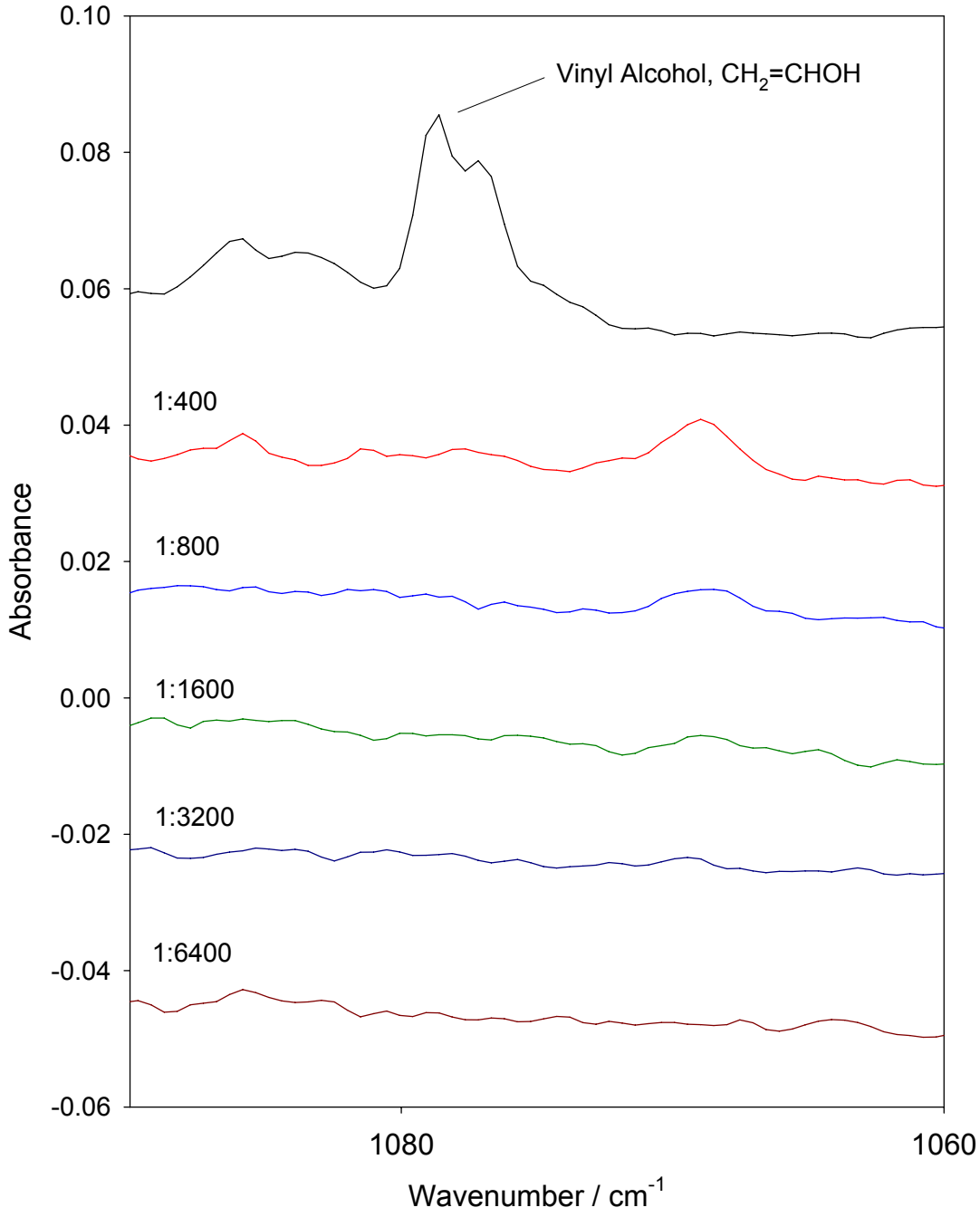

Figure 14: Top (black) is the C—O stretching mode (1079 cm^{-1}) of matrix isolated vinyl alcohol as generated from an electron bombarded acetaldehyde/Ar mixture. Shown below are spectra of the same region for electron bombarded butanal/Ar mixtures at differing butanal partial pressures as labeled.

As a result of this new focus it was decided to change molecules as butanal is a rather large molecule and its gas-phase phase decomposition chemistry is not as well understood as simpler aldehydes as discussed in section 2.3. Thus, propanal was initially investigated in an attempt to use a simpler molecule whose decomposition could be more easily understood. It was also a possibility that propanal might isomerize to its enol tautomer, 1-propen-1-ol, similar to acetone, such that isomerization chemistry might be observed in conjunction with decomposition pathways.

4.2 EBMIS investigation into the gas-phase chemistry of propanal

Similar to butanal, 70μA electron bombardment of 1:800 mixtures of propanal in Ar produced a variety of decomposition products. The alkanes, ethane (2895, 1470, 1467, and 822 cm^{-1}), ethene (3110, 1440, 940, and 829 cm^{-1})[2] and ethyne (3288, 3282, and 736 cm^{-1}) were all observed with the dehydrogenated products appearing as particularly intense features in the electron bombardment spectrum. Some radical species were also generated which included the formyl radical (1863 and 1086cm^{-1}) and several relatively weak features assigned to $CH_2CHO^{\bullet}$ (1542, 1375, 1141, 958 cm^{-1}). Other products characterized were methane (1304 cm^{-1}), ketene (2142 and 969 cm^{-1}), CO (2138 and 2127 cm^{-1}) and finally Ar_2H^+ (904 cm^{-1}). Figures 15 and 16 show different portions of a difference spectrum that was constructed from subtracting a reference spectrum of a deposited 1:800 propanal/Ar mixture from a spectrum of the same mixture but after electron bombardment. As with the earlier

difference spectra shown for the results of butanal, the positive features represent new products whereas the negative features represent remaining propanal. A complete table showing all of the assigned features as well as the unidentified features can be found in Table 3 below. No features were found that suggested the formation of the enol tautomer of propanal, 1-propen-1-ol. Additionally, the observed chemistry was still being convoluted by the multitude of dehydrogenation products observed. Prompted by the desire to investigate the interplay between bimolecular and unimolecular chemistry within the EBMIS system it was decided that the best molecule to work with would be acetaldehyde which readily forms vinyl alcohol.

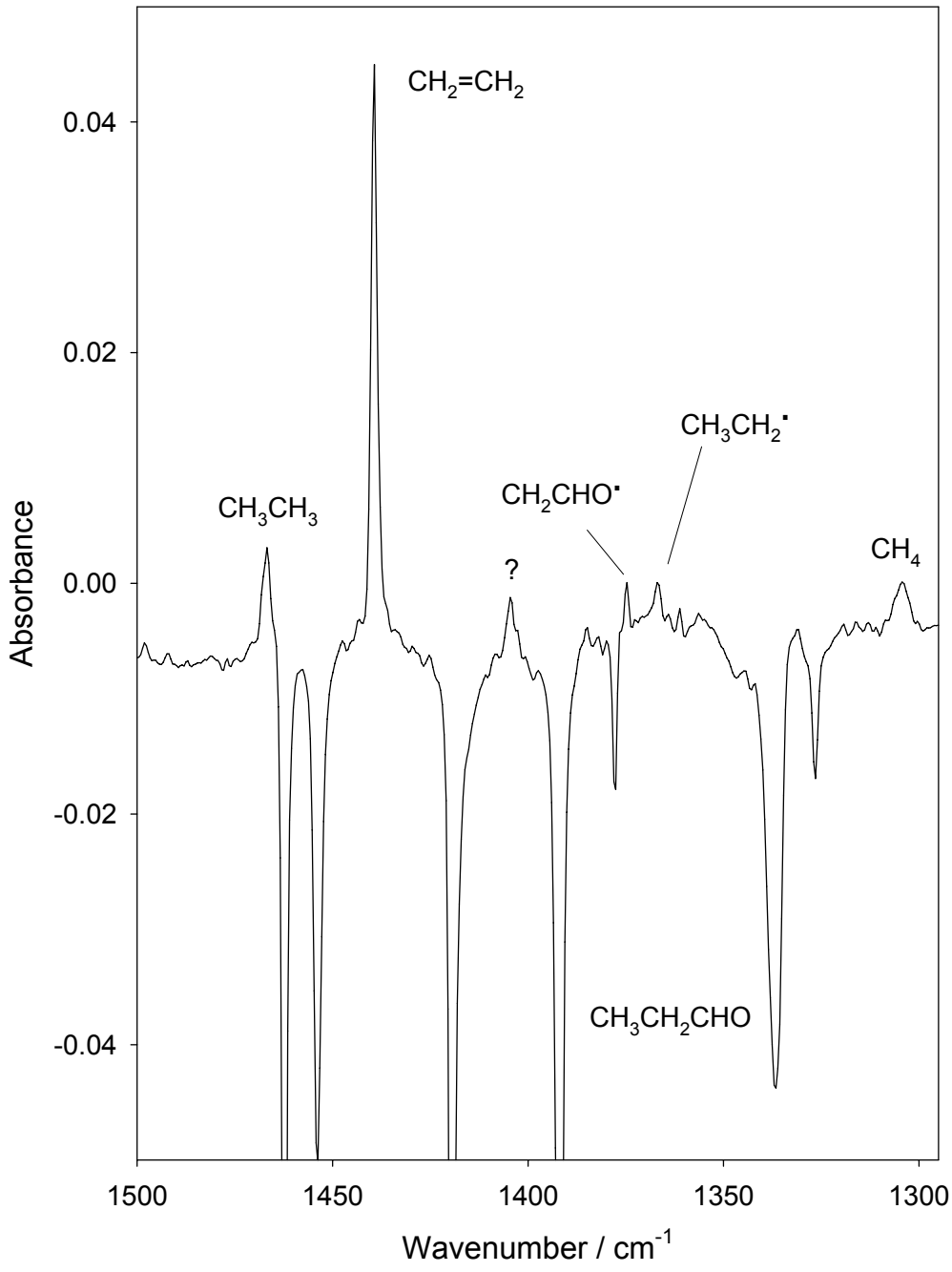

Figure 15: Portion of the infrared spectrum of a 1:800 propanal:Ar sample. Shown is a difference spectrum for the matrix formed under electron bombardment conditions from which the spectrum of a reference spectrum with no electron bombardment is subtracted.

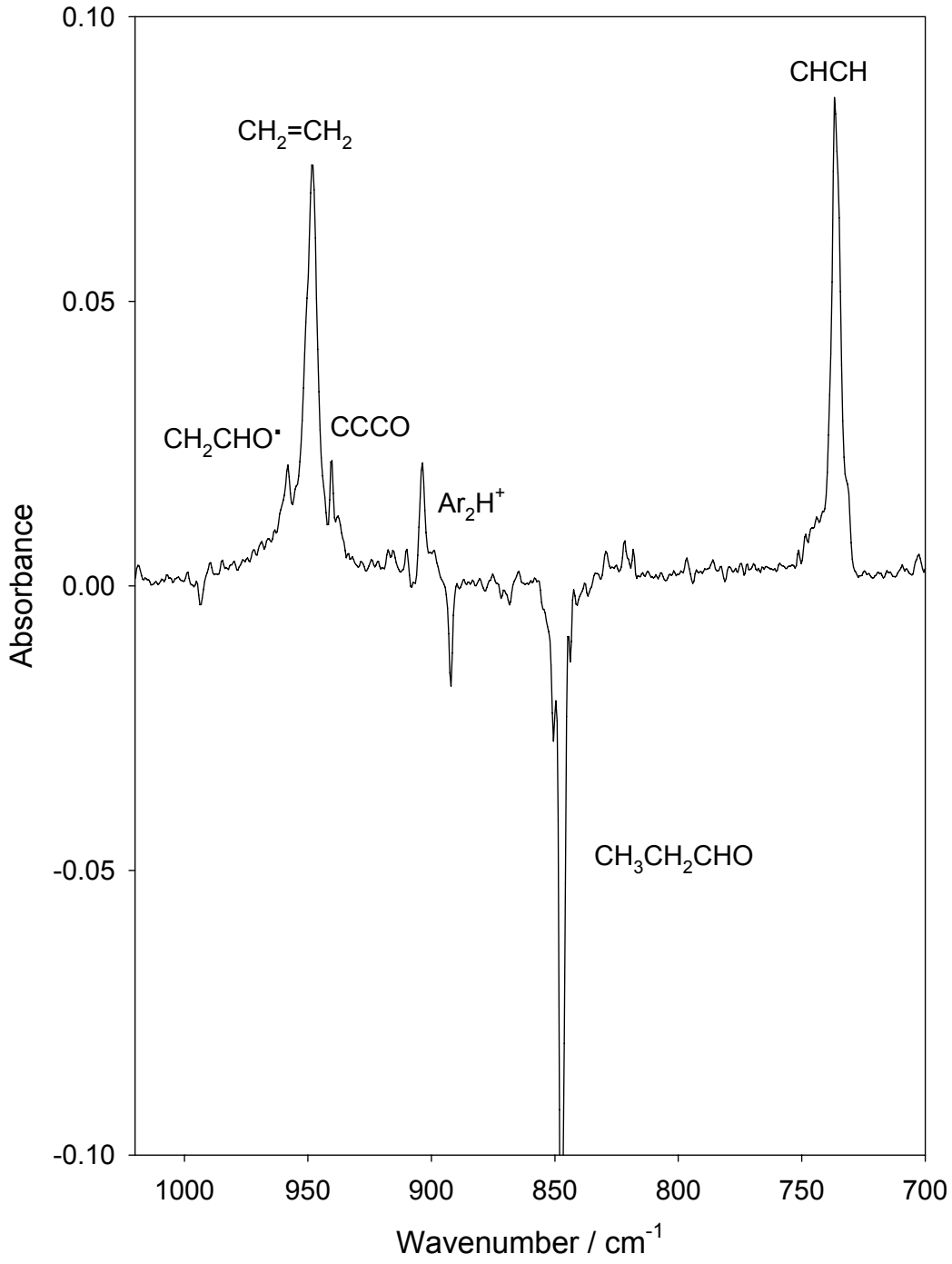

Figure 16: Portion of the infrared spectrum of a 1:800 propanal:Ar sample. Shown is a difference spectrum for the matrix formed under electron bombardment conditions from which the spectrum of a reference spectrum with no electron bombardment is subtracted.

Table 3: Infrared absorption positions of products formed via electron bombardment of a 1:800 mixture of propanal/Ar. Shown also are the unidentified features.

CH_3CH_2CHO in Ar with EB		CH_3CH_2CHO in Ar with EB	
Product	**Wavenumber / cm^{-1} (relative intensity)**	**Product**	**Wavenumber /cm^{-1} (relative intensity)**
		H_2CCO	
CH_3CH_3 (ethane)	2895 (w)	(ketene)	2142 (vs)
	1470 (w)		969 (w)
	1467 (s)	CO	2138 (vs)
	822 (w)		2127 (vs)
		CO-water	
CH_2CH_2 (ethene)	3110 (w)	complex	2149 (m)
	1440 (vs)	Ar_2H^+	904 (s)
	940 (vs)	Unassigned	2979 (m)
	829 (w)		2309 (m)
CHCH (ethyne)	3288 (m)		2247 (m)
	3282 (m)		1860 (m)
	736 (vs)		1714 (m)
CCCO	2243 (s)		1688 (m)
	940 (m)		1404 (m)
$CH_3CH_2^{\bullet}$ (ethyl radical)	3034 (w)		1106 (m)
	1385 (vw)		1092 (m)
	1367 (w)		961 (m)
	535 (m)		938 (m)
$HCO^{\bullet}$ (formyl radical)	1863 (s)		910 (m)
	1086 (w)		745 (m)
$CH_2CHO^{\bullet}$	1541 (w)		731 (s)
	1375 (w)		
	1141 (w)		
	958 (m)		

4.3 EBMIS investigation into the gas-phase chemistry of acetaldehyde

Acetaldehyde (CH_3CHO) provided an ideal molecule to investigate within the EBMIS apparatus as it was small enough that the primary decomposition products could not undergo extensive dehydrogenation as was the case with propanal and butanal. Moreover it is known to isomerize to vinyl alcohol which consequently would allow the comparison of ion-molecule versus unimolecular chemistry to occur.

Electron bombardment of mixtures of CH_3CHO diluted in Ar produced many new features. Neutral fragmentation products characterized via FTIR spectroscopy of the incipient matrix included CH_4 (1305 cm^{-1}), H_2CCO (3063 and 2142 cm^{-1}), CO (2138 cm^{-1}) and the CO-water complex (2148 cm^{-1}). Furthermore, many radical species were generated presumably either by direct formation or by subsequent neutralization by secondary electrons once formed in the matrix. The radical species included, $CH_3CO^{\bullet}$ (1875, 1840, 1321 cm^{-1}), $HCO^{\bullet}$ (1862, 1381, 1086 and 1077 cm^{-1}), $CH_3^{\bullet}$ (606 cm^{-1})[13] and $CH_2CHO^{\bullet}$ (1541 and 525 cm^{-1}). Finally, the isomerization product CH_2CHOH (1662, 1625, 1079, 971, 814 and 413 cm^{-1})[14] was formed as several strong features correlated with the original IR assignment as found by Hawkins and Andrews. Figures 17 and 18 show portions of an infrared spectrum of a 1:800 CH_3CHO:Ar mixture. Shown are difference spectra where the reference spectrum (no electron bombardment) has been subtracted from the spectrum of the resultant matrix post-electron bombardment.

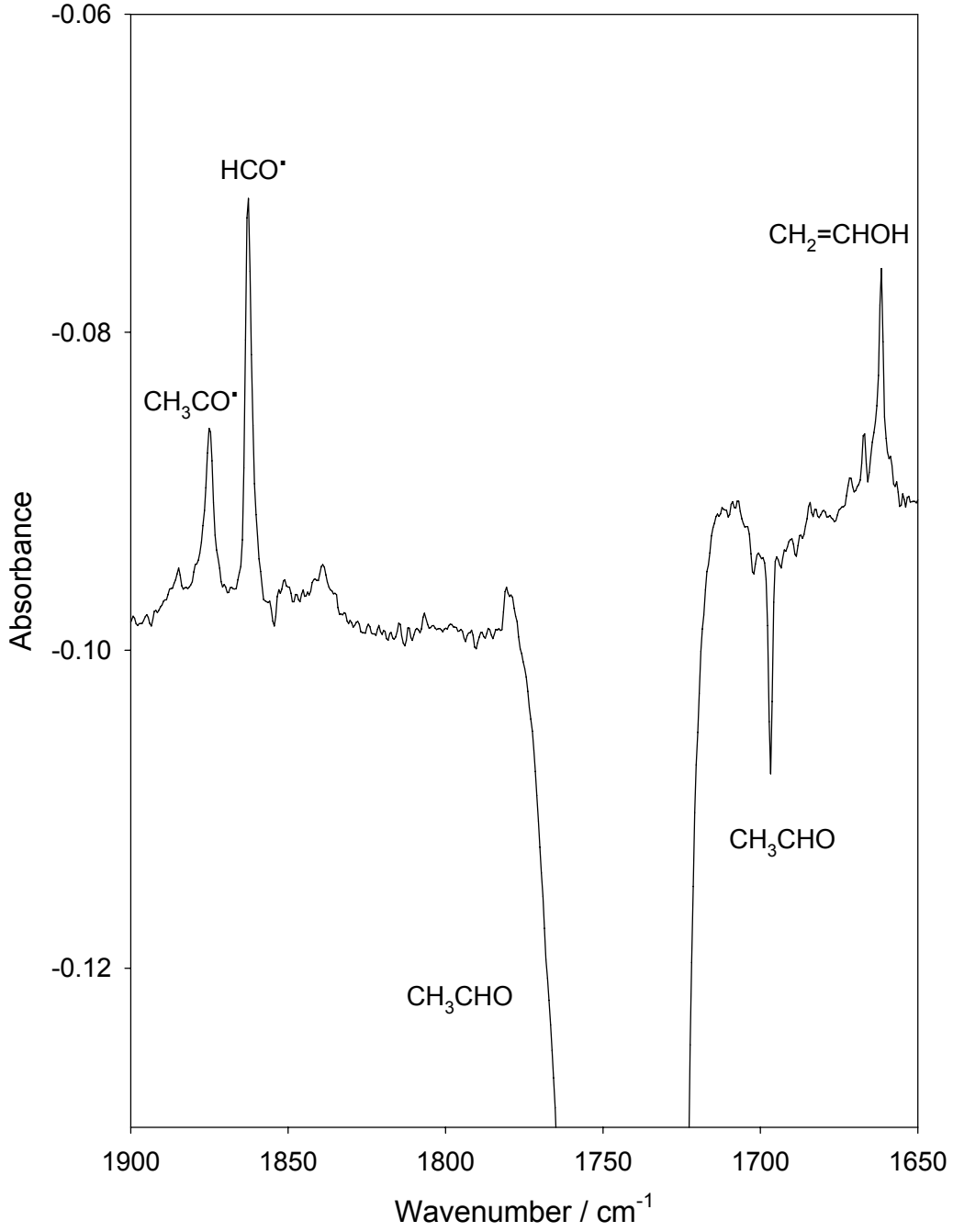

Figure 17: Portion (1900-1650 cm^{-1}) of the infrared spectrum of a 1:800 CH_3CHO:Ar sample. Shown is a difference spectrum for the matrix formed under electron bombardment conditions from which the spectrum of a reference spectrum with no electron bombardment is subtracted.

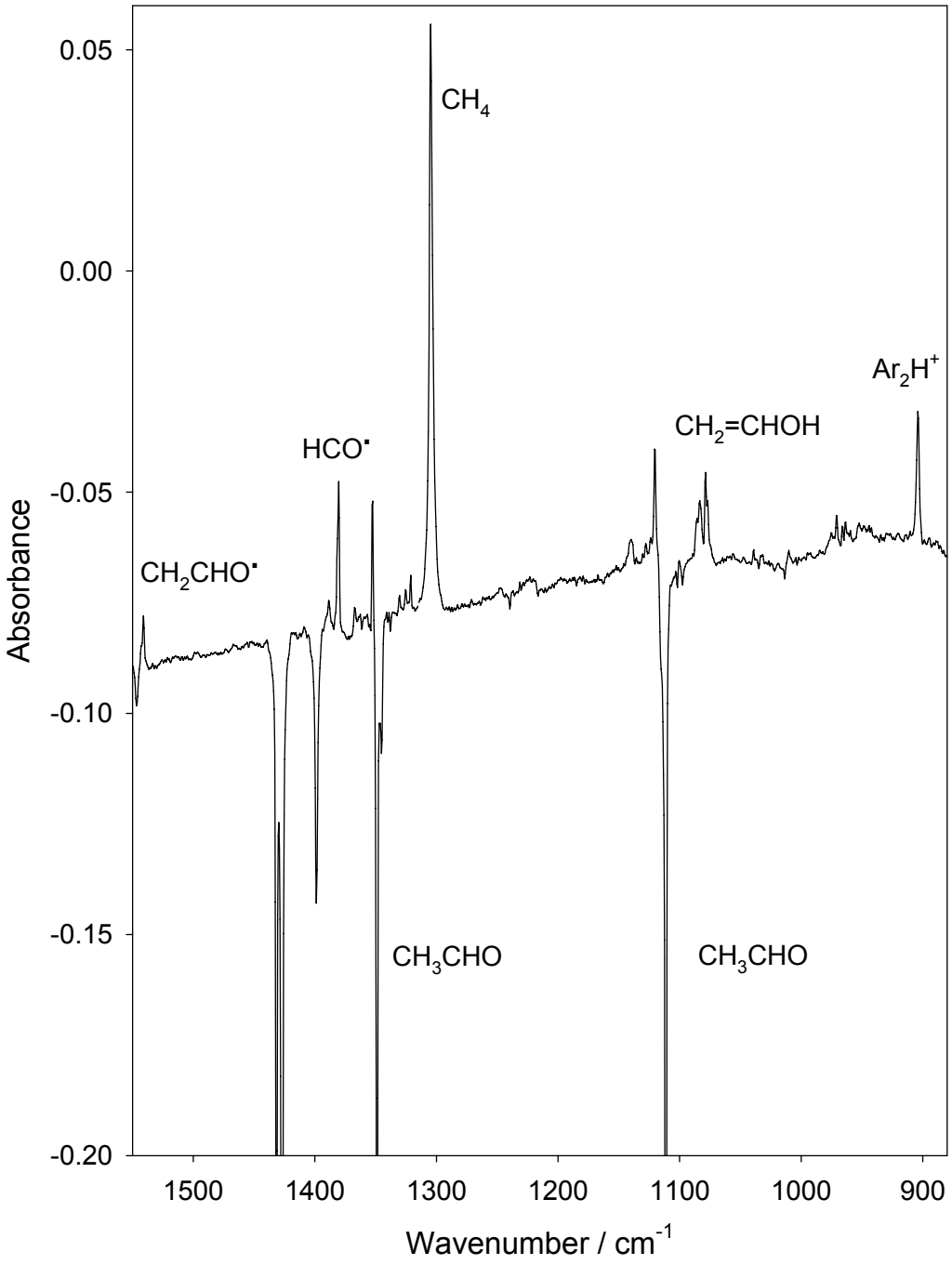

Figure 18: Portion (1550-880 cm^{-1}) of the infrared spectrum of a 1:800 CH_3CHO:Ar sample. Shown is a difference spectrum for the matrix formed under electron bombardment conditions from which the spectrum of a reference spectrum with no electron bombardment is subtracted.

As can be seen from Figure 17 both the acetyl ($CH_3CO^{\bullet}$) and formyl ($HCO^{\bullet}$) radicals are produced in strong yields as evidenced by the relatively intense features at 1875 cm^{-1} and 1863 cm^{-1} respectively. The acetyl radical, in particular, has been difficult to characterize in the Parnis lab. For example, the acetyl radical was not observed in recent work investigating the decomposition and isomerization chemistry of acetone (see section 2.1.2) even though it should be one of the significant decomposition products. Furthermore, the presence of a relatively intense feature at 606 cm^{-1} correlates to the methyl radical as assigned by Jacox.[13] This was another expected product in the acetone work that was not observed.

4.3.1 CD_3CDO/Ar EBMIS results

In order to confirm the above radical assignments the use of the deuterated acetaldehyde, CD_3CDO was employed. This also served to re-confirm the presence of vinyl alcohol as CD_2=CDOD had also been previously characterized through infrared spectroscopy by the extensive work of Rodler *et al.*[15] where nine different isotopomers of vinyl alcohol were characterized. As with the CH_3CHO results, in the infrared spectra of matrices formed following 300V, ~50μA electron bombardment of the gas mixture (1:400 CD_3CDO:Ar) a variety of new features are observed. Figure 19 shows a portion of the CD_3CDO/Ar (1:400) difference spectrum primarily illustrating the new modes that correlate to the deuterated counterpart of the aforementioned radicals as well as deuterated vinyl alcohol.

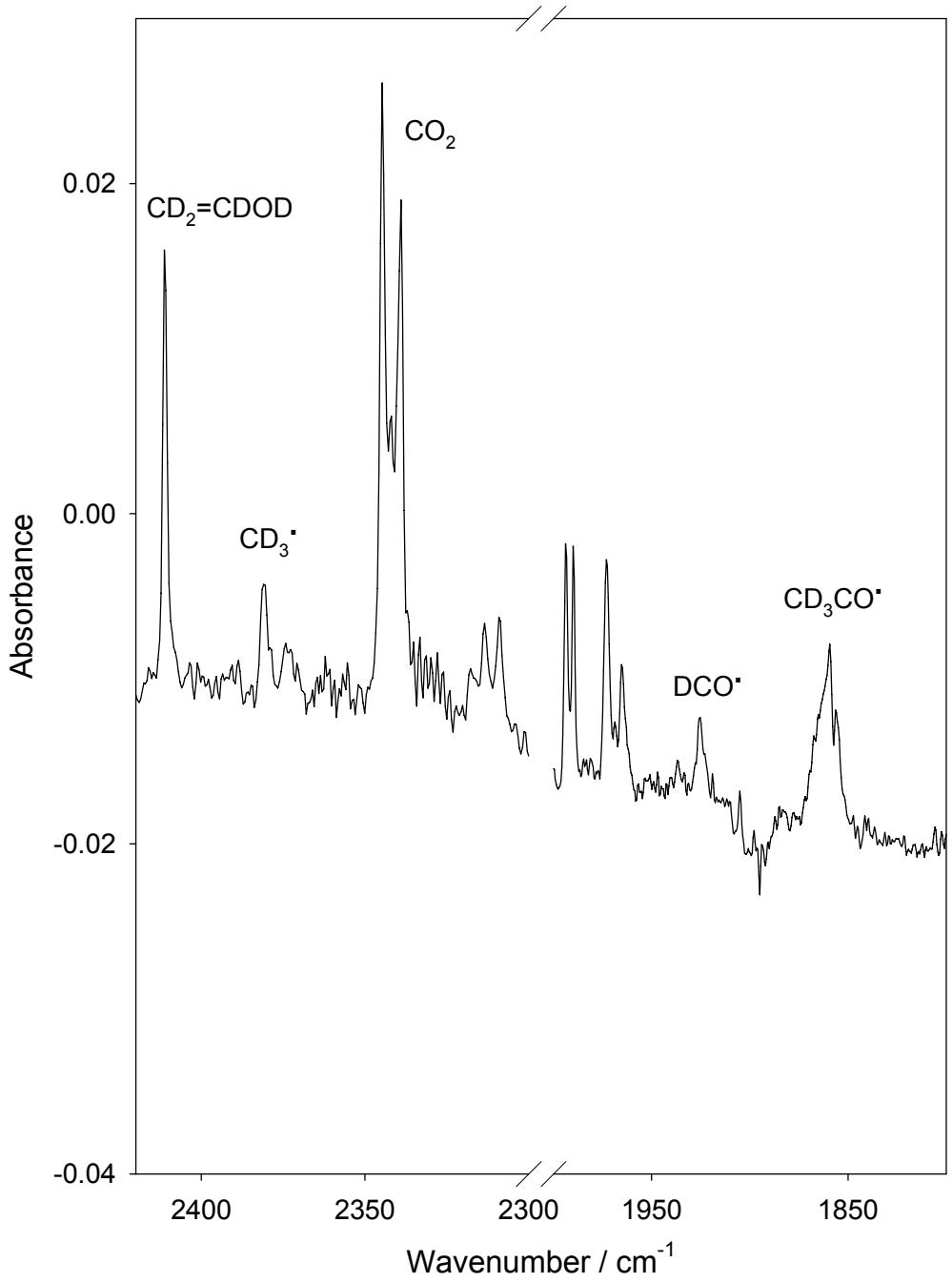

Figure 19: Portion (2420-1800 cm^{-1}) of the infrared spectrum of a 1:400 CD_3CDO:Ar sample. Shown is a difference spectrum for the matrix formed under electron bombardment conditions from which the spectrum of a reference spectrum with no electron bombardment is subtracted.

The deuterated counterparts of all of the assigned products from the CH_3CHO/Ar spectrum were observed in the CD_3CDO/Ar results. Thus the following products were characterized: CD_4 (994 cm^{-1})[16], D_2CCO (2260, 2112 and 849 cm^{-1}), CO (2138 cm^{-1}), CO-water complex (2149 cm^{-1}), $CD_3CO^{\bullet}$ (1856 cm^{-1}), CD_2CDOD (2677, 2411, 1583, 925 and 921 cm^{-1}), $CD_2CDO^{\bullet}$ (1511 and 1223 cm^{-1}), $DCO^{\bullet}$ (1925 and 849 cm^{-1}), $CD_3^{\bullet}$ (2381 and 455 cm^{-1}) and finally Ar_2D^+ (643 cm^{-1})[17]. Table 4 shows a complete list of assigned products for both the CH_3CHO and CD_3CDO results along with the remaining unidentified features.

Table 4: Infrared absorptions of products formed via electron bombardment of CH_3CHO and CD_3CDO in Ar respectively

CH_3CHO in Ar with EB		CH_3CHO in Ar with EB		CD_3CDO in Ar with EB		CD_3CDO in Ar with EB	
	Wavenumber /cm^{-1}		Wavenumber /cm^{-1}		Wavenumber /cm^{-1}		Wavenumber /cm^{-1}
Product	**(rel. int.)**	**Product**	**(rel. int.)**	**Product**	**(rel. int.)**	**Product**	**(rel. int.)**
Methane	1305 (vs)	$HCO^{\bullet}$	1862 (s)	CD_4	994 (vs)	Unassigned	2154 (s)
Ar_2H^+	904 (m)		1381 (m)	D_2CCO	2260 (s)		2119 (s)
H_2CCO (ketene)	3063 (s)		1086 (w)		2112 (vs)		1994 (s)
	2142 (vs)		1077 (m)		849 (w)		1990 (s)
CO	2138 (vs)	CO_2	2345 (vs)	CO	2138 (vs)		1973 (s)
CO-Water Complex	2148 (vs)		2340 (vs)	CO-Water complex	2149 (vs)		1965 (m)
$CH_3CO^{\bullet}$	1875 (s)		663 (w)	$CD_3CO^{\bullet}$	1856 (m)		1734 (s)
	1840 (m)		662 (w)	CD_2CDOD	2677 (m)		1580 (s)
	1321 (w)	$CH_3^{\bullet}$	606 (s)		2411 (s)		1537 (m)
CH_2CHOH	1662 (s)	Unassigned	3240 (s)		1583 (s)		1523 (s)
	1625 (m)		3072 (s)		925 (m)		1407 (m)
	1079 (m)		2308 (m)		921 (s)		1177 (s)
	971 (m)		2031 (s)	CD_2CDO	1511 (m)		1166 (s)
	814 (m)		2023 (s)		1223 (w)		942 (s)
	413 (m)		2019 (vs)	$DCO^{\bullet}$	1925 (m)		648 (m)
CH_2CHO	1541 (m)		1743 (m)	$CD3^{\bullet}$	2381 (m)		644 (m)
	525 (s)		1120 (m)		455 (m)		
			818 (m)				
			517 (m)				

4.3.2 Influence of acetaldehyde partial pressure

The influence of acetaldehyde partial pressure on the observed product distribution was examined as a means of determining which products were being favored at low partial pressures and which products were maximizing at higher acetaldehyde partial pressures. Experiments were performed varying the partial pressures of acetaldehyde corresponding to mole ratio values in the range of 1:6400 to 1:400 (acetaldehyde:Ar). In order to ensure sufficient peak intensity of the resulting products the 300V electron current was maintained at ~50μA while flowing at 1.0 cm^3/min for 2hrs. As previously discussed it is believed that higher partial pressures of acetaldehyde promote bimolecular chemistry and at lower pressures the chemistry transitions into more traditional unimolecular chemistry. Thus, by noticing how the yields of each product vary with partial pressure it can be ascertained whether they are produced via bimolecular routes or via unimolecular decomposition. Figure 20 shows how the peak sizes associated with the formyl radical, $HCO^{\bullet}$ (1863 cm^{-1}) and the acetyl radical, $CH_3CO^{\bullet}$ (1875 cm^{-1}) change with varying acetaldehyde partial pressure.

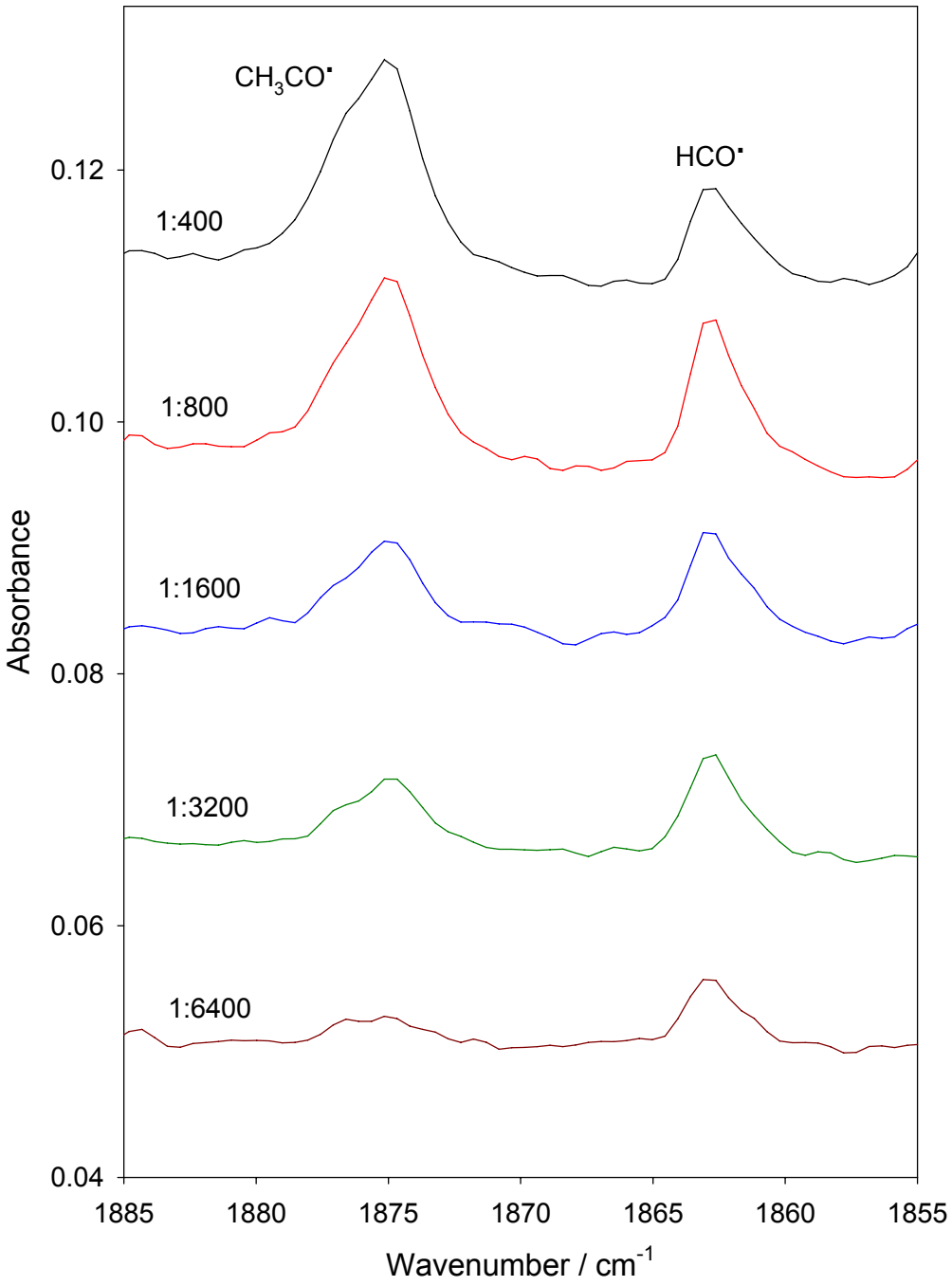

Figure 20: Infrared spectra of electron bombarded acetaldehyde from partial pressures values of 1:400 to 1:6400 (CH_3CHO:Ar) showing the variation of peak intensity for the acetyl radical, $CH_3CO^{\bullet}$, and the formyl radical, $HCO^{\bullet}$.

The concentration range used (1:400 to 1:6400) was chosen as experiments conducted above a 1:400 partial pressure yielded a different chemical outcome with many unidentified features. Further work would need to be done in order to characterize the chemistry occurring in this range. Furthermore, experiments conducted below a 1:6400 concentration did not yield measureable product absorptions with the given flow rate and flow time. Thus the five different partial pressures used provided a substantial change and enough data to show any noticeable trends. As observed from Figure 20 the intensity of the acetyl radical peak at 1875 cm^{-1} drastically declines as the partial pressure of acetaldehyde is decreased. In contrast the intensity of the formyl radical peak at 1863 cm^{-1} remains relatively consistent as the acetaldehyde partial pressure is progressively decreased. Quantitative analysis of these changes for each product can also be performed by measuring the area for a given peak and tracking how that area changes as a function of the partial pressure of acetaldehyde. One important aspect to account for in such analysis, however, is the differing levels of precursor destruction. This complicating factor was previously addressed when discussing a similar series of experiments that were performed using butanal as an attempt to promote the McLafferty Rearrangement to occur. The amount of acetaldehyde that forms products in each experiment can vary. For example if two experiments were to be compared where the acetaldehyde partial pressure were 1:400 and 1:1600 respectively and in the former there was 70% destruction of acetaldehyde, however in the latter only 10% destruction of acetaldehyde then concordantly there would much more

product formation in the former experiment. That would be a result solely of the increased destruction and that would not give information as to which processes were more or less efficient at that concentration. Consequently, in order to extract that information, via such quantitative measuring, the peak areas must be normalized for the amount of acetaldehyde destroyed. For example, if the measured peak area of an acetaldehyde peak from the reference spectrum (deposition without electron bombardment) was 10units and the same peak from the spectrum collected post-electron bombardment was found to have an area of 7units than the difference of 3units would be used to normalize the subsequently measured peak areas of the various products by dividing their measured areas by this difference.

Figures 21 and 22 show the variation in the relative yield of each of the characterized species each normalized to their highest observed value. They are grouped into different Figures as in each Figure the products behave similarly as the acetaldehyde partial pressure is varied. In Figure 21 the products methane, CO, formyl radical, CH_2CHO radical and the methyl radical are plotted. It can be seen that formation of those products is hindered as the partial pressure of acetaldehyde is increased as the normalized measured peak areas are seen to decrease as the acetaldehyde partial pressure is increased. Figure 22 illustrates how the products vinyl alcohol, ketene and the acetyl radical are affected as the partial pressure of acetaldehyde is decreased. From observation of that Figure it can be seen that those products are maximized at intermediate concentrations and are less favored at both the lowest and highest partial pressures

respectively. Recent work with acetone also showed that its enol tautomer, 1-propen-2-ol, and ketene both maximize at intermediate acetone partial pressures and thus this work seems to be congruent with the results of a similar study with acetone.[18]

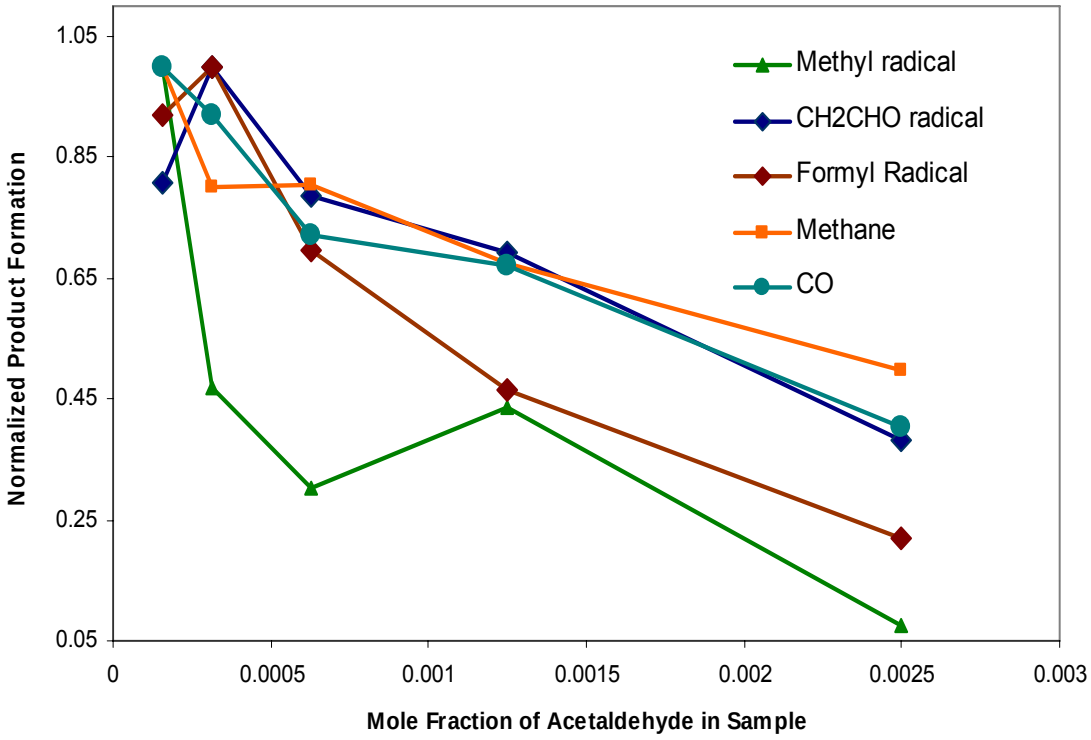

Figure 21: Normalized yield of products associated with unimolecular decomposition that form upon electron bombardment for samples ranging in mole ratio from 1:400 to 1:6400 (plotted as relative mole fraction of acetaldehyde). Yields are normalized with respect to the highest observed value for each product. Absorptions chosen for this plot were: methyl radical (607cm^{-1}), CH_2CHO radical (1541 cm^{-1}), formyl radical (1863 cm^{-1}), methane (1305 cm^{-1}) and CO (2138 cm^{-1}).

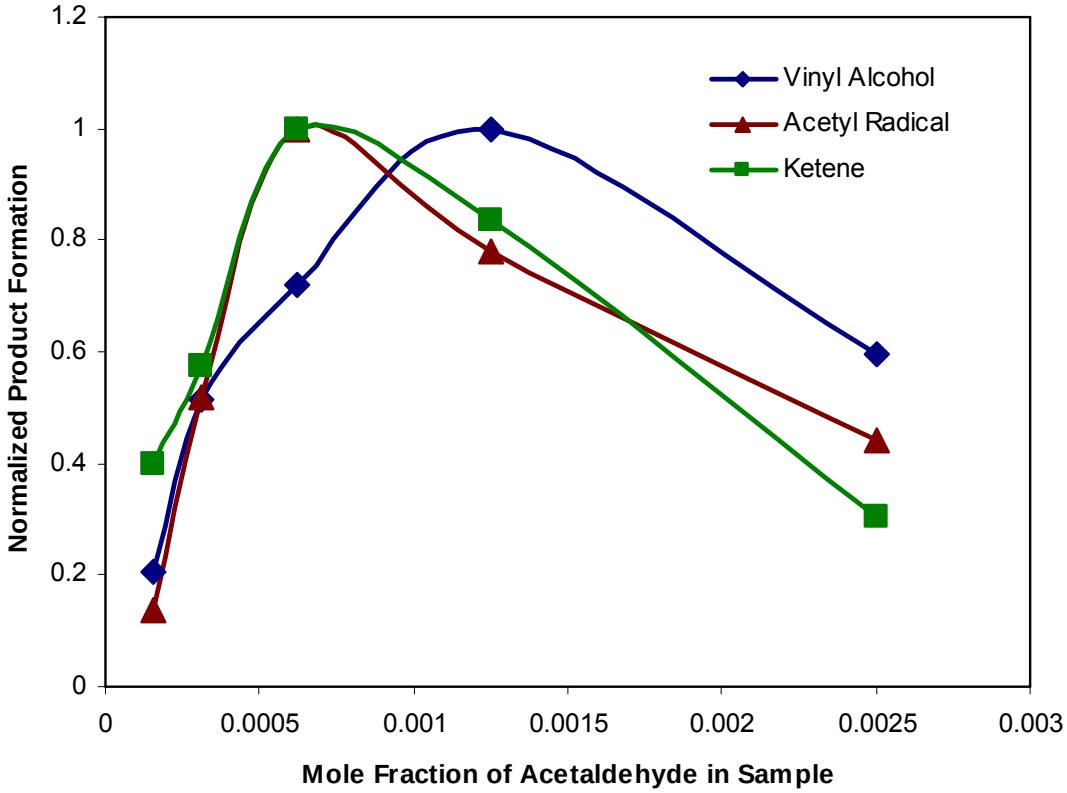

Figure 22: Normalized yield of products associated with bimolecular decomposition that form upon electron bombardment for samples ranging in mole ratio from 1:400 to 1:6400 (plotted as relative mole fraction of acetaldehyde). Yields are normalized with respect to the highest observed value for each product. Absorptions chosen for this plot were: vinyl alcohol (1662cm^{-1}), acetyl radical (1875 cm^{-1}) and ketene (2142 cm^{-1}).

4.3.3 Influence of flow rate on product distribution

Another variable that can be altered so as to study its influence on the resulting chemistry is the total gas flow rate. Increased flow rates correlate with increased pressures in the reaction zone before condensation onto the cold window. Thus products that are favored under low pressure environments should decrease as the flow rate is increased. A 1:400 sample of CH_3CHO:Ar was used for all of the experiments. The 300V electron current applied during electron bombardment was kept at ~50μA for each experiment as well. As increasing the flow rate increases the total gas deposited the corresponding flow times were concurrently adjusted such that the total gas deposited in each experiment remained constant. The flow rates were varied from 0.25 cm^3/min to 2.0 cm^3/min at 0.25 cm^3/min intervals. Thus the total deposition times were correspondingly varied over the range of 2hrs for the lowest flow rate to 15 minutes at the highest flow rate. An additional experiment was performed at 4.0 cm^3/min for 7.5 minutes as well to see if this extreme flow rate further influenced the chemistry. As with the work above dealing with the variation of acetaldehyde partial pressure, there can be variation in the amount of acetaldehyde destroyed between given experiments. Thus, when plotting the change of peak area for the various products as a function of gas flow rate the various peak areas must also be normalized for the varying amounts of acetaldehyde destroyed. Figures 23 and 24 show the variation of normalized product yield as a function of total gas flow. Observation of both Figures show that no discernable trend emerges as

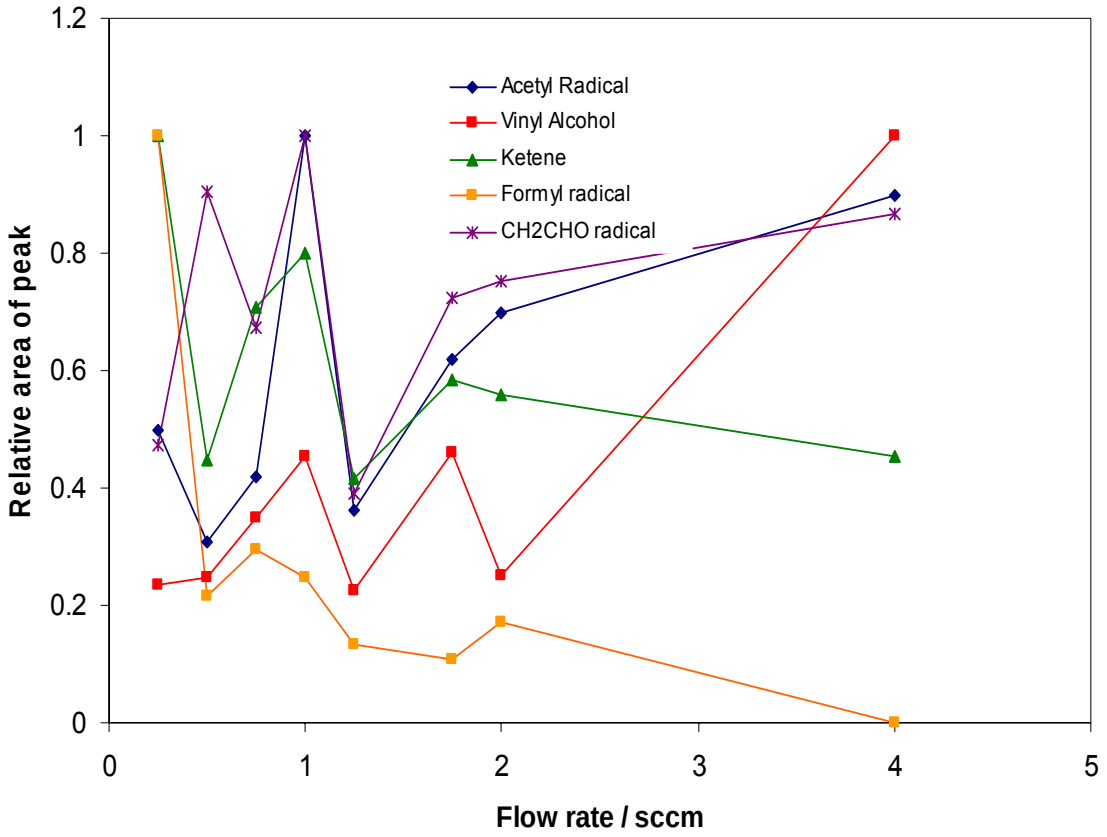

Figure 23: Plots of the relative yield variation for the major products following acetaldehyde ionization in samples of 1:400 CH_3CHO:Ar, as a function of total gas flow rate. Product absorption areas have been normalized with respect to the amount of acetaldehyde destroyed at each flow rate studied between 0.25 and 4sccm and with respect to the highest yield value observed for each molecule. Peaks chosen for each product are the same as those chosen for the partial pressure results.

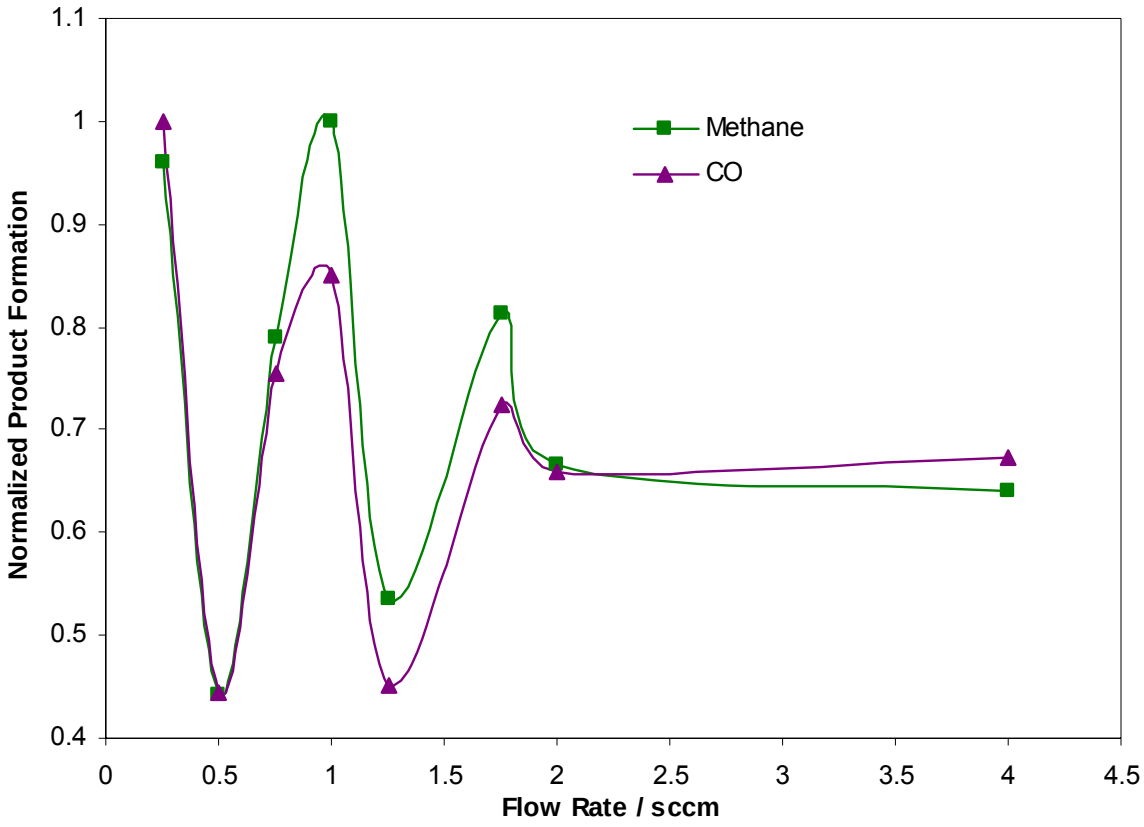

Figure 24: Plots of the relative yield variation for methane and CO following acetaldehyde ionization in samples of 1:400 CH_3CHO:Ar, as a function of total gas flow rate. Product absorption areas have been normalized with respect to the amount of acetaldehyde destroyed at each flow rate studied between 0.25 and 4sccm and with respect to the highest yield value observed for each molecule. Peaks chosen for each product are the same as those chosen for the partial pressure results.

as the product yields fluctuate drastically and in a seemingly random manner. The products methane and CO are shown separately in Figure 24 as it can be observed that these two products vary in an almost identical manner as the flow rate is altered which may suggest that these two products are mechanistically connected as will be explored in the discussion.

4.3.4 CD_3CHO/Ar EBMIS results

As a means of investigating the mechanisms of the formation of the various products experiments were performed using the isotopomer, CD_3CHO. Through the analysis of the isotopomers of the products present mechanistic information could be gathered. There are cases where two or more possible mechanisms can appropriately explain the observed products of electron bombarded acetaldehyde/Ar mixtures. However, when using the isotopomer, CD_3CHO, these different mechanisms should produce specific isotopomers over others and in this way the different mechanisms can be distinguished. For example, methane formation could involve a single CH_3CHO or multiple CH_3CHO molecules. A mixture of CD_3CHO in argon was prepared at a ratio of a 1:400. The 300V electron bombardment experiment was performed at ~50μA and in both the reference and electron bombardment experiments the flow rate and flow time were held at 1.0sccm and 2hrs respectively. The infrared spectra of the resultant electron bombardment matrices showed various new features. The products characterized were, $CD_3^{\bullet}$ (2381 and 455 cm^{-1}), d_3-methane CD_3H (2266 and 1001 cm^{-1}), CD_2CO (2260 and 2112 cm^{-1}), CO (2138 cm^{-1}), CO-water

complex (2149 cm^{-1}), $DCO^{\bullet}$ (1925, 1859 cm^{-1}), $CD_3CO^{\bullet}$ (1856 cm^{-1}), $CD_2CDO^{\bullet}$ (1511 and 1223 cm^{-1}). Figure 25 shows a portion of the difference spectrum of electron bombarded CD_3CHO/Ar mixtures. As can be observed from that Figure the isotopomer of methane, CD_3H, was observed as a very intense feature. The other possible isotopomer, CD_4, was not formed. Figure 26 compares the isotopomers of methane produced when CH_3CHO (CH_4), CD_3CDO (CD_4) or CD_3CHO (CD_3H) are used.

Table 5 below shows all of the assigned features. One product that was not able to be assigned was an isotopomer of vinyl alcohol. Rodler *et al.* have characterized nine isotopomers of vinyl alcohol however none were found to correlate with the observed features in the generated infrared spectrum. Importantly, the isotopomer CD_2=CHOD (resulting from a 1,3-H transfer of CD_3CHO, see section 2.5) was not among those previously characterized and it was therefore thought that this may have been the isotopomer generated upon electron bombardment of CD_3CHO/Ar mixtures. In an effort to provide evidence for the existence of the CD_2=CHOD isotopomer a series of computational calculations were performed in order to generate scaled vibrational frequencies for the putative CD_2=CHOD product.

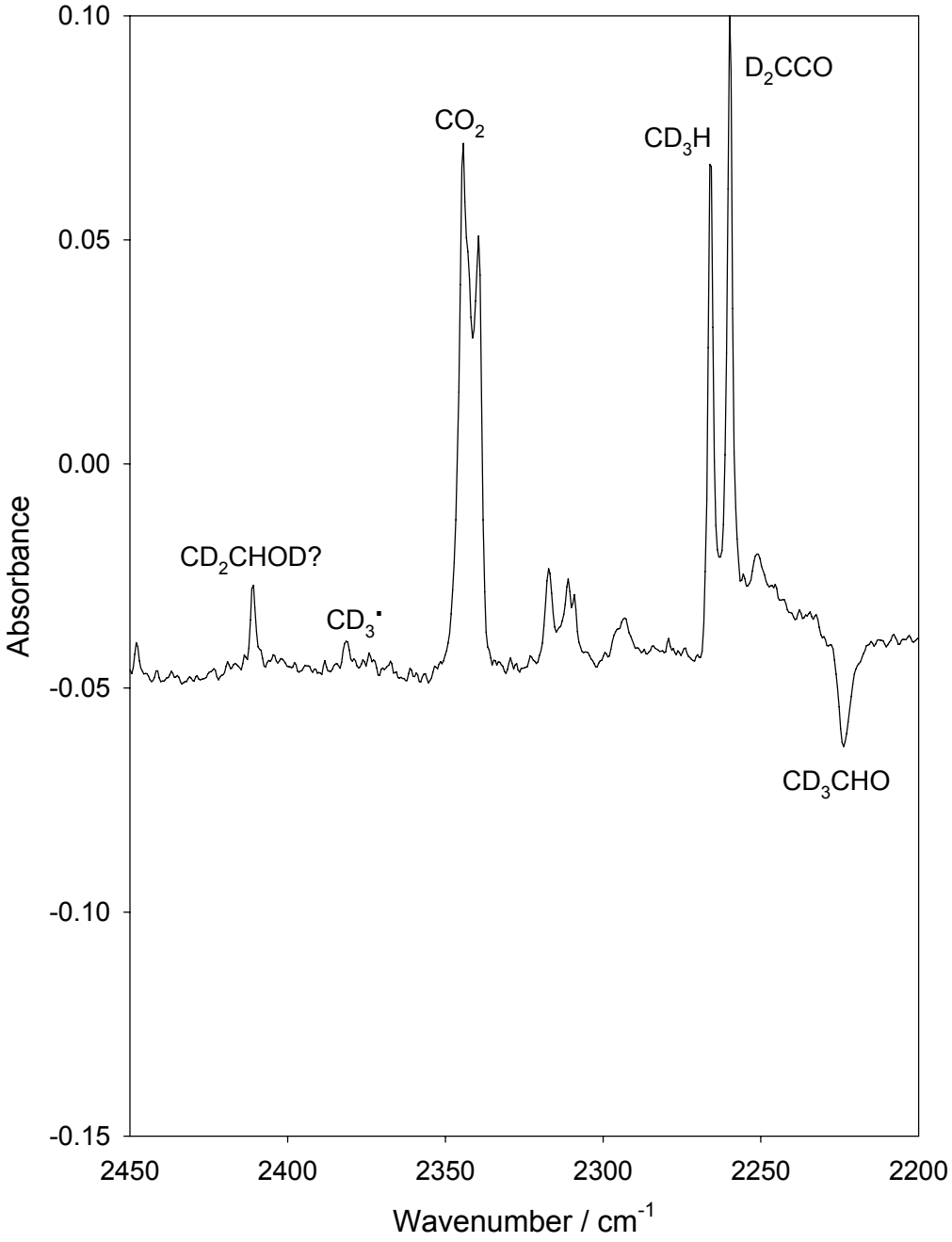

Figure 25: Portion (2450-2200 cm^{-1}) of the infrared spectrum of a 1:400 CD_3CHO:Ar sample. Shown is a difference spectrum for the matrix formed under electron bombardment conditions from which the spectrum of a reference spectrum with no electron bombardment is subtracted.

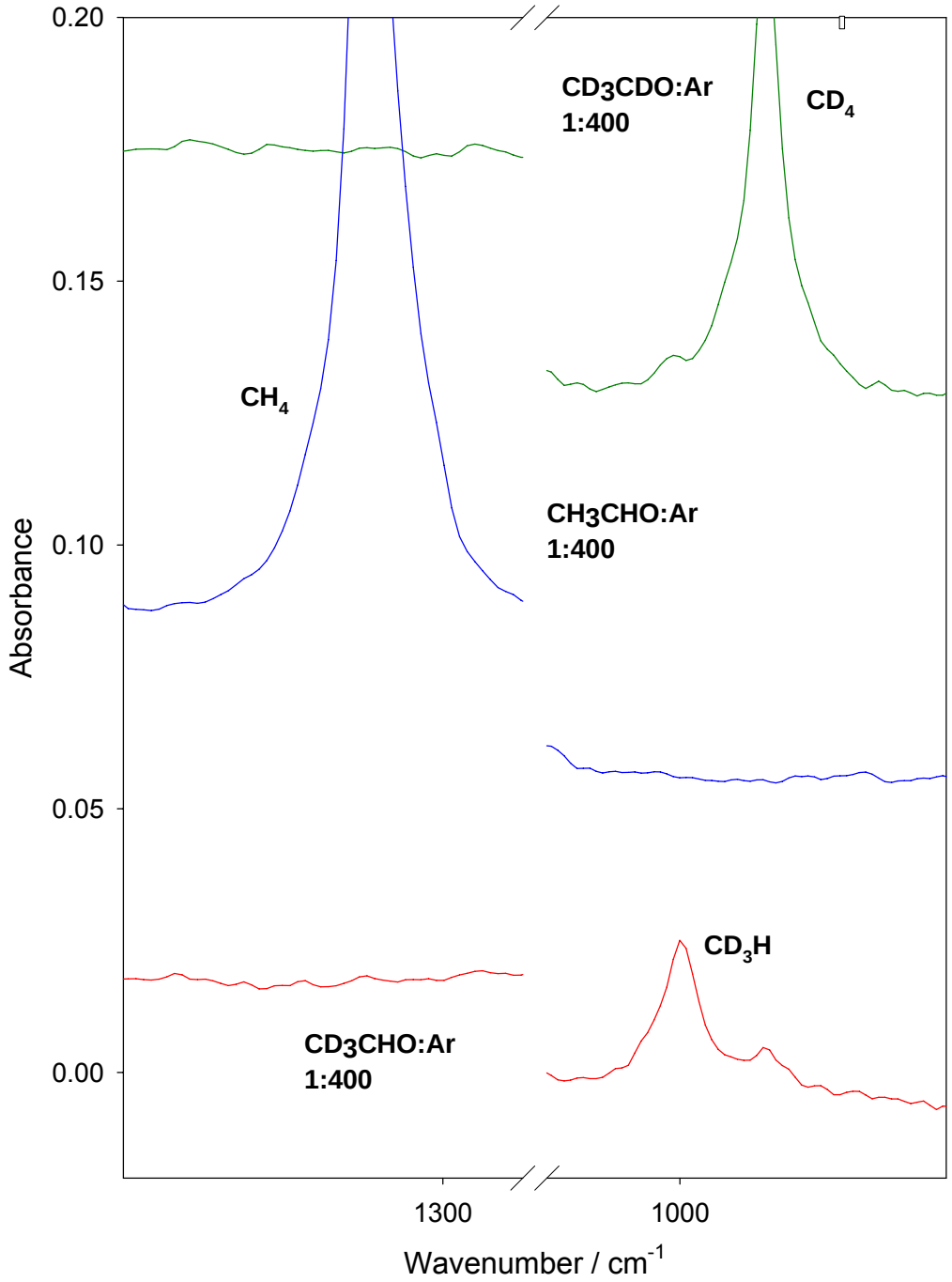

Figure 26: Portion (1310-990 cm^{-1}) of the infrared spectrum of 1:400 samples of CH_3CHO:Ar, CD_3CDO:Ar, and CD_3CHO:Ar respectively. Shown are the different isotopomers of methane produced in each case. For the CD_3CHO case there is a more intense feature associated with CD_3H at 2266 cm^{-1}.

Table 5: Infrared absorptions of characterized products formed via electron bombardment of a 1:400 mixture of CD_3CHO in argon.

CD_3CHO in Ar with EB	
Product	**Wavenumber /cm^{-1} (rel. int.)**
CD_3H	2266 (vs)
	1001 (m)
D_2CCO	2260 (s)
	2112 (vs)
CO	2138 (vs)
CO-Water Complex	2149 (vs)
$CD_3CO^{\bullet}$	1856 (m)
$DCO^{\bullet}$	1925 (m)
	1859 (m)
$CD_3^{\bullet}$	2381 (m)
	455 (m)
CD_2CDO	1511 (m)
	1223 (w)
Ar_2D^+	643 (m)
Unassigned	2119 (vs)
	1994 (s)
	1990 (s)
	1973 (s)
	1965 (m)
	1734 (s)
	1580 (s)
	1523 (s)
	1177 (s)
	1166 (s)
	942 (m)
	648 (m)

4.3.5 Computational study of the vibrational modes of CD_2=CHOD

When using calculated vibrational frequencies as a fingerprint to compare with the observed spectrum scaling factors, specific to the level of theory used, are often employed to improve the accuracy of such calculations.[19] Moreover, a complicating factor when using such computational calculations to aid in analysis of the observed spectrum in this work, is that the features in the spectrum are often shifted by small amounts as a result of the surrounding argon matrix (see section 1.2). Consequently the generation of appropriate scaling factors specific both to the level of theory employed as well as to the argon matrix in this work would be greatly beneficial. In order to generate these scaling factors the many isotopomers characterized by Rodler *et al.* were used to generate mode specific scaling factors by comparing them to calculated values for each isotopomer. These scaling factors were then averaged and applied to the calculated values for the uncharacterized CD_2=CHOD isotopomer. For example, the observed OH stretch of CH_2=CHOD as found by Rodler *et al.*[15] occurs at 2672 cm^{-1} where the calculated value was found to be 2768.85 cm^{-1}. Thus the scaling factor for this mode would be 0.9650 (2672/2768.85). To ensure that these calculated values had better correlation to the spectrum than the main competing isotopomer, CD_2=CDOH (resulting from consecutive 1,2-H-transfers of CD_3CHO, again see section 2.5), the same calculations were also performed on this molecule and compared to the observed spectrum. Table 6 below shows all of the calculations and generated scaling factors. All calculations were optimized first using DFT with the B3LYP functional and 6-311G(d,p) basis set (see section 3.6). The

program GaussView[20] was used to build input structures and visualize output structures. Gassian03[21] was used to do all of the calculations. The structure of vinyl alcohol can be either in an *anti* conformation with the oxygen hydrogen pointing outwards away from the structure or in *syn* conformation with the hydrogen pointing towards the structure. Rodler *et al.*[15] specify that their characterizations are for the *syn* conformation of vinyl alcohol and thus all of the calculations performed have been done using the *syn* conformation. Figure 27 shows as an example the optimized structure of syn-CH_2=CHOH along with corresponding bond lengths and angles.

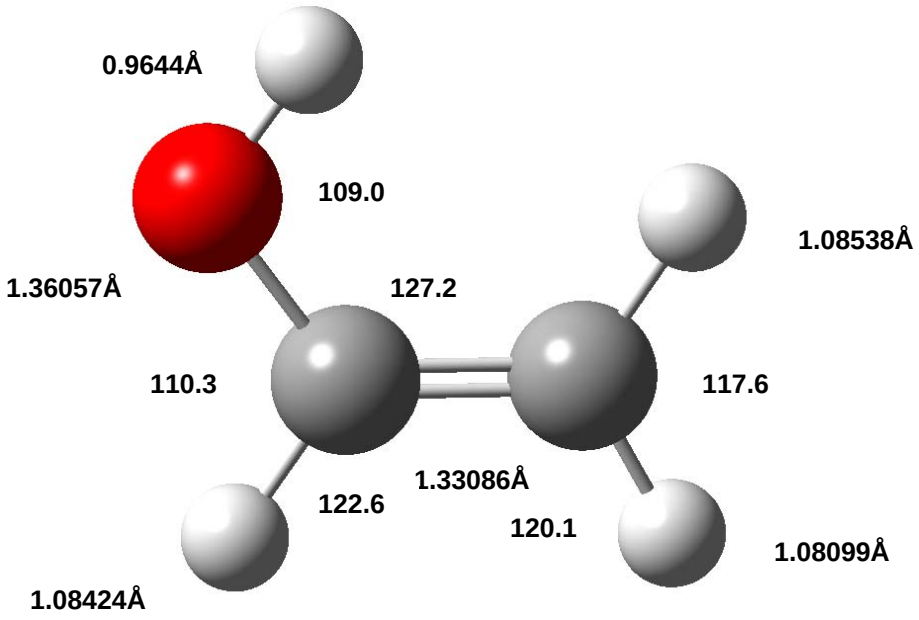

Figure 27: Geometry obtained by B3LYP/6-311G(d,p) theory for syn-CH_2=CHOH.

Table 6: Calculated frequencies (at the B3LYP/6-311(d,p) level of theory) for the various characterized isotopomers of vinyl alcohol as well the generated scaling factors.

			H_2C=CHOD			H_2C=CDOH			D_2C=CHOH		
Mode	**Symmetry**	**Description**	**Obs.**	**Calc.**	**Scaling Factor**	**Obs.**	**Calc.**	**Scaling Factor**	**Obs.**	**Calc.**	**Scaling Factor**
v_1	A'	OH stretch	2672.00	2768.85	0.9650	3621.00	3805.52	0.9515	3622.00	3805.69	0.9517
v_2	A'	CH_2 antisymmetric stretch	-	3237.62	-	-	3235.70	-	-	2408.46	-
v_3	A'	CH stretch	-	3185.94	-	-	2360.86	-	-	3187.28	-
v_4	A'	CH_2 symmetric stretch	-	3139.21	-	-	3139.44	-	-	2299.40	-
v_5	A'	C--C stretch	-	1699.11	-	-	1675.62	-	-	1662.22	-
v_6	A'	CH_2 in-plane deformation	1404.70	1440.92	0.9749	-	1430.62	-	1343.90	817.25	-
v_7	A'	CH in-plane bend	1313.90	1341.92	0.9791	-	819.24	-	-	-	-
v_8	A'	COH in-plane bend	1198.80	1224.45	0.9791	1138.40	1156.17	0.9846	-	-	-
v_9	A'	CO stretch	973.40	1008.72	0.9650	990.00	1011.06	0.9792	990.80	1155.54	0.8574
v_{10}	A'	CH_2 rock	882.00	898.76	0.9814	901.10	916.82	0.9829	-	-	-
v_{11}	A'	CCO in-plane bend	462.90	465.10	0.9953	481.20	486.41	0.9893	422.50	427.64	0.9880
v_{12}	A''	CH_2 twist	960.10	994.69	0.9652	814.10	823.84	0.9882	939.10	964.66	0.9735
v_{13}	A''	CH_2 wag	813.80	823.83	0.9878	798.10	819.24	0.9742	658.70	668.53	0.9853
v_{14}	A''	CH wag	697.80	714.14	0.9771	687.50	704.95	0.9752	-	964.66	-
v_{15}	A''	CO torsion	321.20	366.95	0.8753	411.70	471.56	0.8731	397.40	449.27	0.8845

Table 6 (continued):

			H_2C=CHOH			D_2C=CDOD			D_2C=CDOH		
Mode	**Symmetry**	**Description**	**Obs.**	**Calc.**	**Scaling Factor**	**Obs.**	**Calc.**	**Scaling Factor**	**Obs.**	**Calc.**	**Scaling Factor**
ν_1	A'	OH stretch	3619.90	3805.70	0.9512	2677.00	2769.50	0.9666	3621.60	3805.50	0.9517
ν_2	A'	CH_2 antisymmetric stretch	-	3237.64	-	2411.00	2409.80	1.0005	-	2409.87	-
ν_3	A'	CH stretch	-	3185.27	-	-	2365.68	-	-	2366.30	-
ν_4	A'	CH_2 symmetric stretch	-	3139.21	-	-	2291.17	-	-	2291.25	-
ν_5	A'	C--C stretch	1661.90	1702.79	0.9760	1583.00	1628.03	0.9723	1583.00	1630.90	0.9706
ν_6	A'	CH_2 in-plane deformation	1409.40	1448.41	0.9731	921.00	941.38	0.9784	-	1326.23	-
ν_7	A'	CH in-plane bend	1325.50	1359.11	0.9753	-	991.36	-	-	984.08	-
ν_8	A'	COH in-plane bend	1300.20	1326.63	0.9801	-	1088.38	-	989.10	1000.50	0.9886
ν_9	A'	CO stretch	-	1125.93	-	-	1190.50	-	966.00	1177.22	0.8206
ν_{10}	A'	CH_2 rock	942.60	960.91	0.9809	-	763.99	-	792.10	803.85	0.9854
ν_{11}	A'	CCO in-plane bend	486.10	491.36	0.9893	-	405.95	-	418.20	423.46	0.9876
ν_{12}	A''	CH_2 twist	971.40	997.90	0.9734	-	775.32	-	757.60	777.58	0.9743
ν_{13}	A''	CH_2 wag	813.70	823.83	0.9877	651.00	656.08	0.9923	649.90	658.60	0.9868
ν_{14}	A''	CH wag	698.20	714.55	0.9771	-	566.98	-	-	574.54	-
ν_{15}	A''	CO torsion	413.30	473.58	0.8727	-	347.31	-	398.20	449.27	0.8863

4.4 References for Chapter 4

[1] Robinson, M. *MSc. Thesis*, Queen's University, Kingston, ON, Canada

[2] Molecules such as CO, CH_4, ethane, ethene, ethyne, propane, propene, and propyne and corresponding isotopomers have previously been obtained from commercial sources and have been isolated in Ar under matrix isolation conditions in our own laboratory thus have been characterized via FTIR spectroscopy.

[3] Jacox, M.E. *Chemical Physics*. **1982**, 69, 407.

[4] Jacox, M.E.; Milligan, D.E. *Chemical Physics.* **1974**, 4, 45.

[5] Milligan D. E. and Jacox M. E. *J. Chem. Phys.* **1969**, *51*, 277.

[6] Moore, B.C.; Pimentel, G.C. *J. Chem. Phys.,* **1963**, 38, 2816.

[7] Leroi, G.E.; Ewing, G.E.; Pimentel, G.C. *J. Chem. Phys.* **1964**, 40, 2298.

[8] Khoshkhoo, H.; Nixon, E.B., *Spectromchim. Acta,* **1973**, 23, 603.

[9] DeKock, R.L.; Weltner, W.J. *J. Am. Chem. Soc.* **1971**, 93, 7106.

[10] Pullin, D.E.; Rice, E.H.N.; Rodler, M. *J. Am. Chem. Soc.* **1985**, 107, 7877.

[11] Fridgen, T.D.; Parnis, J.M. *J. Chem. Phys.* **1998**, 109, 2155.

[12] Parnis, J.M.; Thompson, M.G.K.; King, K. Unpublished results, **2008**

[13] Jacox, M.E. *J. Mol. Spectro.* **1977**, 66, 272.

[14] Hawkings, M.; Andrews, L. *J. Am. Chem. Soc.* **1983**, 105, 2523.

[15] Rodler, M.; Blom, C.E.; Bauder, A. *J. Am. Chem. Soc.* **1984**, 106, 4029.

[16] Shimanouchi T. *Table of MolecularVibrational Frequencies Consolidated Volume I*, National Bureau of Standards, **1972**.

[17] Thompson, M.G.K.; Parnis, J.M. *Inorg. Chem.* **2008**, 47, 4045.

[18] Parnis, J.M.; Thompson, M.G.K.; King, K. *Int. J. Mass. Spectrom.* **2009**, in press.

[19] Scott, A.P.; Radom, L. *J. Phys. Chem.* **1996**, 100, 16502.

[20] GaussView, Version 3.09, Dennington II, Roy; Keith, Todd; Millam, John; Eppinnett, Ken; Hovell, W. Lee; and Gilliland, Ray; Semichem, Inc., Shawnee Mission, KS, 2003.

[21] Gaussian 03, Revision C.01 Frisch, M. J.; Trucks, G. W.; Schlegel, H. B.; Scuseria, G. E.; Robb, M. A.; Cheeseman, J. R.; Montgomery, Jr., J. A.; Vreven, T.; Kudin, K. N.; Burant, J. C.; Millam, J. M.; Iyengar, S. S.; Tomasi, J.; Barone, V.; Mennucci, B.; Cossi, M.; Scalmani, G.; Rega, N.; Petersson, G. A.; Nakatsuji, H.; Hada, M.; Ehara, M.; Toyota, K.; Fukuda, R.; Hasegawa, J.; Ishida, M.; Nakajima, T.; Honda, Y.; Kitao, O.; Nakai, H.; Klene, M.; Li, X.; Knox, J. E.; Hratchian, H. P.; Cross, J. B.; Bakken, V.; Adamo, C.; Jaramillo, J.; Gomperts, R.; Stratmann, R. E.; Yazyev, O.; Austin, A. J.; Cammi, R.; Pomelli, C.; Ochterski, J. W.; Ayala, P. Y.; Morokuma, K.; Voth, G. A.; Salvador, P.; Dannenberg, J. J.; Zakrzewski, V. G.; Dapprich, S.; Daniels, A. D.; Strain, M. C.;

Farkas, O.; Malick, D. K.; Rabuck, A. D.; Raghavachari, K.; Foresman, J. B.; Ortiz, J. V.; Cui, Q.; Baboul, A. G.; Clifford, S.; Cioslowski, J.; Stefanov, B. B.; Liu, G.; Liashenko, A.; Piskorz, P.; Komaromi, I.; Martin, R. L.; Fox, D. J.; Keith, T.; Al-Laham, M. A.; Peng, C. Y.; Nanayakkara, A.; Challacombe, M.; Gill, P. M. W.; Johnson, B.; Chen, W.; Wong, M. W.; Gonzalez, C.; and Pople, J. A.; Gaussian, Inc., Wallingford CT, 2004.

Chapter 5

Discussion

5.0 Butanal

From section 4.1 it can be observed that electron bombardment of dilute butanal/Ar mixtures produces a variety of decomposition products. Only two of the observed products can be attributed directly to C—C bond cleavages, $HCO^{\bullet}$ and $CH_2CHO^{\bullet}$. The formyl radical ($HCO^{\bullet}$) can be attributed to α-cleavage which could directly form $HCO^{\bullet}$ or alternatively it could result in the cation, HCO^{+}, which then becomes neutralized while embedded in the matrix upon capturing a stray secondary electron.

Scheme 2: Formation of the formyl radical, $HCO^{\bullet}$, from the α-cleavage of the butanal radical cation.

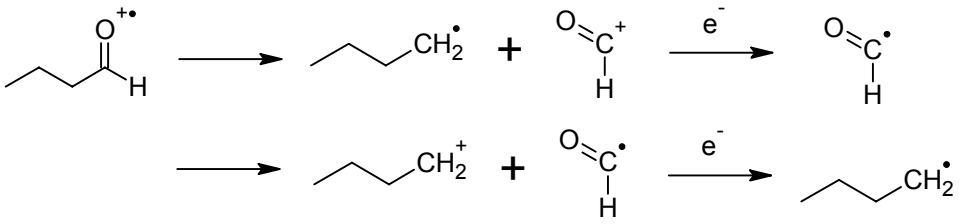

Similarly, the $CH_2CHO^{\bullet}$ radical can be attributed to β-cleavage of the butanal radical cation resulting in either direct formation of the radical or formation of the cation which then becomes neutralized.

Scheme 3: Formation of the $CH_2CHO^{\bullet}$ radical, from the β-cleavage of the butanal radical cation.

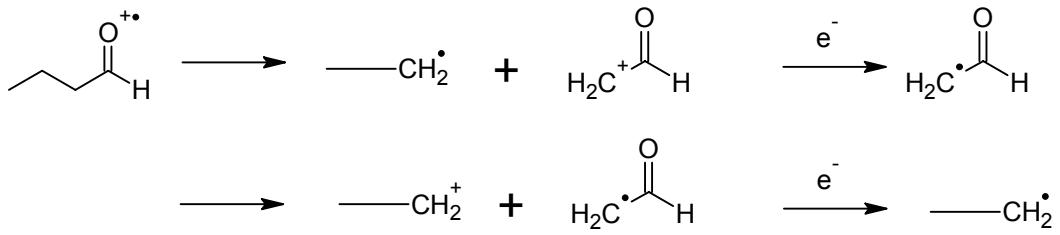

It must be noted, however, that while both reactions (i.e. opposite radical and cation sites of the incipient products) occur to a certain extent, one pathway is often thermodynamically favored. Because most products become neutralized in the EBMIS experiments performed in this work, it is not possible to distinguish between the two possibilities. Thus, in order to determine which of the two incipient fragments will preferably keep the charge Stevenson's rule can be invoked. According to Stevenson's rule, when fragmentation takes place, the positive charge more dominantly remains on the fragment with the lowest ionization energy.[1] Even though one fragmentation route might be dominant it does not preclude the other from occurring and therefore both processes are possible. Schemes 2 and 3 above show the cleavages associated with the formation of $HCO^{\bullet}$ and $CH_2CHO^{\bullet}$ respectively.

In contrast to the radical species $HCO^{\bullet}$ and $CH_2CHO^{\bullet}$, which can be explained by the simple C—C cleavages shown in the scheme above, the other products characterized must stem from additional reactivity of newly formed primary products. Except for ketene (which will be discussed later), these

products are thought to result from hydrogen atom abstraction, hydrogen atom scavenging or dehydrogenation through H_2 loss.

The products that are believed to be formed through H-atom abstraction or scavenging are propane ($CH_3CH_2CH_3$), methane (CH_4) and formaldehyde (H_2CO). As with electrons it has previously been shown that $H^{\bullet}$ and H^+ are small enough to be mobile in an argon matrix.[2] This is also evident by the very intense feature associated with the proton-bound argon dimer, Ar_2H^+ ($904cm^{-1}$). It is possible that there may be free $H^{\bullet}$ available within the matrix that could promote further chemistry. Consequently, a primary product such as the propyl radical ($CH_3CH_2CH_2^{\bullet}$), which would initially be formed upon α-cleavage (see scheme 2) can come into contact with such free H-atoms in the matrix. Such radical recombination chemistry has been previously observed and explored within the EBMIS apparatus. As reviewed in chapter 2, Fridgen and Parnis[3] attribute many of the observed products of electron bombarded oxalyl chloride to such H-atom scavenging and more recently this type of re-encounter chemistry has been probed through the investigation of the decomposition chemistry of acetone[4] and dimethyl ether.[5] The absence of any features that correlate with the propyl radical or methyl radical supports this assertion as these species are probably greatly diminished through the formation of propane and methane respectively.

Although $H^{\bullet}$ atom scavenging by $CH_3^{\bullet}$ and $HCO^{\bullet}$ adequately explains the formation of CH_4 and H_2CO there are further possibilities that can account for the formation of propane. In addition to the possibility of scavenging of *free* $H^{\bullet}$ atoms, hydrogen abstraction might also occur between one radical and a

proximally located species within the matrix. For example, α-cleavage results in the formation of $CH_3CH_2CH_2^{\bullet}$ and $HCO^{\bullet}$ (after subsequent neutralization in the matrix as discussed above) and because of the relatively high pressures of the EBMIS apparatus prior to condensation, the migration of these two incipient species upon initial fragmentation of the parent ion would be inhibited. Thus, it may be likely that upon matrix isolation these two species are proximal to each other which would allow $H^{\bullet}$ abstraction by $CH_3CH_2CH_2^{\bullet}$ from $HCO^{\bullet}$ yielding the two closed-shell species $CH_3CH_2CH_3$ and CO. This also explains the formation of neutral CO which is observed as a very intense feature in all of the spectra generated. Finally, it is possible that radical catonic propane is formed immediately through unimolecular elimination of neutral CO. This is based on a similar process for the unimolecular elimination of CO from propanal which will be further discussed when exploring the propanal results.[6]

The majority of the other products including propene, propyne, ethene, ethyne, CCCO, and the allyl radical can all be explained through progressive H_2 loss of the originally formed products. Suzer and Andrews[7] have studied the matrix-isolated products of electron bombarded ethane/Ar mixtures similar to the EBMIS conditions employed in this work. It was found that such electron bombardment of dilute ethane/Ar mixtures resulted in the formation of dehydrogenated products such as ethene and ethyne. The formation of these products was attributed to multiple ionization events each followed by H_2 loss from the parent species. For example, ethene was formed as a decomposition product of ionized ethane and, in turn, ethyne was formed as a decomposition

product of ionized ethene (which was ionized upon its formation). Furthermore, Parnis *et al.* when investigating the gas-phase chemistry of acetone under EBMIS conditions concluded that the observed formation of ethene, ethyne and CCCO were a result of secondary ionization of ethane through additional charge transfer ionization with $Ar^{\bullet+}$. Thus, propene is formed from H_2 loss of ionized propane and propyne is formed from ionized propene. Scheme 4 shows the purported reaction processes leading the formation of propene and propyne. The allyl radical, $CH_2{=}CHCH_2^{\bullet}$ is believed to stem from immediate H_2 loss of the propyl radical prior to it undergoing any hydrogen abstraction reactions.

Scheme 4: Net reaction processes for propane dehydrogenation leading to propene and propyne.

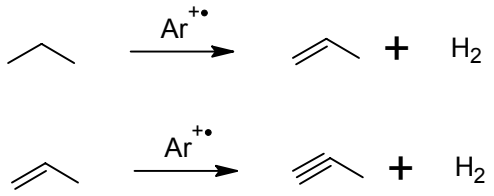

The formation of ethene, ethyne and CCCO are believed to be formed in a similar manner to that of propene and propyne except rather than originating from propane these dehydrogenation products stem from ethane. Although no modes corresponding to ethane were observed it is believed that this is due to the extensive dehydrogenation it undergoes and therefore its initial formation can be implicated. The formation of ethane is believed to occur via $H^{\bullet}$ abstraction of

the ethyl radical subsequent to the β-fragmentation of the initial parent ion. Scheme 5 summarizes the dehydrogenation reactions leading to the production of ethene, ethyne and finally CCCO. The final dehydrogenation product, CCCO, is believed to result from re-encounter chemistry between C_2 and CO as previously explored by Parnis *et al.* Thus, the observation of CCCO provides indirect evidence for the production of fully dehydrogenated product, C_2.

Scheme 5: Net reaction processes for the dehydrogenation of ethane leading to ethene, ethyne and CCCO.

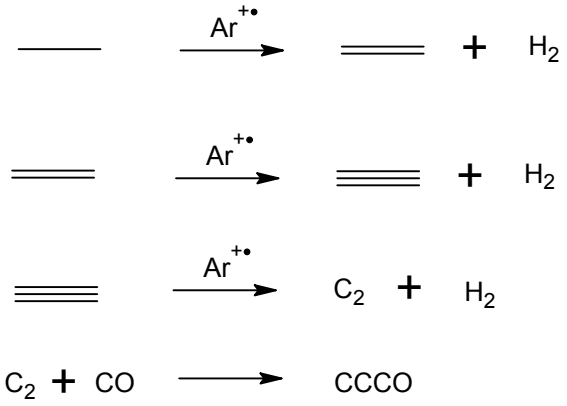

Although support for secondary ionization schemes, explaining the formation of the various dehydrogenation products, can be found in prior studies, the experiments performed at both high (70μA) and low (15μA) electron currents provide further evidence in support of this interpretation. From Figure 13 it can be observed that when only a 15μA current is generated during electron bombardment the features associated with propene, ethyne, and the allyl radical all substantially decrease in intensity. It was mentioned in section 4.1 however

that this may have simply been a result of the decreased parent ion destruction and not a result of dehydrogenation processes being inhibited. If these products were inhibited it would be suspected that less dehydrogenated products would decrease less substantially than more fully dehydrogenated products. From Figure 13 it can be noticed the partially dehydrogenated products propene and the allyl radical still appear as appreciable features in the 15μA spectrum; however, ethyne, a more fully dehydrogenated species, appears as an intense feature in the 70μA spectrum however is completely absent in the 15μA spectrum. This provides support for the mechanism described above as it is believed that under a 15μA current, electron ionization of argon was more limited and therefore the probability that the various alkenes would be further ionized and consequently undergo further dehydrogenation decreases dramatically.

The formation of ketene is believed to be a result of an ion-molecule interaction between CH_2CHO^+ and the $CH_3CH_2^\bullet$ products formed initially after β-fragmentation. As a result of the relatively high pressures of the EBMIS environment it is likely that these two species, upon their formation, would be maintained in close proximity to each other. It is therefore believed that $CH_3CH_2^\bullet$ abstracts the α-H-atom from CH_2CHO^+ which thereby forms ketene and provides another possible route for ethane formation (in fact this is similar to one of the possible mechanisms considered for propane and CO formation as described earlier). It should be noted here that ketene formation is observed when either butanal, propanal or acetaldehyde is used as the precursor molecule and it is thought the mechanism of ketene formation is similar in all three cases where

ketene is a result of bimolecular chemistry. Evidence accrued through work with acetaldehyde supports the bimolecular mechanism of ketene formation (see section 4.3). The mechanism for ketene formation from butanal is shown below in Scheme 6 below.

Scheme 6: Showing the purported general mechanism for ketene formation from $CH_2CHO^{\bullet}$.

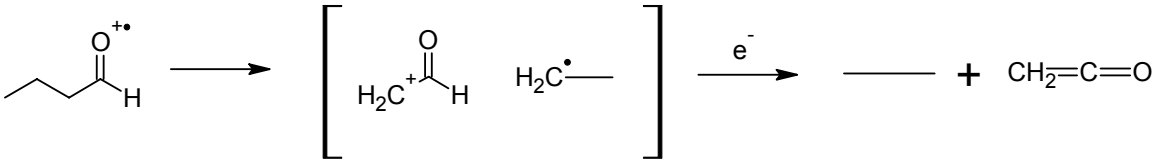

An unexpected result was the observation that the McLafferty Rearrangement (McLR) was not occurring under the EBMIS conditions in this work as evidenced by the lack of presence of any modes associated with vinyl alcohol (one of the expected products of McLR). Figure 14 clearly shows that at all partial pressures of butanal/Ar the McLR does not occur. The appearance energy of the McLR as found by Traeger and Djordjevic[8] is 10.46eV, which is well below the ~16eV that charge transfer ionization with argon would access (see section 2.1.1). As discussed in section 1.3 and illustrated in Figure 4 the rate constants of different reactions change as the energy increases. Although the McLR may initially occur at a lower appearance energy than other competitive fragmentation pathways, as the energy is increased other reaction pathways become accessible and as a result of their loose transition states are

kinetically much faster. Thus, it is possible that because charge transfer ionization with argon transfers such a large amount of energy to the incipient ion it is possible that other unimolecular reactions are being favored over the McLR. Furthermore, the relatively high pressures of the EBMIS apparatus compared to traditional mass spectrometric sources may be why other pathways are being favored over the McLR.

5.1 Propanal

The results of the EBMIS experiments of propanal are very similar to those obtained when butanal was used as the precursor molecule. A variety of decomposition products were obtained of which only three can be attributed to simple C—C bond cleavages, $HCO^{\bullet}$, $CH_2CHO^{\bullet}$ and $CH_3CH_2^{\bullet}$. The appearance energies of the characterized reaction pathways, as reported by Dannacher and Stadelmann[9], are all below the ~16eV energy range associated with charge transfer ionization with argon. Thus, energetically the formation of the above three species can be appropriately accounted for in terms of simple C—C cleavages. These species may have originally been formed as radicals or they may have been formed as cations that were then neutralized in the matrix to form their radical counterparts. A combination of these two processes is also probable.

The radical species, $CH_2CHO^{\bullet}$ is formed from β-cleavage of the parent ion and the formyl radical, $HCO^{\bullet}$ and the ethyl radical, $CH_3CH_2^{\bullet}$ are thought to have formed concurrently upon α-cleavage. Along with the $CH_2CHO^{\bullet}$ radical, the methyl radical, $CH_3^{\bullet}$ is also formed upon β-cleavage. It is believed, however, that

the methyl radical is forming methane from scavenging a hydrogen atom from free H$^{\bullet}$ atoms in the matrix or through the abstraction of an H-atom from another proximally located radical species. Methane formation will be discussed further below when discussing the mechanism of ketene formation. These fragmentation pathways are shown in Scheme 7.

Scheme 7: Reaction pathways leading to the formation of the formyl radical, HCO$^{\bullet}$, the ethyl radical $CH_3CH_2^{\bullet}$, the $CH_2CHO^{\bullet}$ radical and finally methane. The H-atom obtained by methane could be from scavenging a free H$^{\bullet}$ radical or from H-atom abstraction from a proximal radical species.

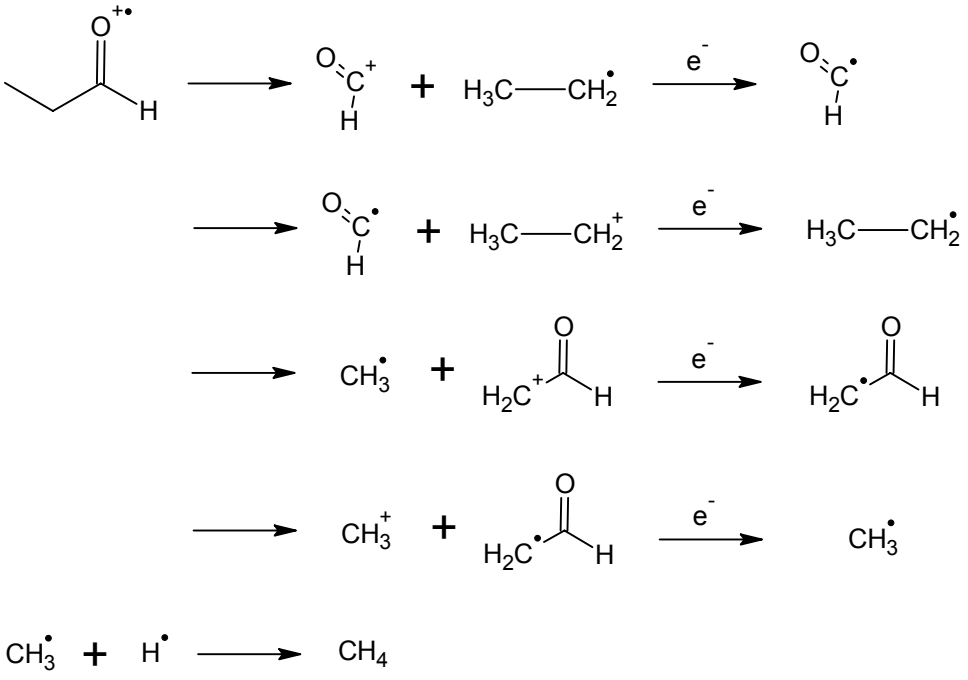

The features in the IR spectra obtained corresponding to HCO$^{\bullet}$ and $CH_3CH_2^{\bullet}$ respectively are relatively weak in intensity and therefore it is believed

that this fragmentation pathway is occurring to a lesser extent than another competitive pathway. As previously explored in terms of some of the products obtained with butanal, upon cleavage, as a result of the relatively high pressures of the EBMIS system, migration of the two incipient species would be inhibited. As a result it is possible the two radical species $HCO^{\bullet}$ and $CH_3CH_2^{\bullet}$ are proximal to each other which would could promote H-atom transfer. Consequently, $CH_3CH_2^{\bullet}$ would abstract the H-atom from $HCO^{\bullet}$ which would result in the simultaneous formation of ethane and CO (Scheme 8a).

It is also possible that neutral CO elimination occurs to form $CH_3CH_2^{\bullet+}$ via an ion-molecule complex and thus ethane formation could occur without the independent radicals forming that subsequently re-encounter (Scheme 8b). This reaction pathway was introduced in section 2.4 while reviewing the gas-phase chemistry of propanal. A paper by Hudson *et al.* investigating the energetics of this process found that, at intermediate energies (11.40-12.0eV), neutral CO elimination is favored over the α-cleavage pathway but that at higher energies (>12.0eV) this is reversed where α-cleavage becomes the dominant pathway. The reason suggested for this is that at higher energies α-cleavage occurs so quickly that there is insufficient time for the implicated ion-molecule interaction to occur. The ~16eV energy range obtained with Ar charge transfer ionization is well above 12.0eV which may suggest that α-cleavage should be favored. Observation of the infrared spectrum showing the matrix-isolated products of electron bombarded propanal shows that the features associated with $CH_3CH_2^{\bullet}$ and $HCO^{\bullet}$ are much weaker than the features corresponding to ethane (and its

dehydrogenated products, see below) and CO. This indicates that ethane and CO are being formed in enough yields so as to lead to intense features in the resultant IR spectrum. As a result of this observation, in contrast to the earlier purely gas-phase studies, it is thought that under EBMIS conditions CO elimination is out-competing α-cleavage.

Scheme 8: (a) Showing a possible mechanism of ethane formation via α-cleavage followed neutralization and then radical-radical recombination (b) another mechanism of ethane formation via an ion-molecule complex with the elimination of neutral CO.

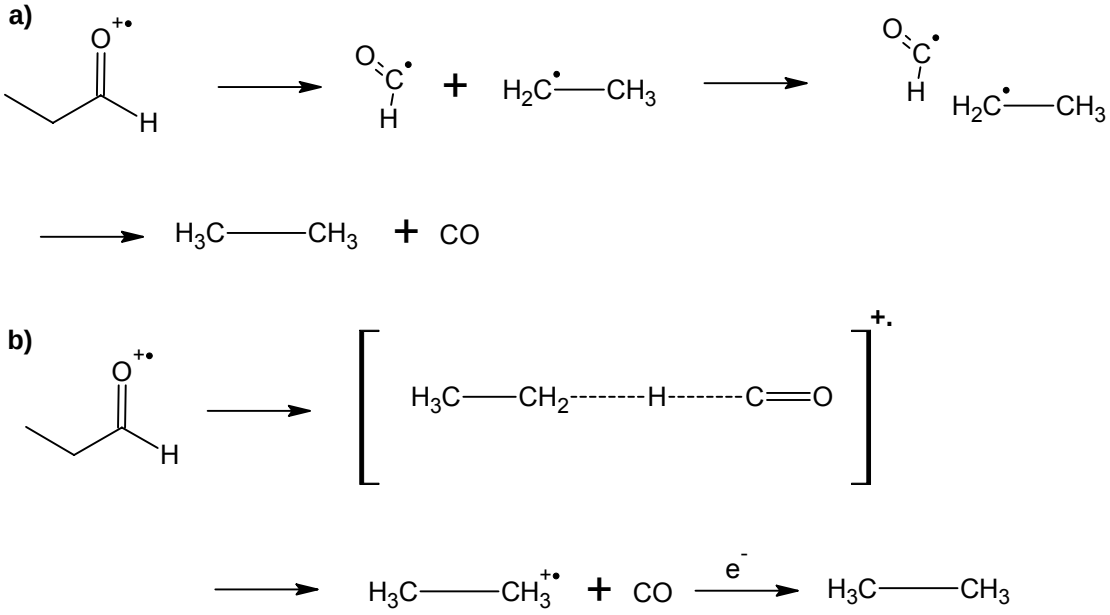

Moreover, in the EBMIS apparatus the relatively higher pressures may be favoring neutral CO elimination as the high pressures would potentially favor the

formation of an ion-molecule complex. Moreover, the higher pressures may inhibit the competing process from occurring as rapidly when compared to other typical gas-phase environments.

As mentioned along with ethane the following dehydrogenation products were also characterized: ethene, ethyne, and CCCO. This type of dehydrogenation chemistry is entirely congruent with the same processes observed with butanal where in additionally propene and propyne were also observed. Overall dehydrogenation chemistry is believed to result from consecutive processes involving neutralization of the incipient product followed by re-ionization and H_2 loss. The product, CCCO, is a believed to be formed through reaction of C_2 with CO. This dehydrogenation chemistry is summarized in Scheme 9.

Scheme 9: Net dehydrogenation reactions beginning with ethane which lead to the formation of ethene, ethyne and CCCO.

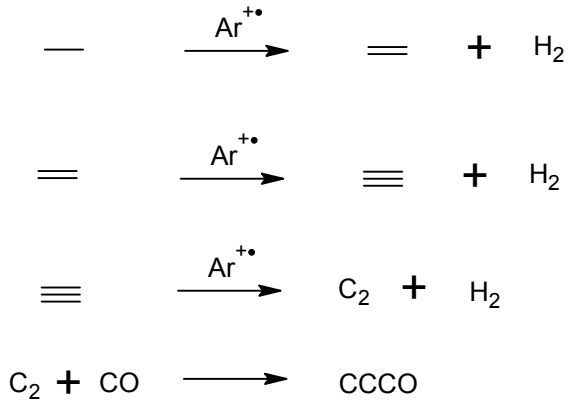

Other than Ar_2H^+ and the CO-water complex, which are two products that always form upon electron bombardment of a carbonyl species diluted in argon, the only other product characterized was ketene. Ketene formation is thought to result from re-encounter chemistry between $CH_3^{\bullet}$ and $CH_2CHO^{\bullet}$ where the methyl radical abstracts the α-H atom from the $CH_2CHO^{\bullet}$ radical thereby concurrently forming methane, CH_4 and ketene CH_2CO. This mechanism is shown in Scheme 10.

Scheme 10: Showing the reaction mechanism from the parent ion leading to methane and ketene formation.

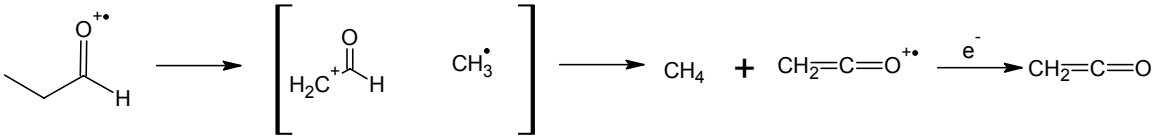

One final aspect that needs to be addressed is why tautomerization of the propanal radical cation to ionized 1-propen-1-ol was not observed to occur despite the enol isomer's greater stability. A theoretical study by Bouma *et al.*[10] found that ionized 1-propen-1-ol was 93kJmol^{-1} more stable than cationic propanal. The greater stability of 1-propen-1-ol over its corresponding keto isomer is even more pronounced in the case of propanal than with acetone where the same study cited above found its enol isomer, 1-propen-2-ol, to be only 40kJmol^{-1} lower in energy. However, despite the favorable thermodynamics no isomerization chemistry was observed for the EBMIS investigation of

propanal. In contrast, acetone isomerizes significantly to 1-propen-2-ol under EBMIS conditions.[11] As reviewed in section 2.1.2 the mechanism of enol formation of acetone in the EBMIS apparatus is believed to be a self-catalyzed 1,3-H-transfer. Consequently, in order for this pathway to be followed two acetone molecules must interact in the correct orientation in order to promote this H-transfer. In kinetics the condition requiring the correct orientation in order for a reaction to proceed has been termed the steric factor. Thus, it is believed that the acetone molecule's more symmetrical structure facilitates this self-catalyzed isomerization reaction as the probability of the two acetone molecules interacting in the correct manner would be much greater than for two propanal molecules which lack this symmetry. Furthermore, acetone only has one competing fragmentation pathway corresponding to the formation of the acetyl and methyl radicals whereas propanal has two possible α-cleavages and a β-cleavage. The additional fragmentation routes offer greater competition for the possible isomerization reaction. These two factors explain why the enol isomer was not observed in the propanal EBMIS studies.

5.2 Acetaldehyde

Electron bombardment of dilute acetaldehyde/Ar mixtures produced many decomposition products. Unlike butanal and propanal the size of the resultant fragments precluded further secondary dehydrogenation reactions from occurring which enabled a more thorough investigation of the chemistry. Furthermore, the tautomer of acetaldehyde, vinyl alcohol was also observed based on the

characterization of Hawkins and Andrews.[12] and consequently experiments were performed to explore how different controllable variables within the EBMIS apparatus effected whether unimolecular or bimolecular products were favored.

The closed-shell species methane and CO as well as the radical species $CH_3CO^{\bullet}$, $HCO^{\bullet}$, $CH_2CHO^{\bullet}$, and $CH_3^{\bullet}$ were all originally thought to be formed through unimolecular decomposition of the parent ion. Methane and CO were believed to be formed simultaneously through an ion-molecule complex leading to the elimination of neutral CO and radical cationic methane. This is a similar process to that described earlier in regards to ethane formation from electron bombardment of propanal/Ar mixtures. However, it is also possible that the methane formation occurs as a result of H-atom abstraction by the methyl radical from a proximally located species. Schemes 11, 12, 13 and 14 below show the possible decomposition routes leading to the aforementioned products. As before cations become neutralized by capturing stray secondary electrons within the matrix and therefore all species are found as radicals or closed-shell neutrals in the case of methane and CO.

Scheme 11: Possible reaction pathways explaining the formation of the acetyl radical, $CH_3CO^{\bullet}$.

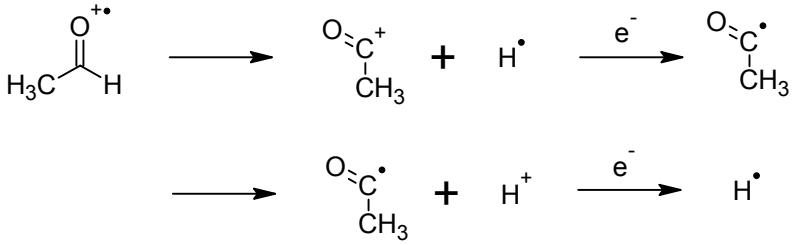

Scheme 12: Possible reaction pathways explaining the formation of the methyl ($CH_3^{\bullet}$) and formyl radicals ($HCO^{\bullet}$).

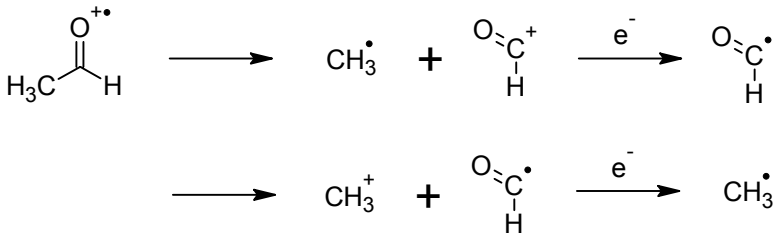

Scheme 13: Possible reaction pathway explaining the formation of CO and methane.

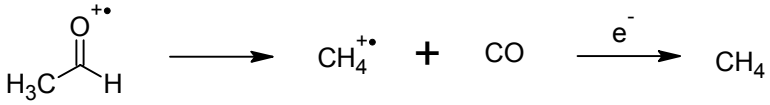

Scheme 14: Possible reaction pathway leading to the formation of the $CH_2CHO^{\bullet}$ radical.

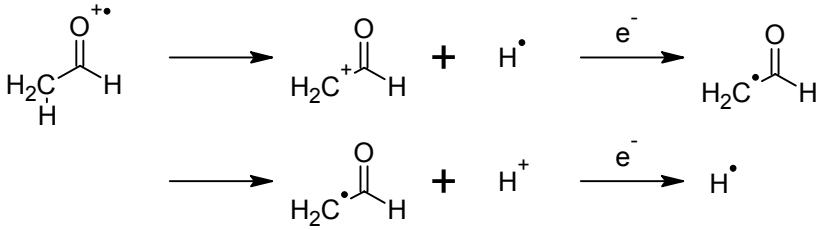

In order to confirm the product assignments experiments were performed with fully deuterated acetaldehyde. In all cases the corresponding deuterated product

was obtained. Thus, the products CD_4, D_2CCO, $CD_3CO^{\bullet}$, CD_2CDOD, $CD_2CDO^{\bullet}$, $DCO^{\bullet}$, $CD_3^{\bullet}$ and Ar_2D^+ were all obtained when using d_4-acetaldehyde, CD_3CDO, as the precursor. The characterization of the acetyl and methyl radicals was particularly important as they confirmed the previous assignments by Jacox[13,14] which were not entirely conclusive.

5.2.1 Product dependence on the partial pressure of acetaldehyde

In order to ascertain further information regarding the nature of the formation of the various products a series of experiments were performed in which the partial pressure of acetaldehyde was varied. It was hoped that these experiments would aid in characterizing the various products as either resulting from unimolecular chemistry or, in contrast, bimolecular chemistry. Previous work has suggested that high partial pressures of the precursor promote bimolecular chemistry and that as the partial pressure is progressively decreased the chemistry transitions into more traditional unimolecular decomposition processes that have been exemplified by previous gas-phase mass spectrometric studies. Thus, it was thought that by observing the changes in product yields that occur as the partial pressure of acetaldehyde was varied the various products could be categorized as either occurring via unimolecular or bimolecular chemistry. For example, as mentioned earlier, methane formation may occur via unimolecular elimination of CO or instead may occur via bimolecular radical-radical recombination. By observing how methane formation

changes with varying acetaldehyde partial pressure evidence can be accrued supporting one of the putative processes.

Figure 21 shows that $CH_3^{\bullet}$, $CH_2CHO^{\bullet}$, $HCO^{\bullet}$, CH_4 and CO all decrease as the partial pressure of acetaldehyde is increased. Thus, these products are maximized at low acetaldehyde partial pressure which mimics more traditional gas-phase environments. Concordantly this suggests that the above products are all formed via unimolecular decomposition. The product $CH_2CHO^{\bullet}$ is not an expected decomposition product as its energetics have not been previously characterized as its appearance energy is precluded from a recent summary of all the known appearance energies for the various decomposition pathways of ionized acetaldehyde.[15] This is most likely due to the fact that it is formed immediately as a radical and therefore methods which probe cations would not be able to gather information on this process. In contrast to Figure 21, Figure 22 shows that the products vinyl alcohol, $CH_3CO^{\bullet}$ and ketene all maximize at intermediate mole ratios of acetaldehyde and are minimized at both low and high partial pressures of acetaldehyde. Thus, it is believed that those three products form as a result of bimolecular chemistry. The observation that ketene product yield is altered in similar way to that of vinyl alcohol suggests that ketene is being formed via a bimolecular interaction which provides evidence for the mechanisms of ketene proposed earlier with respect to ionized butanal and propanal.

It is not completely understood why the products of acetaldehyde ionization that dominate in the intermediate mole ratio range such as vinyl alcohol are observed to diminish at high mole ratios of acetaldehyde:Ar. At these

high pressures it is expected that re-encounter chemistry would be prevalent where initial ionization and isomerization products would interact with each and cause further chemistry to ensue. Parnis *et al.* observed a similar trend with respect to the bimolecular products of ionized acetone. In that investigation it was observed that the products 1-propen-2-ol, and ketene both maximize at intermediate mole ratios and diminish at high mole ratios of acetone:Ar. This effect was explained by attributing the observed diminishing of the two products to an increase in encounters between initial ionization decomposition products with both acetone and the products of methyl radical (an implicated initial decomposition product) reactions with acetone, 1-propen-2-ol and ketene. At high concentrations of acetone new unidentified features were observed that could possibly be from products of these further reactions. Similarly, in this work at high concentrations new modes are observed that may also be a result of products resulting from further re-encounter chemistry. For example, modes of medium intensity at 510cm^{-1}, 512cm^{-1} and 524cm^{-1} appear at a 1:400 mole ratio of acetaldehyde:Ar that are not present at more dilute concentrations. The presence of new unidentified features at these high partial pressures of acetaldehyde suggests that secondary chemistry is occurring which is competing with what would otherwise be more favorable conditions to facilitate the formation of the products being formed via bimolecular interactions. Table 4, in section 4.3.1, shows that there are some major features which have remained unidentified. It is believed these features are also a result of such secondary chemistry based on their diminishment at The primary focus of the investigation

into acetaldehyde was to more fully understand the primary decomposition and isomerization routes it undergoes upon ionization. Consequently, further work would need to be done in order to investigate the more convoluted chemistry, unique to the EBMIS apparatus, which is occurring at high mole ratios.

Another interesting observation from Figure 22 is that the acetyl radical demonstrates variance with acetaldehyde partial pressure typical of bimolecular reactions which is not expected as the acetyl radical could easily be formed through unimolecular α-cleavage. Johnson *et al.*[16] through a photoelectron-photoion coincidence (PEPICO) study of the acetaldehyde molecular ion were able to report the breakdown curves (Figure 28 below) for a variety of decomposition products. A breakdown curve reports how the yield of a specific product varies with the internal energy of the incipient parent ion.

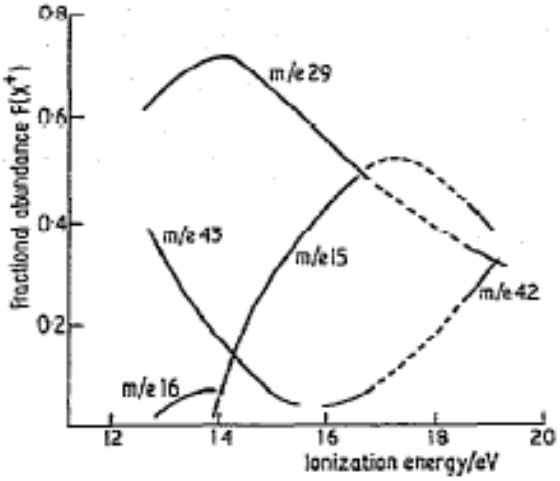

Figure 28: From Johnson *et al.*[16] a breakdown diagram for acetaldehyde.

It should be noted that the cations shown in Figure 28 would appear as radicals (or a close-shell neutral in the case of methane) as a result of neutralization in the matrix from stray secondary electrons. Observation of Figure 28 shows that both the acetyl radical (m/z 43), and ketene (m/z 42) should not be formed via unimolecular decomposition. The curve for m/z 43 shows the production of high yields of that ion at energies around 13eV however at ~16eV, the supposed energy range of Ar change transfer ionization, the curve diminishes substantially. The m/z 42 curve does not start increasing until energies above 17eV are obtained which is beyond the internal energy acetaldehyde would obtain within the EBMIS apparatus. As both ketene and the acetyl radical are produced in very low yields at the ~16eV energy range, these products would not be expected unimolecular products. However, from Figure 22 it is shown that both of these products display variance with acetaldehyde partial pressure typical of bimolecular interactions. The presence of ketene and the acetyl radical can therefore be attributed to bimolecular chemistry instead of unimolecular fragmentation. As a result, the formation of ketene and the acetyl radical are still both congruent with the breakdown curve given by Johnson *et al.*[16] The proposed bimolecular mechanisms for both acetyl radical formation and ketene formation are shown in Schemes 15 and 16 below.

Scheme 15: Possible bimolecular mechanism explaining the formation of the acetyl radical, $CH_3CO^{\bullet}$.

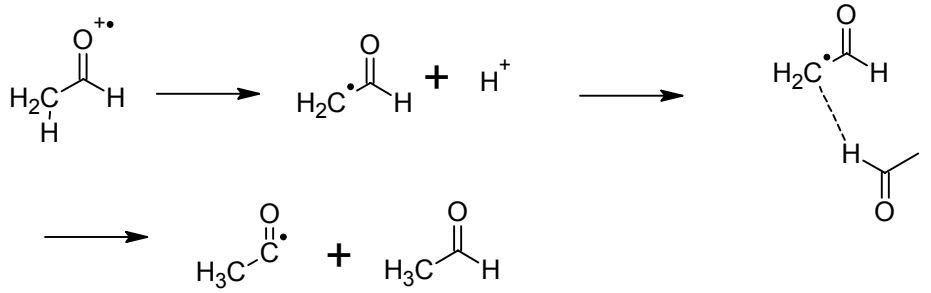

Scheme 16: Possible bimolecular mechanism explaining the formation of ketene, CH_2CO.

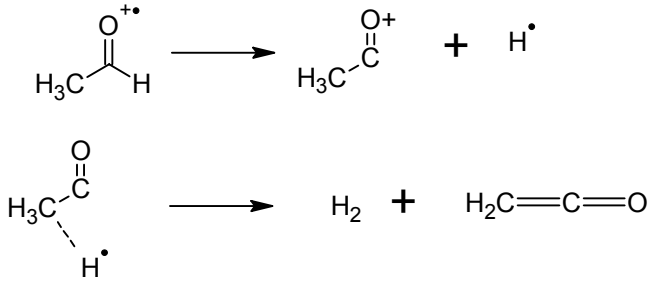

In addition to the acetyl radical and ketene, the breakdown curves for the formyl radical (m/z 29), methane (m/z 16) and the methyl radical (m/z 15) are congruent with these results as all show high product yields around the 16eV energy range and are all observed to occur via unimolecular decomposition as Figure 21 illustrates above. Overall, the breakdown curve in Figure 28 is therefore consistent with all of the observed products. Two products not observed in the breakdown curve are CO and $CH_2CHO^{\bullet}$ as result of their suspected immediate formation as neutrals. The formation of CO is thought to occur simultaneously

with methane which is shown in the breakdown curve and is congruent with the energetics of Ar charge transfer ionization. In contrast, the radical $CH_2CHO^{\bullet}$ does not have an associated cation in the breakdown curve to implicate its presence and therefore this is the one product which cannot be confirmed by the breakdown curve reported by Johnson *et al.*[16]

5.2.2 Influence of flow rate on product distribution

As can be observed from Figure 23 from section 4.3.3 altering the flow rate produced no discernable trend in terms of its effect on product yield. As the flow rate was varied from 0.25cm^3/min to 4.0cm^3/min the various relative peak areas for each specific product fluctuated in a random manner. Thus, the hypothesis that bimolecular products would be favored at high flow rates and unimolecular products would be favored at low flow rates turned out to be false. Because of these results it is thought that altering the flow rate may not have an appreciable effect on the pressure in the reaction zone. This is in contrast to previous flow rate experiments showing that an increase in gas-flow has the effect of increasing the extent of diffusion of various species during condensation as was evident by the increase in diffusion-related chemistry observed at high gas-flow rates.[17]

One interesting result to come from the flow rate experiments concerned how methane and CO product yields were changed as a function of flow rate. Based on the previous series of experiments, where the acetaldehyde partial pressure was varied, it was thought that CO and methane were being formed concurrently as primary unimolecular decomposition products. Examination of

Figure 24 shows that their respective product yields vary almost identically as the flow rate is increased providing further evidence that the two products are mechanistically connected. This is in contrast to the products shown in Figure 23 where no such correlation between two products can be found. Figure 29 below shows a plot of the normalized methane peak areas measured at each flow rate versus the normalized CO peak areas also measured at each flow rate. The linear relationship shown by Figure 29 further exemplifies how methane and CO vary in proportional amounts as the flow rate is altered. Finally, it is worth noting that methane formation in the case of acetaldehyde occurs via a different mechanism than methane formation with propanal and butanal. This is supported, in part, just by examining the relative intensities of the strongest feature associated with methane, the peak at 1305 cm^{-1}. With butanal and propanal, where it is thought that methane is formed via radical-radical recombination reactions, the methane feature in both cases appears similar in intensity. In contrast, the methane feature generated from electron bombardment of acetaldehyde is much greater in intensity which supports that it is being formed more efficiently via unimolecular CO elimination. The methane feature at 1305 cm^{-1} is compared between results of butanal, propanal and acetaldehyde (all at a 1:800 ratio with Ar) as shown in Figure 30 below.

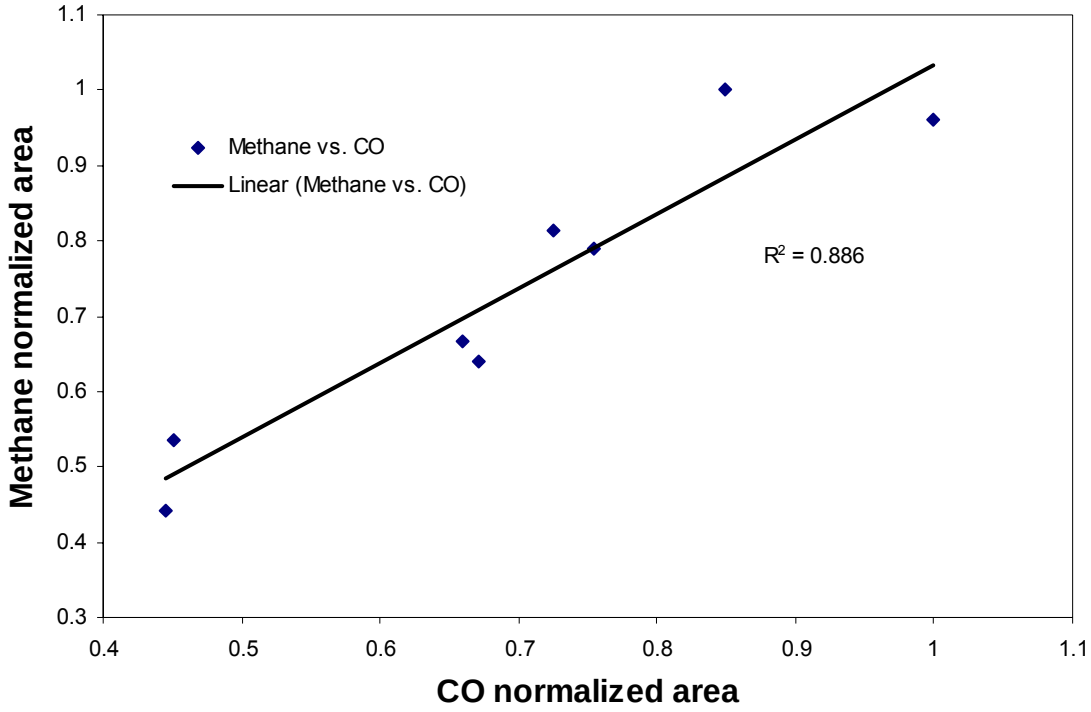

Figure 29: Plot of the normalized methane area versus the CO normalized area for each specific flow rate used.

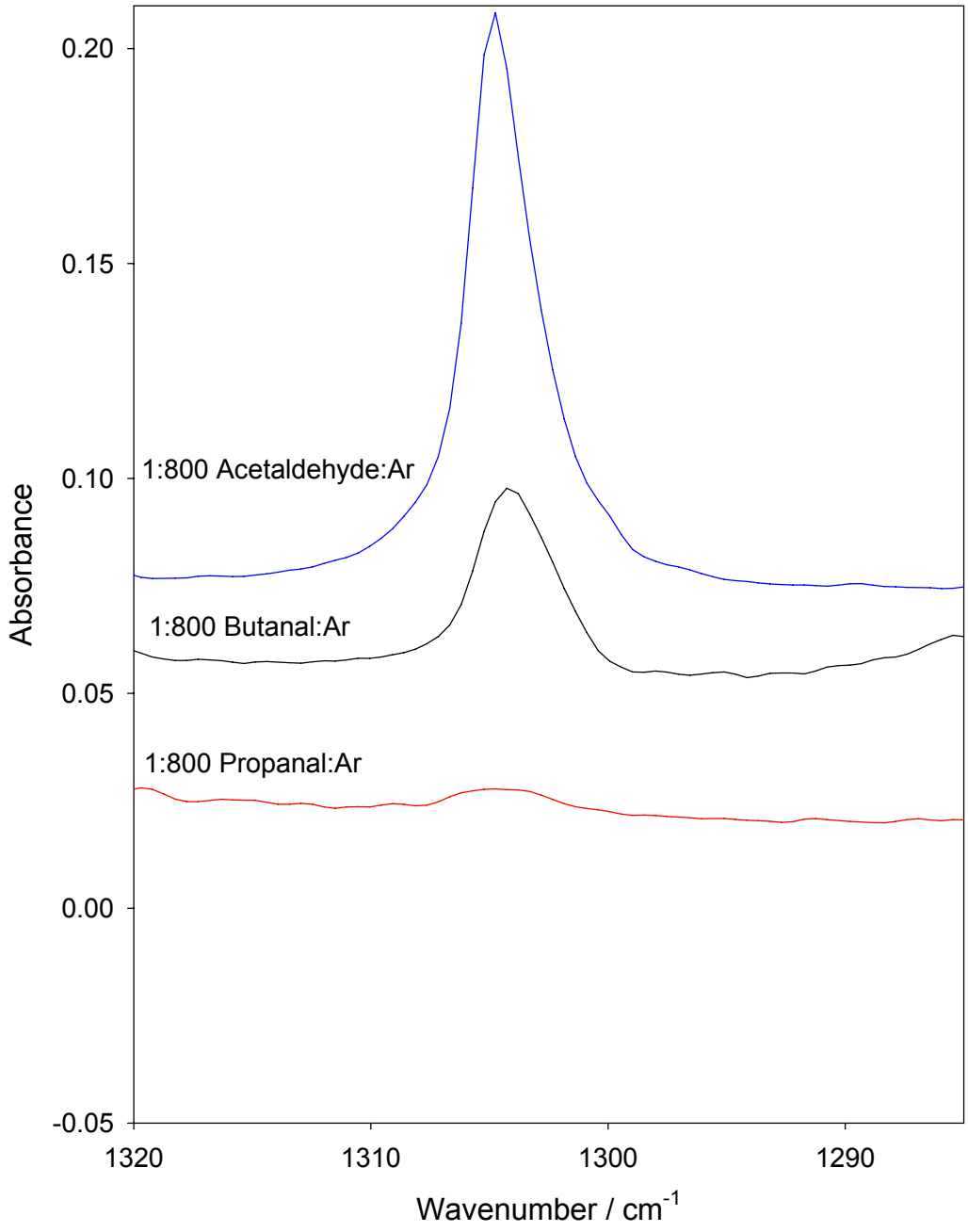

Figure 30: Comparison of the intensity of the methane feature at 1305 cm^{-1} between 1:800 precursor:Ar mixtures of acetaldehyde, butanal and propanal respectively. In each case the electron current was maintained at ~70μA.

5.2.3 CD_3CHO investigation into reaction mechanisms

The isotopomer, CD_3CHO, was used as a means of further investigating the mechanism of a few of the observed products particularly methane and the isomerization product, vinyl alcohol. If methane were being formed through unimolecular elimination of CO, as both the partial pressure and flow rate experiments support, then the use of the CD_3CHO isotopomer should give only CD_3H and not other isotopomers of methane such as CD_4. Figure 26, as found in section 4.3.4 shows that when CD_3CHO is used the only isotopomer generated is CD_3H and therefore this is consistent with the unimolecular elimination of CO. However, it must also be noted that CD_3H could also be formed from the scavenging of free $H^{\bullet}$ atoms by $CD_3^{\bullet}$. Based on the extensive evidence that methane formation occurs via CO elimination such scavenging is not likely to contribute significantly to CD_3H formation.

The use of CD_3CHO was particularly useful in studying the mechanism of acetaldehyde tautomerization. Based on prior studies concerning the gas-phase mechanism of the isomerization of acetaldehyde to vinyl alcohol (see section 2.5) two possible isotopomers of vinyl alcohol were possible when using CD_3CHO as the precursor.[18] If tautomerization were to occur via two consecutive 1,2-H-transfers than the isotopomer expected would be CD_2=CDOH (Scheme 17). In contrast, if the mechanism were a straight a 1,3-H transfer than the isotopomer expected would then be CD_2=CHOD (Scheme 18).

Scheme 17: One possible mechanism of enol formation from 2,2,2-d_3-acetaldehyde (CD_3CHO) consisting of two consecutive 1,2-H-transfers.

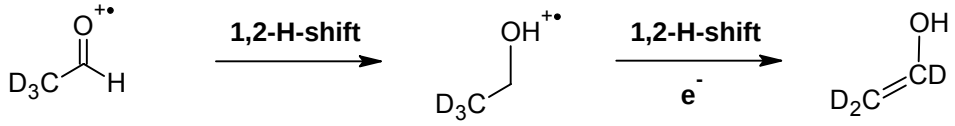

Scheme 18: Another possible mechanism of enol formation from 2,2,2-d_3-acetaldehyde (CD_3CHO) consisting of a direct 1,3-H-transfer.

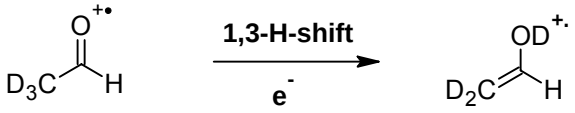

Based on the paper by Haranczyk *et al.* exploring the various mechanisms of vinyl alcohol formation from ionized acetaldehyde it is expected that the isotopomer, CD_2=CHOD would be formed via a direct 1,3-H-shift. This product is also expected based on the result that none of the observed features in electron bombardment spectrum of CD_3CHO were found to correlate with any of the previously characterized isotopomers including CD_2=CDOH; the isotopomer resulting from consecutive 1,2-H-tranfers. Table 7 below shows the features of CD_2=CDOH as characterized by Rodler *et al.*[19] and whether that feature was observed (to within ±5cm^{-1}) in the infrared spectrum of electron bombarded CD_3CHO/Ar.

Table 7: Assigned features of CD_2=CDOH and whether those features were present in the IR spectrum of electron bombarded CD_3CHO/Ar (1:400) mixtures.

	CD_2=CDOH*	
Wavenumber /cm^{-1}	**Assignment**	**Present (Y/N)**
3622	OH stretch	N
1583	C=C stretch	Y
989	COH in-plane bend	N
966	CO stretch	N
792	CH_2 rock	N
758	CH_2 twist	N
418	CCO in-plane bend	N
398	CO torsion	N/A

*As assigned by Rodler *et al.*

As can be observed in the table above the only mode that was found to correlate to an assigned feature of CD_2=CDOH was the C=C stretching mode at 1583cm^{-1}. This is an agreement with an earlier analysis performed by Robinson.[20] Furthermore, the most glaring inconsistency was the absence of any feature corresponding to the OH stretching mode. The lack of correlation between the characterized features of CD_2=CDOH with the observed spectrum indirectly suggests that the isotopomer formed is CD_2=CDOH via the 1,3-H-transfer mechanism. Based on this evidence Scheme 19 shows the final suggested mechanism for enol formation from ionized acetaldehyde. The proton affinity of neutral acetaldehyde is of suitable value to abstract a proton from the initial site and donate it back to the oxygen to form vinyl alcohol. Consequently, the 1,3-H-transfer is believed to be self-catalyzed through an ion-molecule interaction between ionized acetaldehyde and neutral acetaldehyde. This is in agreement with the theoretical work of Haranczyk *et al.* as well as the mechanism put forth for acetone enolization under EBMIS conditions.

Scheme 19: Proposed self-catalyzed 1,3-H-transfer mechanism for formation of vinyl alcohol from the tautomerization of the acetaldehyde radical cation.

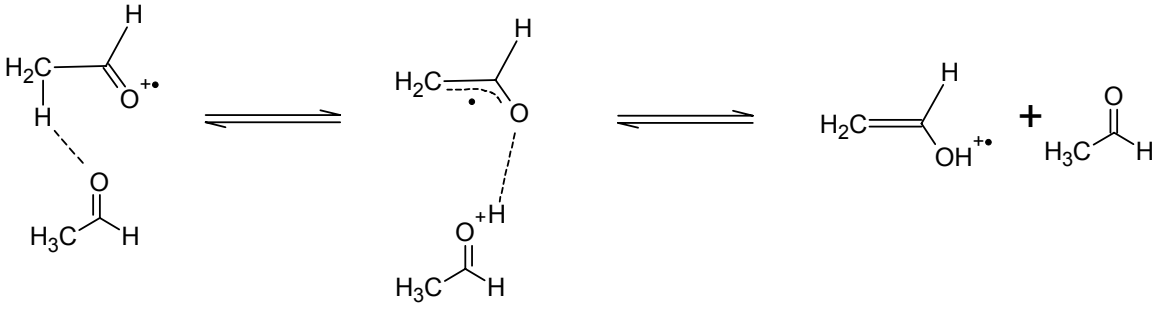

5.2.4 Computational results

Despite the above indirect evidence of CD_2CHOD formation a direct characterization of the isomer was still desired. Thus, as a means of characterizing spectroscopically the CD_2CHOD isotopomer, a computational study (at the B3LYP/6-311G(d,p) level) was employed where the vibrational modes of CD_2CHOD could be calculated and compared with the observed spectrum. Also in order to show that the calculated values of that isotopomer correlated better than the competing isomer, CD_2CDOH, the same calculations and subsequent scaling of resultant frequencies was performed on CD_2CDOH as well. Table 8 shows the average scaling factors for each mode applied to the calculated values of CD_2=CHOD and CD_2=CDOH with the scaled values compared to the observed spectral features.

Table 8: Comparison of the calculated wavenumbers (B3LYP/6-311G(d,p)) for CD_2=CDOH and CD_2=CHOD versus the observed features in electron bombarded CD_3CHO/Ar mixtures.

Mode	Description	Av. scaling factor	Calc. D_2C=CHOD	Calc. D_2C=CDOH	D_2C=CHOD scaled	Observed	D_2C=CDOH scaled	Observed
ν_1	OH (OD) stretch	0.9563	2768.89	3805.5	**2647.85309**	**2632**	3639.15	NF
ν_2	CD_2 antisymmetric stretch	1.0005	2409.03	2409.87	**2410.22962**	**2411**	**2411.07**	**2411**
ν_5	C—C stretch	0.973	1656.74	1630.9	**1611.98427**	**1614**	1586.842	NF
	-	-	-	-	-	**1609**	-	-
	-	-	-	-	-	**1606**	-	-
ν_6	CD_2 in-plane deformation	0.9754	944.38	1326.23	**921.173823**	**920**	**961.6381**	**966**
	-	-	-	-	-	**926**	-	**963**
ν_8	COH (COD) in-plane bend	0.9831	1074.81	1000.5	**1056.63635**	**1052**	983.5828	NF
ν_{12}	CD_2 twist	0.9749	961.2	777.58	**937.103756**	**941**	758.0869	NF
	-	-	-	-	-	**933**	-	-
ν_{13}	CD_2 wag	0.9857	666.88	658.6	**657.328926**	**659**	**649.1675**	**650**
	-	-	-	-	-	**658**	-	**-**

NF: not found within 5cm^{-1}

Table 8 clearly shows that the calculated values for CD_2CHOD correlate better with the observed features than do the calculated values for CD_2CDOH. For the former isotopomer 12 different modes in the IR spectrum were found to lie within $5cm^{-1}$ of the calculated values. In contrast, for the latter isotopomer only 4 different modes in the IR spectrum were found to lie within $5cm^{-1}$ of the calculated values. Based on those computational results a tentative assignment of the various modes of the CD_2=CHOD isotopomer are put forth in Table 9 below. For convenience, where more than one mode was observed to correlate with a calculated value, the mode closest to the calculated value was used. Finally, it is recognized that some modes are not characterized which is a result those modes not displaying features in the infrared spectrum. This could be a result of the fact that those modes are weaker in intensity and therefore would not be observed or additionally those characterized modes might be located in a region populated with peaks of CD_3CHO itself. This would result in making their identification more difficult as the large modes of the precursor would overshadow the possible smaller modes associated with CD_2CHOD.

Table 9: Tentative assignment of the vinyl alcohol isotopomer, CD_2=CHOD.

Mode	Symmetry	Description	Wavenumber / cm^{-1}
ν_1	A'	OD stretch	2632
ν_2	A'	CD_2 antisymmetric stretch	2411
ν_5	A'	C=C stretch	1609
ν_6	A'	CD_2 in-plane deformation	920
ν_8	A'	COD in -plane bend	1052
ν_{12}	A"	CD_2 twist	933
ν_{13}	A"	CD_2 wag	658

5.3 References for Chapter 5

[1] Gross, J. *Mass Spectrometry, a textbook.* Springer, New York, **2004**.

[2] Jacox, M. E.; Milligan, D. E. J. Chem. Phys. 1965, 43, 866.

[3] Fridgen, T.D.; Parnis, J.M. *J. Phys. Chem. A.* **1997**, 101, 5117.

[4] Parnis, J.M.; Thompson, M.G.K.; King, K. *J. Mass. Spectrom.* **2009**, in press.

[5] Thompson, M.G.K.; Parnis, J.M. *J. Phys. Chem. A.* **2008**, 112, 12109.

[6] Hudson, C.E.; McAdoo, D.J.; Griffin, L.L.; Traeger, J.C. *J. Am. Soc. Mass Spectrom.* **2003**, 14, 136.

[7] Suzer, S.; Andrews, L. *J. Phys. Chem.* **1989**, 93, 2123.

[8] Traeger, J.C.; Djordjevic, M. *Eur. Mass Spectrom.* **1999**, 5, 319.

[9] Dannacher, J.; Stadelmann, J.P. *Int. J. Mass Spectrom.* **2001**, 208, 147.

[10] Bouma, W.J.; MacLeod, J.K.; Radom, L. *J. Am. Chem. Soc.* **1980**, 102, 2246.

[11] Zhang, X.K.; Parnis, J.M.; Lewars, E.G.; March, R.E. *Can. J. Chem.*, **1997**, 75, 276.

[12] Hawkings, M.; Andrews, L. *J. Am. Chem. Soc.* **1983**, 105, 2523.

[13] Jacox, M.E. *Chemical Physics*. **1982**, 69, 407.

[14] Jacox, M.E. *J. Mol. Spectro.* **1977**, 66, 272.

[15] Gluch, K.; Cytawa, J.; Michalak, L. *Int. J. Mass Spectrom.* **2008**, 273, 20.

[16] Johnson, K.; Powis, I.; Danby, C.J. *Chemical Physics*. **1982**, 70, 329.

[17] Thompson, M.G.K.; Parnis, J.M. *Inorg. Chem.* **2008**, 47, 4045.

[18] Haranczyk, M.; Burgers, P.C.; Ruttink, P.J.A. *Int. J. Mass Spectrom.* **2002**, 220, 53.

[19] Rodler, M.; Blom, C.E.; Bauder, A. *J. Am. Chem. Soc.* **1984**, 106, 4029.

[20] Robinson, Mark. MSc. Thesis, Queen's University, Kingston, Ontario, Canada, **2005**.

Chapter 6

Summary

Electron bombardment of butanal:Ar mixtures produced many decomposition products associated with parent ion decomposition and secondary reactions. Products included propane, propene, propyne, ethene, ethyne, CCCO, ketene, formaldehyde, CO, CH_2=$CHCH_2^{\bullet}$, $CH_2CHO^{\bullet}$, the formyl radical, $HCO^{\bullet}$ and methane. Electron bombardment of propanal:Ar mixtures also produced a variety of products attributable to extensive fragmentation of the parent ion and secondary chemistry. Products included ethyl radical, ethane, ethene, ethyne, CO, $CH_2CHO^{\bullet}$, $HCO^{\bullet}$ and methane. In both cases primary products were believed to be formed as a result of C—C cleavages of the parent ion whereby closed-shell neutral species resulted from subsequent scavenging of free $H^{\bullet}$ atoms and/or hydrogen abstraction between two proximally located species. Dehydrogenation products of propane and ethane were proposed to result from multiple product ionization events and this process was found to be dependent on the applied electron current.

Electron bombardment of acetaldehyde:Ar mixtures produced many products including methane, CO, $HCO^{\bullet}$, $CH_3CO^{\bullet}$, $CH_2CHO^{\bullet}$, $CH_3^{\bullet}$ and ketene. The isomerization product, vinyl alcohol, was also observed. All observed products were found to be consistent with previous studies performed with acetaldehyde. Variations in the acetaldehyde:Ar mole ratios resulted in dramatic variations in the products formed, demonstrating a transition from unimolecular

chemistry at low acetaldehyde concentrations to processes consistent with bimolecular chemistry at intermediate mole ratios. Using this technique it was found that the products methane, CO, $HCO^{\bullet}$, $CH_2CHO^{\bullet}$ and $CH_3^{\bullet}$ are formed via unimolecular decomposition of the parent ion. In contrast, it was found that ketene, $CH_3CO^{\bullet}$, and vinyl alcohol formation involves bimolecular processes. The variation of precursor:Ar mole ratios has therefore been found to give fundamental information regarding the mechanisms of gas-phase reactions. These results are in good accord with published gas-phase ion chemistry studies.

By observing how a given product fluctuates while altering the precursor:Ar ratio the product can easily be categorized as either occurring via a unimolecular or bimolecular process. This technique could therefore be very beneficial in obtaining mechanistic information in cases where this information would have remained ambiguous using other methods. Variations in the total flow rate of gas resulted in random changes in product yields but provided further evidence for unimolecular methane formation via the elimination of neutral CO.

$$CH_3CHO^{\bullet+} \rightarrow CH_4^{\bullet+} + CO \qquad (50)$$

Finally, an investigation into the mechanism of vinyl alcohol formation using the acetaldehyde isotopomer, CD_3CHO, in conjunction with computational methods provided further evidence that enol formation occurs at a result of a direct self-catalyzed 1,3-H-transfer and not consecutive 1,2-H-transfers. Based on the

comparison of calculated vibrational modes to the observed spectrum a tentative vibrational assignment of the suspected isotopomer, CD_2=CHOD was given.

$$CD_2\mathbf{D}CHO^{\bullet+} + CD_3CHO \text{ (1,3-H-transfer)} \rightarrow CD_2{=}CHO\mathbf{D}^{\bullet+} + CD_3CHO \qquad (51)$$